

UC Berkeley

UC Berkeley Electronic Theses and Dissertations

Title

Nanostructure Control of Biologically Inspired Polymers

Permalink

<https://escholarship.org/uc/item/89z332v7>

Author

Rosales, Adrienne

Publication Date

2013

Peer reviewed|Thesis/dissertation

Nanostructure Control of Biologically Inspired Polymers

By

Adrienne Marie Rosales

A dissertation submitted in partial satisfaction of the

requirements for the degree of

Doctor of Philosophy

in

Chemical Engineering

in the

Graduate Division

of the

University of California, Berkeley

Committee in charge:

Professor Rachel A. Segalman, Chair

Professor Nitash P. Balsara

Professor Matthew B. Francis

Spring 2013

Nanostructure Control of Biologically Inspired Polymers

© 2012

By Adrienne Marie Rosales

Abstract

Nanostructure Control of Biologically Inspired Polymers

by

Adrienne Marie Rosales

Doctor of Philosophy in Chemical Engineering

University of California, Berkeley

Professor Rachel A. Segalman, Chair

Biological polymers, such as polypeptides, are responsible for many of life's most sophisticated functions due to precisely evolved hierarchical structures. These protein structures are the result of monodisperse sequences of amino acids that fold into well-defined chain shapes and tertiary structures. Recently, there has been much interest in the design of such sequence-specific polymers for materials applications in fields ranging from biotechnology to separations membranes. Non-natural polymers offer the stability and robustness necessary for materials applications; however, our ability to control monomer sequence in non-natural polymers has traditionally operated on a much simpler level. In addition, the relationship between monomer sequence and self-assembly is not well understood for biological molecules, much less synthetic polymers. Thus, there is a need to explore self-assembly phase space with sequence using a model system. Polypeptoids are non-natural, sequence-specific polymers that offer the opportunity to probe the effect of sequence on self-assembly.

A variety of monomer interactions have an impact on polymer properties, such as chirality, hydrophobicity, and electrostatic interactions. Thus, a necessary starting point for this project was to investigate monomer sequence effects on the bulk properties of polypeptoid homopolymers. It was found that several polypeptoids have experimentally accessible melting transitions that are dependent on the choice of side chains, and it was shown that this transition is tuned by the incorporation of "defects" or a comonomer. The polypeptoid chain shape is also controlled with the choice of monomer and monomer sequence. By using at least 50% monomers with bulky, chiral side chains, the polypeptoid backbone is sterically twisted into a helix, and as found for the first time in this work, the persistence length is increased. However, this persistence length, which is a measure of the stiffness of the polymer, is small compared to other folded helices, indicating the conformational flexibility of polypeptoid chains.

With a firmer understanding of how monomer sequence and composition influence polypeptoid bulk properties, we designed block copolymer systems for self-assembly. Because the governing parameters of block copolymer self-assembly are well understood, this architecture provides a convenient starting point for probing the effect of changing polymer sequence. We found that polystyrene-polypeptoid block copolymers readily self-assemble into hexagonally-packed and lamellar morphologies with long range order, and furthermore, sequence control of the

polypeptoid block enables us to tune the strength of segregation (and therefore the order-disorder transition) of the block copolymer. Polypeptoid chain shape also affects self-assembly. In classical synthetic block copolymers, it has typically been difficult to change chain shape without also changing polymer chemistry and therefore other factors affecting self-assembly. The advantage of the polypeptoid system is that it is modular, as the side chain chemistry (and therefore polymer properties) can easily be changed without changing the backbone chemistry. Thus, we have decoupled conformational effects from chemical composition by comparing the self-assembly of block copolymers containing either a helical peptoid block or its racemic, non-helical analog. The increase in the persistence length of the peptoid block due to helicity translates to an increase in the morphological domain spacing.

In this work, we further the understanding of the effect of monomer sequence on bulk polypeptoid properties and self-assembly. Our findings pave the way for the rational design of structured synthetic polymers with tunable, sequence-specific properties.

Table of Contents

Table of Contents.....	i
List of Figures.....	iii
List of Tables.....	v
Acknowledgements.....	vi
Chapter 1. Introduction.....	1
1.1 Polymer Sequence Control.....	1
1.2. Sequence Effects on Polymer Properties.....	4
1.3. Sequence Effects on Copolymer Conformation and Self-Assembly.....	6
1.4. Polypeptoids.....	8
1.5 Peptoid Structure Formation.....	9
1.6 Tuning Bulk Self-Assembly with Polymer Sequence.....	13
Chapter 2. Control of Crystallization and Melting Behavior in Sequence Specific Polypeptoids.....	19
2.1. Introduction.....	19
2.2. Experimental Methods.....	21
2.3. Results and Discussion.....	25
2.3.1. Thermal Stability and Processability.....	25
2.3.2. Controlling T_m by Varying Sidechains.....	26
2.3.3. Controlling T_m with Sequence Defects.....	30
2.3.4. Controlling the Distribution of Sequence Defects.....	37
2.4. Conclusions.....	41
2.5. Acknowledgements.....	41
2.6. Appendix.....	42
2.7. References.....	43
Chapter 3. Determination of the Persistence Length of Helical and Non-helical Polypeptoids in Solution.....	45
3.1. Introduction.....	45
3.2. Experimental Methods.....	46
3.3. Results and Discussion.....	48

3.3.1. Circular Dichroism.....	48
3.3.2. Small Angle Neutron Scattering.....	52
3.4. Conclusions.....	59
3.5. Acknowledgements.....	59
3.6. Appendix.....	60
3.7 References.....	67
Chapter 4. Tunable Phase Behavior of Polystyrene-Polypeptoid Block Copolymers	69
4.1 Introduction.....	69
4.2. Experimental Methods.....	71
4.3. Results and Discussion.....	73
4.3.1. Synthesis of Polypeptoids and Polystyrene-Polypeptoid Block Copolymers.....	73
4.3.2. Thermal Properties of Polypeptoids.....	75
4.3.3. Self-Assembly of PS-b-Nme Block Copolymers.....	75
4.3.4. Tuning Segregation Strength with the Introduction of N-(2-Phenylethyl)glycine Residues.....	81
4.4. Conclusions.....	86
4.5. Acknowledgements.....	86
4.6. Appendix	87
4.7. References.....	91
Chapter 5. Effect of Chain Shape on Peptoid Block Copolymer Self-Assembly.....	94
5.1. Introduction.....	94
5.2. Experimental Methods.....	95
5.3. Results and Discussion.....	99
5.4. Conclusions.....	107
5.5. Acknowledgements.....	107
5.6. Appendix.....	108
5.7. References.....	112
Chapter 6. Conclusions and Future Outlook.....	113

List of Figures

Figure 1.1.	Strategies for Polymer Sequence Control.....	5
Figure 1.2.	Solid Phase Synthesis of Peptoids.....	10
Figure 2.1.	Model Acetylated Peptoid 15-mer.....	23
Figure 2.2.	Thermal Properties of a Model Peptide vs. a Model Peptoid.....	27
Figure 2.3.	Tuning Melting Transition with Side Chain Length.....	28
Figure 2.4.	XRD of pNpe15.....	31
Figure 2.5.	POM of pNpe15.....	31
Figure 2.6.	Heat Rate Dependence of Crystallization for pNpe15.....	32
Figure 2.7.	Defect Scheme for Peptoids.....	33
Figure 2.8.	Thermal Behavior of Peptoids with Nhx Defects.....	35
Figure 2.9.	Thermal Behavior of Peptoids with Nme Defects.....	36
Figure 2.10.	Melting Point Comparison of Peptoids with Defects.....	38
Figure 2.11.	Thermal Behavior of pNpe15 Peptoids with Defects.....	39
Figure 2.12.	XRD Patterns for pNia15 Copolymers with 2 Defects Each.....	40
Figure 2.13.	X-Ray Diffraction of Polypeptoids of Various Molecular Lengths.....	42
Figure 3.1.	Structure of Helical and Non-Helical Peptoids.....	47
Figure 3.2.	CD of Helical Peptoids.....	51
Figure 3.3.	CD at Various Temperatures and in Methanol.....	53
Figure 3.4.	SANS of Polypeptoids.....	54
Figure 3.5.	Persistence Length as a Function of Chain Length.....	58
Figure 3.6.	Guinier Plots of Polypeptoids.....	61
Figure 3.7.	Persistence Length Fits.....	63
Figure 3.8.	Structure of Racemic Peptoid.....	64
Figure 3.9.	CD of Racemic Peptoid.....	64
Figure 3.10.	Variable Temperature CD.....	66
Figure 4.2.	Conjugation reaction scheme for polystyrene and an example polypeptoid.....	74
Figure 4.3.	Peptoid structure with alkyne functionalization.....	74
Figure 4.4.	GPC for block copolymers containing Nme or (Nme-co-Npe) polypeptoids...	78
Figure 4.5.	DSC thermograms of Nme and (Nme-co-Npe) peptoid copolymers.....	78

Figure 4.6.	DSC traces for SNme block copolymers.....	80
Figure 4.7.	SAXS of SNme Block Copolymers.....	80
Figure 4.8.	TEM of Block Copolymers.....	83
Figure 4.9.	SAXS heating scan for S ₃₂ Nme ₄₈	83
Figure 4.10.	DSC heating traces for representative S(Nme-co-Npe) block copolymers.....	84
Figure 4.11.	SAXS of S(Nme-co-Npe) Block Copolymers.....	84
Figure 4.11.	Analytical HPLC traces for (Nme) _N polypeptoids.....	87
Figure 4.12.	Analytical HPLC traces for (Nme-co-Npe) _N polypeptoids.....	87
Figure 4.13.	Magnified SAXS for S ₈₄ Nme ₂₄	88
Figure 4.14.	Inverse intensity vs. inverse temperature plots to determine ODTs for SNme block copolymers.....	89
Figure 4.15.	Inverse intensity vs. inverse temperature plots to determine ODTs for S(Nme-co-Npe) block copolymers.....	90
Figure 5.1.	CD of P(nBA-peptoid) Block Copolymers.....	102
Figure 5.2.	SAXS of P(nBA-peptoid) Block Copolymers.....	103
Figure 5.3.	Domain Spacing of P(nBA-peptoid) Block Copolymers.....	105
Figure 5.4.	Domain Spacing and CD of Sequence Specific P(nBA-peptoid) Block Copolymers.....	106
Figure 5.5.	Representative GPC Traces for Block Copolymers.....	108
Figure 5.6.	Circular Dichroism for Peptoid Homopolymers.....	109
Figure 5.7.	Domain spacings of the block copolymers with Equation 5.1 fits.....	111

List of Tables

Table 2.1.	N-substituted glycine side chains.....	23
Table 2.2.	Analytical data for a series of peptoid 15-mers.....	24
Table 2.3.	pNia15 copolymers with various sequence distributions of 2 defects.....	40
Table 3.1.	Molecular design of non-helical and helical polypeptoids.....	49
Table 3.2.	Fitted parameters for Compounds 1 and 2 with $n = 6$	56
Table 3.3.	Fitted Peptoid Parameters allowing Contour Length to Fluctuate.....	65
Table 4.1.	Polypeptoids synthesized and their characteristics.....	76
Table 4.2.	Polystyrene-polypeptoid block copolymers.....	77
Table 4.3.	ODT Comparison for Analogous SNme and S(Nme-co-Npe) Block Copolymers.....	85
Table 5.1.	Characterization of polypeptoids.....	97
Table 5.2.	Characterization of poly(n-butyl acrylate-peptoid) block copolymers.....	98

Acknowledgements

First, I would like to express my deep gratitude to my advisors. Rachel has provided an incredible amount of support and has given me license to be creative and independent throughout my PhD. Ron Zuckermann has also been a wonderful mentor, and I have deeply appreciated his advice and scientific guidance. Together, they have both imparted me with a solid scientific foundation, as well as provided strong examples of compassionate leadership.

I would also like to thank all of my present and former labmates for their help, insightful discussions, and friendship. I am extremely lucky to have worked with such a talented and motivated group of individuals, many of whom continue to be among my closest friends. I would especially like to thank Hannah Murnen, who started the polypeptoid project with me. She spent innumerable hours on scientific brainstorming and troubleshooting with me, and her friendship helped to make our project truly fun. I would also like to especially thank Megan Hoarfrost, Bryan McCulloch, Victor Ho, and Miguel Modestino for their encouragement, discussions (both serious and fun), and friendship that helped to foster a truly collaborative lab dynamic. In addition, I am deeply appreciative of the opportunity to work with Wendy van Zoelen and Hilda Buss on the polypeptoid project; they have both contributed much insight to our mini group. Bryan Boudouris and Boris Russ have also been extremely helpful with experimental techniques and advice without which I could not have achieved some of the work here. Finally, there are numerous individuals from both the Segalman and Zuckermann groups that have been an extremely helpful and essential part of my experience here: Barbara Ekerdt, Shannon Yee, Byoung-Chul Lee, Gloria Olivier, Jing Sun, Tammy Chu, Chun Long Chen, Nelson Coates, Eddie Buehler, Cynthia Chen, William Chang, Jibin Sun, Joe Feser, Yanika Schneider, Yuefei Tao, Justin Virgili, Saar Kirmeyer, Jon Malen, Young-rae Hong, Kevin See, Kasper Moth-Poulsen, Robert Wang, and Joe Chen.

I would also like to thank Nitash Balsara, Matthew Francis, Matthew Tirrell, and Dave Schaffer for the advice and guidance that they have provided me through serving on my qualifying exam and thesis committees, as well as through informal scientific discussions. Steven Kline, Volker Urban, Alex Hexemer and his group, and John Pople have all provided essential assistance at their various beamlines for which I am truly grateful. In addition, Andrey Dobrynin was extremely helpful with the analysis of our polyelectrolyte peptoid data. In addition, I am deeply appreciative of several members of the College of Chemistry staff for their aid throughout my PhD: Aileen Harris, Rocio Sanchez, Fred Deakin, Cheryn Gliebe, and Carlet Altamirano.

Finally, I am deeply grateful to my family and friends, especially Michael, who have provided me with so much support throughout my time in graduate school.

Chapter 1. Introduction

Polymer sequence has a profound effect on polymer properties and structure. Understanding the relationship between monomer sequence, properties, and structure will be important as the need for advanced functional materials increases in fields ranging from sensors to biomaterials. Current research efforts have focused on biological polymers such as polypeptides for applications where monomer sequence definition is necessary. While these biological polymers have excellent sequence control, they are limited in their monomer set, stability, and availability, making them less suited for materials purposes. Furthermore, it is extremely difficult to predict *de novo* structures from a biological polymer sequence. Conversely, sequence control is difficult in synthetic polymer systems due to conventional polymerization methods, but the chemical diversity, robustness, and low cost exceeds that of natural polymers. As polymer physicists explore an increasingly complex phase space,^{1,2} the question of the monomer sequence effect on polymer self-assembly grows more pressing. The creation of new materials with tunable properties and structures thus requires a biologically-inspired approach that combines the sequence-specificity of natural polymers with the versatility of synthetic systems.

In practice, many sequence-specific synthetic molecules have been oligomeric in nature and are termed “foldamers.”³⁻⁵ Research on the properties of sequenced polymers, however, is just emerging. This work investigates the effect of monomer sequence on bulk polymer properties and self-assembly using polypeptoids, or N-substituted glycines. The thermal and conformational properties of sequence-defined homopolymers are probed. The gained insight is then used to tune the self-assembly of a polypeptoid-polymer block copolymer.

1.1 Polymer Sequence Control

In order to probe the effect of monomer sequence on polymer properties, one needs excellent synthetic control over the insertion of monomers into the polymer chain. Broadly, approaches to achieve this goal fit into three areas: harnessing the cellular machinery to modify biological polymer backbones or side chains, exploiting the kinetics of conventional polymerizations, and building non-natural polymers via solid phase synthesis.

Modification of Biological Synthesis

One strategy for the sequence control of synthetic polymers is to engineer existing biosynthetic methods to include non-natural molecules. In nature, the cell creates polypeptides during the process of translation. Researchers have adapted this process to the laboratory using recombinant genes, enabling the production of large (gram scale) batch sizes of monodisperse, designed peptide sequences.⁶ As one way toward achieving non-natural functionalities, a plethora of non-natural amino acids have been successfully incorporated into polypeptide chains, thereby expanding the side-chain diversity for these systems. A thorough review of these methods is found elsewhere.^{7,8} Engineering the peptide backbone has proven to be a more difficult task because nature has optimized the ribosome and transfer RNAs (tRNAs) to work with the amino

acid construct. However, it has been shown that tRNAs can bind molecules with similar spacing and chemistry to amino acids.⁹⁻¹² For example, Ohta and coworkers developed a flexizyme system to charge t-RNAs with α -hydroxy acids, yielding ha-tRNAs. Then, the codons that call specific tRNAs can be reassigned to these non-natural tRNAs, leading to the production of polyesters.^{9,10} Recently, similar approaches have led to other non-natural backbones such as N-methyl peptides,¹¹ and polypeptoids.¹² Optimization of these systems is underway, as they currently suffer from low yields and reaction efficiencies.

The biological synthesis of polynucleotides has also provided inspiration for the synthesis of sequence-defined non-natural polymers. Biological synthesis of polynucleotides uses base pairs of complementary nucleic acids; thus, a mother polymer provides a template for a daughter polymer consisting of complementary monomers in a defined sequence. To increase chemical diversity, the four natural nucleic acids have been chemically modified to create a large library of functional moieties.¹³ In addition, polynucleotides with modified backbones have also been synthesized,^{14,15} such as peptide nucleic acids¹⁶ and threose nucleic acids.¹⁷ Importantly, the general concept for using a template to direct the assembly of monomer units has been adapted to a variety of synthetic polymers.¹⁸⁻²² For example, aniline monomers were linked to a duplex DNA template, which was then treated with hydrogen peroxide and horseradish peroxidase to polymerize the anilines.²⁰ Novel, DNA-free templates have also been designed to direct the polymerization of methacrylate/acrylate systems (using a naphthalene template)²¹ and styrene/4-vinyl-pyridine systems (using a palladium template)²² into repeating sequence motifs. In these systems, the template was removed after polymerization, yielding sequence-controlled copolymers of high molecular weight but also high polydispersities.

The advantage of adapting templated syntheses to non-natural polymers is that compatibility with cellular components is not necessary. However, one must create a template with the desired sequence motif. In addition, it can be difficult to control the reaction, leading to large polydispersities. More conventional polymerizations, such as step-growth or chain-growth methods, can exert better control over polydispersity, and recently, many new strategies have been developed for macromolecular sequence control. Most sequence-controlled polymers to date consist of repeating or periodic sequences, but some notable developments may enable greater freedom over sequence design in synthetic systems.

Sequence-controlled Polymerizations

Conventional chain-growth polymerization methods typically offer a low level of sequence control and a high amount of chain-to-chain heterogeneity. Radical and anionic polymerizations are sensitive to differences in the reactivity ratios of the monomers,^{23,24} which can lead to uncontrolled gradient or blocky sequences. Recently, however, polymer chemists are exploiting these kinetic differences via monomer design, feed composition, and reaction times to produce controlled monomer distributions.²⁵⁻²⁷ In one example, single N-substituted maleimides were incorporated into precise regions of a polystyrene chain using a sequential addition strategy.^{26,27}

A primary batch of the styrene monomer was allowed to reach high conversion before the maleimide was added to the feed. As the maleimide/styrene pair has a strong tendency to alternate, the maleimide reacted immediately; then, the styrene chain growth was refreshed by adding more styrene to the feed. Although this strategy leads to a narrow region of maleimide incorporation, copolymerization still leads to some chain-to-chain differences.

Researchers have also designed novel catalysts and initiators to control monomer sequence during chain-growth polymerizations.²⁸⁻³⁰ For chiral molecules, catalysts are extremely sensitive to stereochemistry, enabling the controlled synthesis of a polymer with a particular tacticity. This selectivity was applied to the polymerization of chiral β -lactones using a syndiospecific catalyst.³¹ By using two different β -lactones (differing in the substituent) of enantiomerically pure opposite chiralities, nearly monodisperse polyesters with an alternating sequence of side chains could be synthesized at high molecular weights in excellent yield. Another recent strategy combined a templating initiator and a catalyst to achieve extreme selectivity in the precise radical addition of one alkene monomer.^{32,33} Essentially, the templating initiator contained a chemical moiety that was recognizable to the desired monomer; this was demonstrated with initiators containing an amino group³² or a size-selective crown ether³³ to “recognize” a carboxy-containing methacrylic acid or sodium methacrylate, respectively. Although this concept was only demonstrated in a short oligomer, it sets the stage for the design of catalysts that can selectively add specific monomers of widely different types, thereby enhancing both sequence control and chain-to-chain homogeneity.

Finally, many polymer chemists have developed new step-growth polymerizations for sequence control because they offer homogeneous sequences (chain to chain), although they exclusively produce repeating or periodic motifs. In step-growth polymerizations, difunctional monomers that contain complementary reactive termini lead to alternating sequences of 2 or 3 monomers; nylons, which are composed of diacids and diamines, are a classic example. Recently, repeating sequence copolymers have been synthesized via the step-growth polymerization of short low molecular weight segments prepared by other synthesis or polymerization methods.³⁴⁻³⁷ In one study, these segments, termed “segmers,” were monodisperse lactic-co-glycolic-co-caprolactic acid units of 2 to 8 monomers in length.³⁶ In a similar approach, short polystyrene segments containing a substituted maleimide were functionalized into α -alkyne, ω -azido oligomers and polymerized stepwise using copper-catalyzed click chemistry.³⁴ Periodic sequences of branched polyolefins have also been obtained using acyclic diene metathesis (ADMET) polymerization.^{38,39} In this step-growth method, the polymerization of α,ω -dienes is driven by the production of ethylene; a number of polyethylenes have been synthesized with side chains such as alkyl chains,^{38,39} halogens,^{40,41} or acid groups^{42,43} on every n th monomer. While these solution-phase step-growth polymerizations lead to sequence-controlled polymers of high molecular weight, they also tend to lead to high polydispersities. To date, only step-growth syntheses on a solid phase offer complete monodispersity in both sequence control and chain length.

Solid Phase Synthesis

Current solid-phase methods are largely developments of the Merrifield method,⁴⁴ in which molecules are synthesized stepwise on a solid support (such as polystyrene resin), then cleaved from the resin and purified using chromatography. Both natural^{45,46} (polypeptides, polynucleic acids, polysaccharides) and non-natural⁴⁷⁻⁴⁹ (polyamidoamines,⁵⁰ polyacetylenes,⁵¹ polypeptoids⁵²) polymers can be synthesized on solid supports with exact control over sequence and chain length, although chain lengths can be limited to less than 50 monomers for many backbones. Polypeptoids, however, show high coupling efficiencies in excess of 99% even up to 50 monomers.⁵³ While these chain lengths are at the lower limit of what defines a polymer, these macromolecules still present the opportunity to rigorously probe sequence-related questions in materials science and polymer physics.

1.2 Sequence Effects on Polymer Properties

With the drastic improvement in sequence control of synthetic polymers, the next step is to examine the sequence effect on polymer properties. Due to their synthetic ease, many property-focused studies have compared periodic and random sequences. In these studies, researchers have demonstrated that chain-to-chain sequence homogeneity has a significant effect on thermomechanical properties, such as crystallization behavior, whereas random copolymer behavior tends to be influenced by stretches of homopolymer blocks within the chains. Research on more complex structure-property relationships is just emerging.

Monomer sequence plays a strong role in the crystallization properties of copolymers because a small amount of comonomer can act as a crystalline defect. Recent work has demonstrated that polyolefin copolymers with precisely placed branches show significantly more uniform crystal sizes and more narrow transitions than their random analogues.^{38,40,54} In one study, precisely-sequenced polyethylenes with pendant chlorine groups were found to form thicker crystals and exhibit sharper melting and crystallization peaks than randomly-sequenced polyethylenes, suggesting the Cl atoms act as crystalline defects and that crystallization in random systems is dominated by the longest stretches of polyethylene within the chains.⁴⁰ Similarly, precise ethylene/1-hexene copolymers showed narrow lamella thicknesses that corresponded to the distance between branches, while random ethylene/1-hexene copolymers exhibited much larger lamella with a broader thickness distribution.³⁸ Finally, precise ethylene/acid ionomers have shown a remarkable increase in the order of ionic aggregates compared to random ionomers; the precise ionomers exhibited the first case of ionic aggregates packing on a face-centered cubic lattice, as probed by X-ray scattering.^{55,56}

Control over crystalline lamella thickness has also been demonstrated with periodic sequences of bioinspired materials. Since the 1960s, it has been well known that long chains of polypeptides can crystallize into chain-folded lamellae, similar to many synthetic polymers such as the polyolefins described above. More recently, crystalline lamellar mats have been designed using

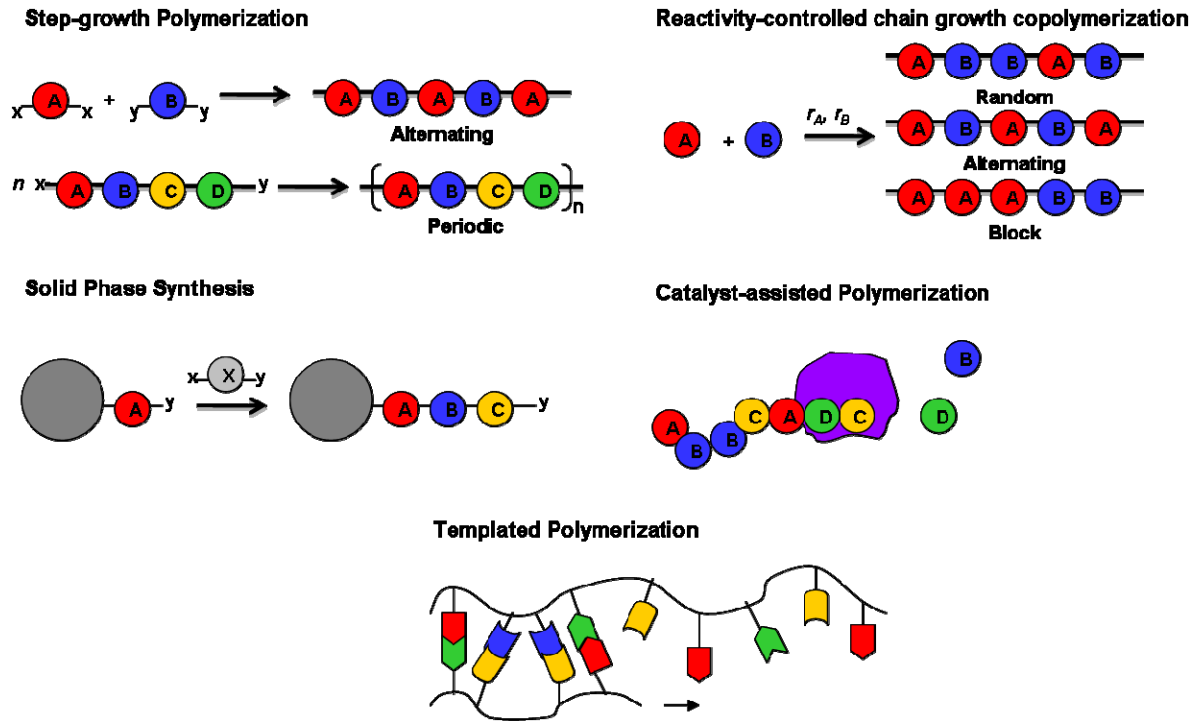


Figure 1.1. Strategies for polymer sequence control (modified from Lutz, J.F.).

monodisperse periodic polypeptides of alanine (A), glycine (G), and glutamic acid (E) in the sequence $[(AG)_x(EG)_n]$, where x varies from 3 to 6.^{57,58} The alanyl-glycyl units crystallize into antiparallel β -sheets, and the E residues induce chain folding; thus, the thickness of the lamellar crystal increases for longer AG sequences.

For amorphous polymers, sequence effects manifest in glass transition differences. Much recent work with gradient copolymers, for example, has shown that the breadth of the glass transition can be manipulated using the strength of segregation of the two comonomers.⁵⁹⁻⁶¹ In general, very strongly segregated gradient copolymers show large T_g breadths that span the width of the difference between the homopolymer T_g s, whereas moderately to weakly segregated gradient copolymers have much smaller T_g breadths that fluctuate with the strength of the gradient. More exact sequences have also been shown to affect T_g . Repeating sequence copolymers of glycolic (G), lactic (L), and caprolactic (C) acid were synthesized by polymerizing short “segmers” of known sequence. For binary copolymers containing only C and L or only G and C, it was found that the T_g could be more accurately predicted by the Fox equation for the precise copolymers compared to random copolymers of the same composition.³⁶ It was proposed that the deviation of the random copolymers was due to stretches of homopolymer blocks within the chains. When two copolymers of the same composition but different sequence were compared (e.g., GGCC vs. GC), the T_g was approximately the same. However, ternary copolymers exhibited a significant difference in T_g ; the T_g of poly(GLC) was 8°C higher than that of poly(LGC). Both of these T_g s deviated from that predicted by the Fox equation, yet the reason for this deviation remains unclear.³⁶

Precise monomer sequences also allow for tunability of polymer properties in solution. Preliminary work with synthetic copolymers has demonstrated a sequence effect on polymer cloud point transitions⁶² and the coil-to-globule transition. In another study, the rate of degradation was controlled with precise poly(lactic-co-glycolic acid) (PLGA); the precise copolymer degraded more slowly and in a more uniform fashion than random copolymers with the same L:G composition.^{63,64} It is proposed that for the random copolymer, the hydrolysis of the more accessible glycolic units occurs first and then slows as the sterically inaccessible units are left, whereas the sequenced copolymer degrades evenly. This property enables the design of controlled release profiles of small molecules, as demonstrated with Rhodamine-B.

It is anticipated that sequence effects will extend to other types of properties, such as mechanical, optical, and conductive, and these will become evident as sequence-specific polymers are needed for those applications. As the ability to synthesize more complex sequence-defined polymers increases, so will the ability to tune polymer properties with sequence.

1.3 Sequence Effects on Copolymer Conformation and Self-Assembly

Because the monomer sequence of most synthetic copolymers is a random distribution, there is no structure-directing information, and the bulk state is either fully amorphous or some mixture

of amorphous and crystalline domains. Likewise, solution phases are typically heterogeneous mixtures of Gaussian-like coils or molten globules. Block copolymers offer one exception to this behavior, as the A-B structure allows the equilibrium formation of nanostructures with long range order. The block sequence motif has provided a convenient starting point to probe the effect of sequence on self-assembly.⁶⁵ Bioconjugates,⁶⁶⁻⁷¹ especially, have utilized a structure-directing biological block, such as peptidic α -helices,⁷²⁻⁷⁵ β -sheets,⁷⁶⁻⁸¹ or even folded proteins,^{82,83} to create new hierarchically ordered materials in the bulk. However, many bioconjugate structures are solution cast and therefore kinetically-controlled. One reason for this is that the biopolymer is sensitive to heat, and thus it is necessary to avoid thermal annealing to prevent degradation. Sequence-controlled non-natural polymers offer the opportunity to design hierarchical self-assembled structures in a robust way both in solution and in the bulk.

Sequence effects on self-assembly of copolymers in solution

Although sequence control of synthetic polymers has drastically improved, it is still difficult to design an appropriate sequence to target a desired morphology. To understand the sequence-structure relationship, theorists have taken a reductionist approach and classified the 20 amino acids as either hydrophilic (H) or hydrophobic (P); simulations show that globular proteins tend to have blocky sequences of H and P monomers such that the P “blocks” form a hydrophobic core.⁸⁴ Recently, this approach has been extended to synthetic polymers to design protein-like sequences that will “fold” in solution.^{85,86} Experimental validation of this concept is difficult, however, due to the low level of sequence control for most synthetic polymers. Many blocky sequences are created by chemically modifying collapsed polymer chains in poor solvents (i.e., decorating the outside of a globule), though these methods are not precise. Despite the presence of heterogeneous sequences, there are slight differences in the coil-to-globule transition of a blocky copolymer and a random copolymer.⁸⁷ It is likely that these differences will be clarified with more precise sequence control.

Chain collapse can also be controlled with more synthetically-accessible sequences. The use of monomers with highly directional interactions, such as hydrogen bonding moieties, can dictate “folding” with simple repeating sequences⁸⁸ or precise pairwise locations in the polymer chain.⁸⁹ Intramolecular ligations, via the use of click chemistry, have also driven the collapse of polymer chains with precisely located reactive groups into various kinds of looped structures in solution.^{90,91} For these studies, the change in chain conformation was probed using a combination of size exclusion chromatography, NMR, and FT-IR.

Sequence effects on self-assembly of copolymers in the solid state

Solid state structures have largely been generated using block architectures. Although multiblock copolymers have a very low level of sequence control, the order, number, and length of the blocks affect the self-assembled morphology because self-assembly is dictated by the number of A-B contacts.¹ For instance, in a series of linear styrene-isoprene block polymers of constant

total molecular weight and composition (50:50 styrene:isoprene), increasing the number of AB blocks (decreasing block length) was found to drastically decrease the domain spacing of the lamellar morphology from 50 nm for a diblock to 19 nm for a hexablock.⁹² In addition, increasing the number of blocks results in a higher fraction of bridging in the polymer, and this bridging enables the multiblocks to sustain an applied load to much higher strain than the diblock. In a similar series of styrene-methyl methacrylate multiblocks, it was shown that a greater number of blocks leads to better compatibilization of a styrene-methyl methacrylate interface.⁹³

Similar to bioconjugates, sequence-specific non-natural polymers have been used to direct hierarchical order in block systems. The sequence-specific part of the hybrid is typically synthesized using solid-phase methods and then conjugated to a synthetic polymer block. Many sequence-specific synthetic polymers form secondary structures that lend certain material properties to the block system. For example, oligoamide-poly(ethylene glycol) block copolymers form birefringent liquid crystalline phases at elevated temperatures due to the hydrogen-bonded β -sheet-like structures of the oligoamides.⁹⁴ Similarly, hydrogen bonding interactions in N-alkyl ureas direct urea-PEG conjugates into supramolecular fibers. Tuning the sequence of these conjugates enabled hydrogen bonding and π - π interactions to be decoupled; the π - π interactions were not a requirement for fiber formation.⁹⁵

As block length decreases in a copolymer, the monomer sequence eventually resembles a “blocky-random” type motif. The self-assembly of these systems are not governed by classical block copolymer thermodynamics and may lead to structures beyond the predicted block copolymer phases. While these types of copolymers have been more studied in solution (as described above), there has also been much interest in how these blocky polymers adsorb and assemble on surfaces^{96,97} or in the bulk.^{56,98} Notably, blocky copolymers of styrene and 4-bromostyrene showed a stronger adsorption onto surfaces than random copolymers. These copolymers were synthesized by modifying collapsed globular chains in solution, and it is anticipated that precise sequences would show an even more significant difference.

1.4 Polypeptoids

Of all the sequence-defined peptidomimetics, polypeptoids (or N-substituted glycines) are particularly interesting for materials science studies due to their ease of synthesis, chemical diversity, ability to form secondary structures, and biological relevance. Originally developed as part of a drug discovery program in the late 1980s,^{99,100} polypeptoids are structurally similar to α -peptides, yet their N-substitution confers a proteolytic stability that makes them desirable for therapeutic applications.^{101,102} Because of their pharmaceutical origins, peptoid chemistry was developed in a sequence-defined way using solid-phase supports. It is therefore amenable to combinatorial library synthesis and screening methods,⁵³ rendering the molecules attractive for binding¹⁰³ and molecular recognition applications.

Polypeptoids offer ease of synthesis compared to other peptidomimetics. The solid phase synthesis of polypeptoids is a submonomer method involving the use of an activated carboxylic acid and a primary amine (Figure 1.2). Typically, the first step involves acylation of an amine (commonly that of a derivatized Rink amide resin) using *N,N*-diisopropylcarbodiimide and bromoacetic acid, and the second step involves displacement of the bromide by the primary amine. These steps are iterated, usually by an automated synthesizer, to form a linear chain of defined sequence and length. The peptoid chain is cleaved from the resin using an acid such as trifluoroacetic acid (TFA). Variations on the synthesis method have recently been summarized in an excellent review.⁵²

There are several strengths of the submonomer method. In particular, the use of primary amines to introduce the side chain moiety renders the synthesis of polypeptoids to be relatively inexpensive compared to that of α -peptides. In addition, hundreds of these primary amines are commercially available, enabling a large chemical diversity with which to explore self-assembly phase space. Most importantly, the efficiency associated with each step of the synthesis is typically in excess of 99%, meaning that chains up to 50 monomers in length can be readily constructed. While these chain lengths are significantly shorter than those achieved by conventional polymerizations, they are long with respect to most sequence-defined oligomers and sufficient for chain folding and hierarchical ordering.

1.5 Peptoid Structure Formation

Polypeptoids are an ideal system to probe self-assembly, as sequence specificity enables the encoding of structural information into the polymer chain. Here, we summarize the development of peptoid secondary structure and recent developments in peptoid self-assembly.

Peptoid Secondary Structures

The general strategy for peptoid secondary structure formation has been the control of the *cis/trans* isomerism of the backbone tertiary amide. Local interactions such as steric repulsion, hydrophobic interactions, and $n \rightarrow \pi^*$ interactions have all been exploited to yield a variety of folded peptoid structures. Much of this part of the field has been driven by the crystallization and structure analysis of short peptoid oligomers in the solid state; however, the design rules elucidated by these compounds have already begun to inform structure formation in longer peptoid polymers.¹⁰⁴ The next step to understanding these molecules as materials is to examine the impact of these secondary structures on material properties.

The peptoid helix is the most well characterized peptoid secondary structure. The first peptoid helices were designed to contain bulky, α -chiral side chains, such as *N*-(*S*)-(1-phenylethyl)glycine and *N*-(*S*)-(1-carboxyethyl)glycine, that sterically twist the peptoid backbone into a helical conformation.¹⁰⁵ Crystal structures of a pentamer containing *N*-(1-cyclohexylethyl)glycine residues showed the helix contained approximately 3 residues per turn (a pitch of ~ 6.7 Å) and an all *cis* amide bond configuration¹⁰⁶; this structure strongly resembles

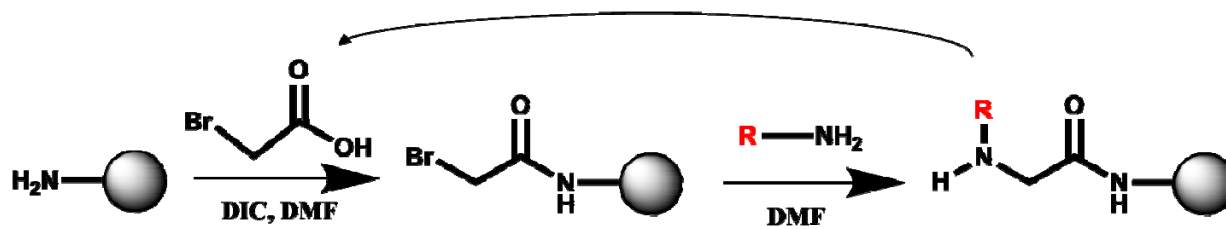


Figure 1.2. Solid Phase Synthesis of Peptoids. Stepwise synthesis enables complete monodispersity and sequence control.

the peptide polyproline-type-I helix. Furthermore, a set of rules was elucidated for peptoid helix formation^{107,108}: the incorporation of at least 50% α -chiral residues (in particular at the i and $i + 3$ positions), an α -chiral residue at the C-terminus, and chain lengths greater than 10 monomers. However, despite the well-ordered crystal, 2D NMR studies in solution indicated a large amount of conformational heterogeneity, which in turn affects peptoid properties.

One approach to stabilizing the amide bond in the *cis* configuration has been to incorporate side chains that enhance the $n \rightarrow \pi^*$ interaction between the lone pair on the carbonyl oxygen of the backbone and the π^* orbital of an adjacent aromatic side chain. Systematic studies of small peptoid model compounds revealed that phenyl side chains with electron-withdrawing or positively charged groups, such as pyridinium groups, strengthened the $n \rightarrow \pi^*$ interaction and favored *cis* amide bond formation.^{109,110} In longer peptoid chains, this interaction was enhanced in concert with increased steric bulk using a naphthyl side chain, leading to extremely stable peptoid helices with almost no *trans* amide bond configuration in solution.^{110,111} Recent studies have expanded upon this theme. The triazolium side chain led exclusively to the *cis* amide bond configuration, in part enhanced by hydrogen bonding between the backbone carbonyl oxygen and the triazolium proton.¹¹² This finding suggests that longer peptoid helices could be functionalized with a variety of side chains via azide-alkyne click chemistry without disrupting the structural integrity of the helix.

More recently, another approach to enhancing peptoid helix formation has been the incorporation of functional groups at sequence positions i and $i + 3$ that introduce specific stabilizing bonds along the helix face. Covalent bonds such as triazoles¹¹³ or lactam bridges¹¹⁴ have successfully been incorporated into the helix. In another approach, functionalized *N*-(*S*)-(1-phenylethyl)glycine residues with groups capable of hydrogen bonding or forming disulfide bonds were shown to readily incorporate into peptoid heptamers.¹¹⁵ In all of these studies, enhanced ellipticity is shown via circular dichroism studies. However, the conformational heterogeneity has not been explored with 2D NMR either in solution or solid state, and it remains to be seen whether these covalent or hydrogen bonds rigidify the peptoid backbone.

Whereas the general strategy to induce peptoid helix formation has been the stabilization of the *cis*-amide configuration, other structures can be obtained with a *trans*-amide configuration or the design of specific *cis* and *trans* bonds. For example, *N*-aryl glycines strongly prefer the *trans*-amide bond configuration and can form helices reminiscent of polyproline type-II structures.¹¹⁶ In achiral peptoids, the strategic placement of a *trans*-inducer such as the *N*-aryl glycine¹¹⁷ or a *cis*-inducer such as the triazole¹¹⁸ has led to the formation of turn structures. Turn structures have also been observed in achiral peptoid macrocycles via the *cis*-amide bond configuration.¹¹⁹

Hydrogen bonding interactions have also been used to stabilize other secondary structures in polypeptoids. For example, peptoid trimers containing *N*-hydroxy amides capable of hydrogen bonding with the backbone carbonyls were shown to crystallize into sheet-like structures reminiscent of β -sheets.¹²⁰ In peptoid nonamers of *N*-(*S*)-(1-phenylethyl)glycine, hydrogen bonds

were found to stabilize a threaded loop conformation in organic solvents; in this case, the backbone carbonyls could hydrogen bond with the nitrogens at both the N-terminus and the C-terminus.¹²¹

Peptoid Self-Assembly in Solution

Polypeptoids have demonstrated a number of examples of sequence-controlled hierarchical structures in solution that can inform structure formation in the solid state. In particular, this self-assembly has largely relied on hydrophobic interactions. Although sequence control is not a synthetic issue, one still needs to select the appropriate sequence to dictate chain folding. Several approaches to answer this question have been taken: combinatorial library screening, theoretical prediction, and biological inspiration.

The first example of polypeptoid single chain folding relied on the hydrophobic associations of helices into a helical bundle. A combinatorial library of peptoid sequences 15 monomers in length was synthesized, and the sequences were screened for 1,8-ANS binding, which is a dye that exhibits strong fluorescence when bound in a hydrophobic environment.¹²² From this selection process, it was found that the sequence of hydrophobic residues was extremely important to 1,8-ANS binding and that polypeptoid helices presented the best conformation for binding. Furthermore, these helices were shown to aggregate in solution due to hydrophobic interactions. Thus, it was hypothesized that covalently linking the helices together into longer peptoid chains (via disulfide and oxime linkages) would stabilize the cooperative folding process. FRET quenching studies during equilibrium denaturant titrations led to the identification of several polypeptoids that showed cooperative transitions from tertiary interactions.¹²³ While these structures are not unique, they are first steps toward dictating a non-natural chain into a nanostructure using monomer sequence.

Theoretical prediction via the HP model¹²⁴ has also dictated polypeptoid chain collapse. Polypeptoids have provided clear experimental validation of the HP model using a theoretically-provided blocky sequence of hydrophobic (“H”) N-methylglycine monomers and hydrophilic (“P”) N-(2-carboxyethyl)glycine monomers.¹²⁵ For this study, two sequence-specific 50-mer polypeptoids were synthesized and conjugated via click chemistry, achieving a 100-mer with an unambiguous blocky sequence. As a control, a polypeptoid with the same amount of H and P monomers was used, but the sequence was simply repeating instead of blocky. Using acetonitrile titrations, it was shown that the blocky HP sequence formed a tighter globule in aqueous solution that was more stable to acetonitrile than the control sequence; the blocky sequence “unfolded” at approximately 10 M acetonitrile, whereas the control sequence unfolded at approximately 7 M acetonitrile.

Finally, biology has provided inspiration for peptoid hydrophobic sequence patterning. In an alternating sequence reminiscent of peptide β -sheets, peptoid chains were designed to have alternating hydrophobic N-(2-phenylethyl)glycines and oppositely charged ionic groups on

complementary strands, leading to the observation of well-defined, two-dimensional nanosheet structures.¹²⁶ Furthermore, X-Ray diffraction studies showed that this nanosheet is actually a bilayer that is 2.7 nm thick with a highly ordered aromatic core. More recent studies led to an optimized sequence design in which both the anionic and cationic residues are incorporated into a single strand using a block architecture, where each block is still an alternating sequence of hydrophobic and hydrophilic residues.¹²⁷ The chain retains the ability to self-assemble with other chains into nanosheets.

Other block sequence motifs have also yielded hierarchically ordered peptoid nanostructures. A partially charged amphiphilic peptoid 30-mer, (N-(2-phenylethyl)glycine)₁₅-b-(N-(2-carboxyethyl)glycine)₁₅, self-assembles into giant, homochiral superhelices in solution.¹²⁸ This diblock copolymer first forms lamellar stacks in solution that then twist into a supramolecular, homochiral helix (the origin of the chirality is currently unknown). In non-sequence-specific, cyclic systems, amphiphilic diblocks form cylindrical micelles in methanol solution.¹²⁹ In the solid state, block architectures provide the maximum driving force for microphase separation while retaining sequence definition.

1.6 Tuning Bulk Self-Assembly with Polymer Sequence

Prior work on sequence-controlled polymers in the bulk state has demonstrated that these polymers exhibit significantly different properties compared to random copolymers and therefore have the potential to influence self-assembly in a tunable way. To date, sequence-defined self-assembling systems in the bulk state have largely consisted of bioconjugates or biological block copolymer systems. The biological block has the ability to direct self-assembly into numerous hierarchical structures; however, many of these structures are lyotropic and non-equilibrium due to strong intermolecular interactions and temperature instability of the biological block. In contrast, polypeptoids lack intermolecular hydrogen bonding interactions and offer a route to tractable sequence-defined systems.

This thesis describes the development of polypeptoid-based block copolymers for the study of sequence effects on self-assembly. First, peptoid thermal properties such as melting transitions and degradation temperatures are characterized in Chapter 2. In addition, the effect of various side chain substituents on peptoid chain conformation is examined in Chapter 3. Together, these peptoid homopolymer characteristics are used to control peptoid-based block copolymer properties such as order-disorder transition (Chapter 4) and domain spacing (Chapter 5). Finally, the impact of this work and the outlook for polypeptoid materials is discussed in Chapter 6.

1.7 References

- (1) Bates, F. S.; Hillmyer, M. A.; Lodge, T. P.; Bates, C. M.; Delaney, K. T.; Fredrickson, G. H. *Science* **2012**, *336*, 434-440.
- (2) Bates, F. S.; Fredrickson, G. H. *Physics Today* **1999**, *52*, 32-38.
- (3) Horne, W. S.; Gellman, S. H. *Accounts of Chemical Research* **2008**, *41*, 1399-1408.
- (4) Martinek, T. A.; Fulop, F. *Chem. Soc. Rev.* **2012**, *41*, 687-702.

- (5) Zhang, D.-W.; Zhao, X.; Hou, J.-L.; Li, Z.-T. *Chemical Reviews* **2012**, *112*, 5271-5316.
- (6) Deming, T. J. *Adv. Mater.* **1997**, *9*, 299-&.
- (7) Link, A. J.; Mock, M. L.; Tirrell, D. A. *Curr. Opin. Biotechnol.* **2003**, *14*, 603-609.
- (8) Murakami, H.; Ohta, A.; Ashigai, H.; Suga, H. *Nat. Methods* **2006**, *3*, 357-359.
- (9) Ohta, A.; Murakami, H.; Higashimura, E.; Suga, H. *Chemistry & Biology* **2007**, *14*, 1315-1322.
- (10) Ohta, A.; Murakami, H.; Suga, H. *Chembiochem* **2008**, *9*, 2773-2778.
- (11) Subtelny, A. O.; Hartman, M. C. T.; Szostak, J. W. *Journal of the American Chemical Society* **2008**, *130*, 6131-6136.
- (12) Kawakami, T.; Murakami, H.; Suga, H. *Journal of the American Chemical Society* **2008**, *130*, 16861-+.
- (13) Hirao, I. *Current Opinion in Chemical Biology* **2006**, *10*, 622-627.
- (14) Brudno, Y.; Liu, D. R. *Chemistry & Biology* **2009**, *16*, 265-276.
- (15) McHale, R.; Oâ€™Reilly, R. K. *Macromolecules* **2012**, *45*, 7665-7675.
- (16) Brudno, Y.; Birnbaum, M. E.; Kleiner, R. E.; Liu, D. R. *Nature Chemical Biology* **2010**, *6*, 148-155.
- (17) Chaput, J. C.; Szostak, J. W. *Journal of the American Chemical Society* **2003**, *125*, 9274-9275.
- (18) Połowiński, S. *Prog. Polym. Sci.* **2002**, *27*, 537-577.
- (19) Milnes, P. J.; McKee, M. L.; Bath, J.; Song, L.; Stulz, E.; Turberfield, A. J.; O'Reilly, R. K. *Chemical Communications* **2012**, *48*, 5614-5616.
- (20) Datta, B.; Schuster, G. B. *Journal of the American Chemical Society* **2008**, *130*, 2965-2973.
- (21) Hibi, Y.; Tokuoka, S.; Terashima, T.; Ouchi, M.; Sawamoto, M. *Polym. Chem.* **2011**, *2*, 341-347.
- (22) Hibi, Y.; Ouchi, M.; Sawamoto, M. *Angewandte Chemie International Edition* **2011**, *50*, 7434-7437.
- (23) Mayo, F. R.; Lewis, F. M. *Journal of the American Chemical Society* **1944**, *66*, 1594-1601.
- (24) Lutz, J. F.; Pakula, T.; Matyjaszewski, K. In *Advances in Controlled/Living Radical Polymerization*; Matyjaszewski, K., Ed.; Amer Chemical Soc: Washington, 2003; Vol. 854, p 268-282.
- (25) Minoda, M.; Sawamoto, M.; Higashimura, T. *Macromolecules* **1990**, *23*, 4889-4895.
- (26) Pfeifer, S.; Lutz, J.-F. o. *Journal of the American Chemical Society* **2007**, *129*, 9542-9543.
- (27) Zamfir, M. L., J.-F. *Nature Communications* **2012**, *3*, 1138.
- (28) Brulé, E.; Guo, J.; Coates, G. W.; Thomas, C. M. *Macromolecular Rapid Communications* **2011**, *32*, 169-185.
- (29) Ouchi, M.; Terashima, T.; Sawamoto, M. *Accounts of Chemical Research* **2008**, *41*, 1120-1132.
- (30) Ouchi, M.; Terashima, T.; Sawamoto, M. *Chemical Reviews* **2009**, *109*, 4963-5050.
- (31) Kramer, J. W.; Treitler, D. S.; Dunn, E. W.; Castro, P. M.; Roisnel, T.; Thomas, C. M.; Coates, G. W. *Journal of the American Chemical Society* **2009**, *131*, 16042-+.
- (32) Ida, S.; Terashima, T.; Ouchi, M.; Sawamoto, M. *Journal of the American Chemical Society* **2009**, *131*, 10808-10809.
- (33) Ida, S.; Ouchi, M.; Sawamoto, M. *Journal of the American Chemical Society* **2010**, *132*, 14748-14750.
- (34) Berthet, M.-A.; Zarafshani, Z.; Pfeifer, S.; Lutz, J.-F. o. *Macromolecules* **2009**, *43*, 44-50.
- (35) Wong, E. H. H.; Stenzel, M. H.; Junkers, T.; Barner-Kowollik, C. *Journal of Polymer Science Part A: Polymer Chemistry* **2011**, *49*, 2118-2126.
- (36) Weiss, R. M.; Jones, E. M.; Shafer, D. E.; Stayshich, R. M.; Meyer, T. Y. *Journal of Polymer Science Part A: Polymer Chemistry* **2011**, *49*, 1847-1855.

- (37) Stayshich, R. M.; Meyer, T. Y. *Journal of the American Chemical Society* **2010**, *132*, 10920-10934.
- (38) Rojast, G.; Wagener, K. B. *Macromolecules* **2009**, *42*, 1934-1947.
- (39) Rojas, G.; Berda, E. B.; Wagener, K. B. *Polymer* **2008**, *49*, 2985-2995.
- (40) Boz, E.; Wagener, K. B.; Ghosal, A.; Fu, R. Q.; Alamo, R. G. *Macromolecules* **2006**, *39*, 4437-4447.
- (41) Boz, E.; Nemeth, A. J.; Wagener, K. B.; Jeon, K.; Smith, R.; Nazirov, F.; Bockstaller, M. R.; Alamo, R. G. *Macromolecules* **2008**, *41*, 1647-1653.
- (42) Opper, K. L.; Markova, D.; Klapper, M.; Muñ'llen, K.; Wagener, K. B. *Macromolecules* **2010**, *43*, 3690-3698.
- (43) Baughman, T. W.; Chan, C. D.; Winey, K. I.; Wagener, K. B. *Macromolecules* **2007**, *40*, 6564-6571.
- (44) Merrifield, R. *Advances in Enzymology and Related Areas of Molecular Biology* **1969**, *32*, 221-&.
- (45) Albericio, F. *Current Opinion in Chemical Biology* **2004**, *8*, 211-221.
- (46) Plante, O. J.; Palmacci, E. R.; Seeberger, P. H. *Science* **2001**, *291*, 1523-1527.
- (47) Franz, N.; Kreutzer, G.; Klok, H. A. *Synlett* **2006**, 1793-1815.
- (48) Briehn, C. A.; Bauerle, P. *Chemical Communications* **2002**, 1015-1023.
- (49) Wendeborn, S.; De Mesmaeker, A.; Brill, W. K. D.; Berteina, S. *Accounts of Chemical Research* **2000**, *33*, 215-224.
- (50) Hartmann, L.; Krause, E.; Antonietti, M.; BÄ¶rner, H. G. *Biomacromolecules* **2006**, *7*, 1239-1244.
- (51) Young, J. K.; Nelson, J. C.; Moore, J. S. *Journal of the American Chemical Society* **1994**, *116*, 10841-10842.
- (52) Culf, A. S.; Ouellette, R. J. *Molecules* **2010**, *15*, 5282-5335.
- (53) Figliozzi, G. M.; Goldsmith, R.; Ng, S. C.; Banville, S. C.; Zuckermann, R. N. *Combinatorial Chemistry* **1996**, *267*, 437-447.
- (54) Berda, E. B.; Baughman, T. W.; Wagener, K. B. *Journal of Polymer Science Part A: Polymer Chemistry* **2006**, *44*, 4981-4989.
- (55) Buitrago, C. F.; Opper, K. L.; Wagener, K. B.; Winey, K. I. *ACS Macro Lett.* **2012**, *1*, 71-74.
- (56) Seitz, M. E.; Chan, C. D.; Opper, K. L.; Baughman, T. W.; Wagener, K. B.; Winey, K. I. *Journal of the American Chemical Society* **2010**, *132*, 8165-8174.
- (57) Krejchi, M. T.; Atkins, E. D. T.; Waddon, A. J.; Fournier, M. J.; Mason, T. L.; Tirrell, D. A. *Science* **1994**, *265*, 1427-1432.
- (58) Krejchi, M. T.; Cooper, S. J.; Deguchi, Y.; Atkins, E. D. T.; Fournier, M. J.; Mason, T. L.; Tirrell, D. A. *Macromolecules* **1997**, *30*, 5012-5024.
- (59) Mok, M. M.; Kim, J.; Wong, C. L. H.; Marrou, S. R.; Woo, D. J.; Dettmer, C. M.; Nguyen, S. T.; Ellison, C. J.; Shull, K. R.; Torkelson, J. M. *Macromolecules* **2009**, *42*, 7863-7876.
- (60) Jakubowski, W.; Juhari, A.; Best, A.; Koynov, K.; Pakula, T.; Matyjaszewski, K. *Polymer* **2008**, *49*, 1567-1578.
- (61) Kim, J.; Mok, M. M.; Sandoval, R. W.; Woo, D. J.; Torkelson, J. M. *Macromolecules* **2006**, *39*, 6152-6160.
- (62) Gallow, K. C.; Jhon, Y. K.; Tang, W.; Genzer, J.; Loo, Y. L. *J. Polym. Sci. Pt. B-Polym. Phys.* **2011**, *49*, 629-637.
- (63) Li, J.; Rothstein, S. N.; Little, S. R.; Edenborn, H. M.; Meyer, T. Y. *Journal of the American Chemical Society* **2012**, *134*, 16352-16359.
- (64) Li, J.; Stayshich, R. M.; Meyer, T. Y. *Journal of the American Chemical Society* **2011**, *133*, 6910-6913.
- (65) Ganesan, V.; Kumar, N. A.; Pryamitsyn, V. *Macromolecules* **2012**, *45*, 6281-6297.
- (66) Klok, H. A. *Macromolecules* **2009**, *42*, 7990-8000.

- (67) Borner, H. G. *Prog. Polym. Sci.* **2009**, *34*, 811-851.
- (68) Borner, H. G.; Schlaad, H. *Soft Matter* **2007**, *3*, 394-408.
- (69) Rabotyagova, O. S.; Cebe, P.; Kaplan, D. L. *Biomacromolecules* **2011**, *12*, 269-289.
- (70) Schnitzler, T.; Herrmann, A. *Accounts of Chemical Research* **2012**, *45*, 1419-1430.
- (71) Lutz, J. F.; Borner, H. G. *Prog. Polym. Sci.* **2008**, *33*, 1-39.
- (72) Perly, B.; Douy, A.; Gallot, B. *Makromolekulare Chemie-Macromolecular Chemistry and Physics* **1976**, *177*, 2569-2589.
- (73) Klok, H. A.; Lecommandoux, S. In *Peptide Hybrid Polymers*; Klok, H. A., Schlaad, H., Eds.; Springer-Verlag Berlin: Berlin, 2006; Vol. 202, p 75-111.
- (74) Douy, A.; Gallot, B. *Polymer* **1982**, *23*, 1039-1044.
- (75) Klok, H. A.; Langenwalter, J. F.; Lecommandoux, S. *Macromolecules* **2000**, *33*, 7819-7826.
- (76) Jatsch, A.; Schillinger, E. K.; Schmid, S.; Bauerle, P. *Journal of Materials Chemistry* **2010**, *20*, 3563-3578.
- (77) Shaytan, A. K.; Schillinger, E. K.; Khalatur, P. G.; Mena-Osteritz, E.; Hentschel, J.; Borner, H. G.; Bauerle, P.; Khokhlov, A. R. *ACS Nano* **2011**, *5*, 6894-6909.
- (78) Klok, H.-A.; Rosler, A.; Gotz, G.; Mena-Osteritz, E.; Bauerle, P. *Org. Biomol. Chem.* **2004**, *2*, 3541-3544.
- (79) Schillinger, E. K.; Mena-Osteritz, E.; Hentschel, J.; Borner, H. G.; Bauerle, P. *Adv. Mater.* **2009**, *21*, 1562-+.
- (80) Diegelmann, S. R.; Gorham, J. M.; Tovar, J. D. *Journal of the American Chemical Society* **2008**, *130*, 13840-13841.
- (81) Frauenrath, H.; Jahnke, E. *Chemistry – A European Journal* **2008**, *14*, 2942-2955.
- (82) Thomas, C. S.; Glassman, M. J.; Olsen, B. D. *ACS Nano* **2011**, *5*, 5697-5707.
- (83) Thomas, C. S.; Xu, L. Z.; Olsen, B. D. *Biomacromolecules* **2012**, *13*, 2781-2792.
- (84) Dill, K. A.; Bromberg, S.; Yue, K. Z.; Fiebig, K. M.; Yee, D. P.; Thomas, P. D.; Chan, H. S. *Protein Sci.* **1995**, *4*, 561-602.
- (85) Khokhlov, A. R.; Khalatur, P. G. *Phys. Rev. Lett.* **1999**, *82*, 3456-3459.
- (86) Ashbaugh, H. S. *The Journal of Physical Chemistry B* **2009**, *113*, 14043-14046.
- (87) Siu; Zhang, G.; Wu, C. *Macromolecules* **2002**, *35*, 2723-2727.
- (88) Englebienne, P.; Hilbers, P. A. J.; Meijer, E. W.; De Greef, T. F. A.; Markvoort, A. J. *Soft Matter* **2012**, *8*, 7610-7616.
- (89) Altintas, O.; Lejeune, E.; Gerstel, P.; Barner-Kowollik, C. *Polym. Chem.* **2012**, *3*, 640-651.
- (90) Schmidt, B.; Fechler, N.; Falkenhagen, J.; Lutz, J. F. *Nat. Chem.* **2011**, *3*, 234-238.
- (91) Sugai, N.; Heguri, H.; Yamamoto, T.; Tezuka, Y. *Journal of the American Chemical Society* **2011**, *133*, 19694-19697.
- (92) Spontak, R. J.; Smith, S. D. *Journal of Polymer Science Part B: Polymer Physics* **2001**, *39*, 947-955.
- (93) Eastwood, E. A.; Dadmun, M. D. *Macromolecules* **2002**, *35*, 5069-5077.
- (94) Bohle, A.; Brunklaus, G.; Hansen, M. R.; Schleuss, T. W.; Kilbinger, A. F. M.; Seltmann, J.; Spiess, H. W. *Macromolecules* **2010**, *43*, 4978-4985.
- (95) Chen, X.; Ding, K.; Ayres, N. *Polym. Chem.* **2011**, *2*, 2635-2642.
- (96) Jayaraman, A.; Hall, C. K.; Genzer, J. *Phys. Rev. Lett.* **2005**, *94*, 4.
- (97) Jhon, Y. K.; Semler, J. J.; Genzer, J.; Beevers, M.; Gus'kova, O. A.; Khalatur, P. G.; Khokhlov, A. R. *Macromolecules* **2009**, *42*, 2843-2853.
- (98) Jang, S. S.; Molinero, V.; Cagin, T.; Goddard, W. A. *J. Phys. Chem. B* **2004**, *108*, 3149-3157.
- (99) Zuckermann, R. N. *Peptide Science* **2011**, *96*, 545-555.
- (100) Simon, R. J.; Kania, R. S.; Zuckermann, R. N.; Huebner, V. D.; Jewell, D. A.; Banville, S.; Ng, S.; Wang, L.; Rosenberg, S.; Marlowe, C. K.; Spellmeyer, D. C.; Tan, R. Y.; Frankel, A. D.;

Santi, D. V.; Cohen, F. E.; Bartlett, P. A. *Proceedings of the National Academy of Sciences of the United States of America* **1992**, *89*, 9367-9371.

(101) Dohm, M. T.; Kapoor, R.; Barron, A. E. *Current Pharmaceutical Design* **2011**, *17*, 2732-2747.

(102) Zuckermann, R. N.; Kodadek, T. *Current Opinion in Molecular Therapeutics* **2009**, *11*, 299-307.

(103) Reddy, M. M.; Wilson, R.; Wilson, J.; Connell, S.; Gocke, A.; Hynan, L.; German, D.; Kodadek, T. *Cell* **2011**, *144*, 132-142.

(104) Guo, L.; Li, J. H.; Brown, Z.; Ghale, K.; Zhang, D. H. *Biopolymers* **2011**, *96*, 596-603.

(105) Kirshenbaum, K.; Barron, A. E.; Goldsmith, R. A.; Armand, P.; Bradley, E. K.; Truong, K. T. V.; Dill, K. A.; Cohen, F. E.; Zuckermann, R. N. *Proceedings of the National Academy of Sciences of the United States of America* **1998**, *95*, 4303-4308.

(106) Wu, C. W.; Kirshenbaum, K.; Sanborn, T. J.; Patch, J. A.; Huang, K.; Dill, K. A.; Zuckermann, R. N.; Barron, A. E. *Journal of the American Chemical Society* **2003**, *125*, 13525-13530.

(107) Wu, C. W.; Sanborn, T. J.; Zuckermann, R. N.; Barron, A. E. *Journal of the American Chemical Society* **2001**, *123*, 2958-2963.

(108) Wu, C. W.; Sanborn, T. J.; Huang, K.; Zuckermann, R. N.; Barron, A. E. *Journal of the American Chemical Society* **2001**, *123*, 6778-6784.

(109) Gorske, B. C.; Bastian, B. L.; Geske, G. D.; Blackwell, H. E. *Journal of the American Chemical Society* **2007**, *129*, 8928-8929.

(110) Gorske, B. C.; Stringer, J. R.; Bastian, B. L.; Fowler, S. A.; Blackwell, H. E. *Journal of the American Chemical Society* **2009**, *131*, 16555-16567.

(111) Stringer, J. R.; Crapster, J. A.; Guzei, I. A.; Blackwell, H. E. *Journal of the American Chemical Society* **2011**, *133*, 15559-15567.

(112) Caumes, C. c.; Roy, O.; Faure, S.; Taillefumier, C. *Journal of the American Chemical Society* **2012**, *134*, 9553-9556.

(113) Holub, J. M.; Jang, H.; Kirshenbaum, K. *Organic Letters* **2007**, *9*, 3275-3278.

(114) Vaz, B.; Brunsveld, L. *Org. Biomol. Chem.* **2008**, *6*, 2988-2994.

(115) Seo, J.; Barron, A. E.; Zuckermann, R. N. *Organic Letters* **2010**, *12*, 492-495.

(116) Shah, N. H.; Butterfoss, G. L.; Nguyen, K.; Yoo, B.; Bonneau, R.; Rabenstein, D. L.; Kirshenbaum, K. *Journal of the American Chemical Society* **2008**, *130*, 16622-16632.

(117) Stringer, J. R.; Crapster, J. A.; Guzei, I. A.; Blackwell, H. E. *Journal of Organic Chemistry* **2010**, *75*, 6068-6078.

(118) Pokorski, J. K.; Jenkins, L. M. M.; Feng, H. Q.; Durell, S. R.; Bai, Y. W.; Appella, D. H. *Organic Letters* **2007**, *9*, 2381-2383.

(119) Shin, S. B. Y.; Kirshenbaum, K. *Organic Letters* **2007**, *9*, 5003-5006.

(120) Crapster, J. A.; Stringer, J. R.; Guzei, I. A.; Blackwell, H. E. *Biopolymers* **2011**, *96*, 604-616.

(121) Huang, K.; Wu, C. W.; Sanborn, T. J.; Patch, J. A.; Kirshenbaum, K.; Zuckermann, R. N.; Barron, A. E.; Radhakrishnan, I. *Journal of the American Chemical Society* **2006**, *128*, 1733-1738.

(122) Burkoth, T. S.; Beausoleil, E.; Kaur, S.; Tang, D.; Cohen, F. E.; Zuckermann, R. N. *Chemistry & Biology* **2002**, *9*, 647-654.

(123) Lee, B. C.; Zuckermann, R. N.; Dill, K. A. *Journal of the American Chemical Society* **2005**, *127*, 10999-11009.

(124) Sun, S.; Brem, R.; Chan, H. S.; Dill, K. A. *Protein Engineering* **1995**, *8*, 1205-1213.

(125) Murnen, H. K.; Khokhlov, A. R.; Khalatur, P. G.; Segalman, R. A.; Zuckermann, R. N. *Macromolecules* **2012**, *45*, 5229-5236.

(126) Nam, K. T.; Shelby, S. A.; Choi, P. H.; Marciel, A. B.; Chen, R.; Tan, L.; Chu, T. K.; Mesch, R. A.; Lee, B. C.; Connolly, M. D.; Kisielowski, C.; Zuckermann, R. N. *Nature Materials* **2010**, *9*, 454-460.

- (127) Kudirka, R.; Tran, H.; Sanii, B.; Nam, K. T.; Choi, P. H.; Venkateswaran, N.; Chen, R.; Whitelam, S.; Zuckermann, R. N. *Biopolymers* **2011**, *96*, 586-595.
- (128) Murnen, H. K.; Rosales, A. M.; Jaworsk, J. N.; Segalman, R. A.; Zuckermann, R. N. *Journal of the American Chemical Society* **2010**, *132*, 16112-16119.
- (129) Lee, C.-U.; Smart, T. P.; Guo, L.; Epps, T. H.; Zhang, D. *Macromolecules* **2011**, *44*, 9574-9585.

Chapter 2. Control of Crystallization and Melting Behavior in Sequence Specific Polypeptoids

Reproduced with permission from Adrienne M. Rosales, Hannah K. Murnen, Ronald N. Zuckermann, and Rachel A. Segalman, *Macromolecules*, 2010, 43(13), pp. 5627-5636. Copyright (2010), American Chemical Society.

The sequence specificity of a class of biologically inspired polymers based on N-substituted glycines (polypeptoids) allows for a degree of tunability in the crystallization and thermal behavior not available in classical polymer systems. It is demonstrated that a series of peptoid homopolymers are stable up to temperatures of 250-300°C and are crystalline with reversible melting transitions ranging from 150°C to 225°C. Defects inserted at precise locations along the polymer backbone (as monomer substitutions) enable control of the melting temperature. Melting points decrease with increased defect content, and X-ray diffraction (XRD) indicates defect inclusion in the crystal lattice. In addition, it is demonstrated that the distribution of the defects for a given content level affects the thermal properties of the peptoid chain.

2.1. Introduction

The ability to control the thermal processability and physical properties of polymers depends to a large extent on controlling their crystallization. While many processing variables can affect the rate of crystallization or percent crystallinity of a given polymer, inherent properties such as the melting temperature depend on the chemical nature of the polymer. One of the easiest routes to altering these properties is through copolymerization, either with a chemically dissimilar monomer or a structural isomer. The chemical or steric interaction of the specific monomer substitution or co-monomer with the main chain can strongly influence the crystallinity and melting behavior.¹ A large and fascinating body of work with copolymers, polyethylenes in particular, has provided much insight on how the type, content, and distribution of the co-unit affect melting.²⁻⁷ Although there is much theoretical interest in the effects of sequence distribution on copolymer melting^{8, 9}, experimental control of such systems has been difficult synthetically. Experimentally, the concept of introducing defects at precise locations in a polymer sequence and the subsequent effect on crystallinity is relatively unexplored.

In general, the introduction of a co-monomer into a crystalline homopolymer chain presents two possible cases: the co-unit either enters the crystal lattice of the polymer chain or it is excluded from it. Flory developed the equilibrium theory of crystallization for the case in which the co-monomer is excluded from the crystalline phase and essentially acts as a defect in the polymer chain, thereby depressing the melting point.^{10, 11} For this case, the melting temperature T_m of the copolymer can be given by

$$\frac{1}{T_m} = \frac{1}{T_m^0} - \frac{R \ln p}{\Delta H} \quad 2.1$$

where T_m^0 is the melting temperature of the pure homopolymer, ΔH is the enthalpy of fusion per monomer unit, and p is the probability that a crystallizable monomer is followed by another such unit. The most well studied case is that of purely random copolymers, in which p is equal to the mole fraction of crystallizable units (X). In agreement with the behavior predicted by Flory, several empirical studies have found a correlation between increasing co-monomer content (decreasing X) and decreasing levels of crystallinity.¹²⁻¹⁶ Much interest has also been focused on the role that the heterogeneity of the co-monomer content distribution plays in the thermal properties of a copolymer.^{3, 17-19} Various stepwise DSC methods have been used to separate sequences of different co-monomer content levels. Such DSC methods generally involve multiple annealing stages at decreasing temperature intervals to selectively crystallize copolymers of various compositions, which can then be detected upon the next heating run.²⁰ Despite the progress in narrowing co-monomer distributions, there is still a lack of control in which these sequences can be specified in an exact, monodisperse fashion.

Recently, a level of sequence control has been achieved in which co-monomer units are placed on every n th carbon along a polyethylene chain using acyclic diene metathesis (ADMET) polymerization.²¹ These precision copolymers have provided insight on how the distribution of short alkyl branches along the chain affects melting behavior; namely, it was found that systems with precise co-monomer placement tolerate a higher amount of defects compared to random systems before crystallinity is disrupted.^{22, 23} Bockstaller, et al, performed similar experiments with halogenated co-monomers and found that while both random and regularly placed co-monomers depress the melting temperature, the resulting crystalline lamellae are different in morphology.^{7, 24} While these precision copolymers are a significant effort in understanding the interplay between polymer sequence and physical properties, greater control over defect placement and defect chemistry is clearly needed to gain further insight and to finely tune polymer properties.

In contrast to the systems studied above, biologically derived and biologically inspired polymers can be sequence-specific. Polypeptides of defined sequence can be synthesized by solid-phase synthesis methods and hold the potential to create systems in which polymer primary structure can be manipulated to control polymer thermal properties. However, polypeptide thermal processability is poor due to the dominant effect of intra- and intermolecular hydrogen bonding on melting behavior. Alternatively, a variety of peptidomimetic oligomer systems allow access to a wide range of sequence-specific materials²⁵. Of these, polypeptoids offer an ideal platform to explore thermal behavior due to their ease of synthesis and unique structure. Polypeptoids are based on an N-substituted glycine backbone (as shown in Figure 2.1)²⁶ and have simplified intermolecular interactions as compared to polypeptides and other peptidomimetic oligomers. Whereas peptide chains are dominated by hydrogen bonding

interactions, the N-substitution in peptoid polymers precludes the presence of hydrogen bond donors along the backbone. While most sequence-specific polymers require complex and low yielding synthetic routes, peptoids utilize a rapid, solid-phase submonomer synthetic method^{26, 27} that results in monodisperse chains up to 50 monomers in length in high yield and relatively large batch sizes from hundreds of different readily available monomers. Polypeptoids therefore possess both the chemical diversity and the synthetic efficiency necessary for investigating the interplay of monomer sequence and thermal properties.

In this work, polypeptoids are shown to be thermally stable to very high temperatures and to have crystallinity which is easily controlled through the placement of sequence specific defects. We have synthesized a variety of polypeptoids of exactly 15 monomers in length to characterize their thermal properties and stability (Figure 2.1, Tables 2.1 and 2.2). Although 15 monomers is short compared to other polymers, this length allows for exquisite control over molecular sequence and more importantly, enables the investigation of changes in crystalline structure with very subtle monomer changes. Many of these molecules exhibit crystalline structures with accessible melting transitions. To illustrate the tunability of these transitions, we have inserted defects into the peptoid homopolymers via a side chain substitution at specific locations with the result that crystallization and hence the melting temperature is either decreased or suppressed completely. The type, content, and distribution of the defects have all been varied with exact control and monodispersity. This sequence specificity leads to increased understanding of the effects of these defects on the thermal behavior.

2.2 Experimental Methods

Synthesis Polypeptoids were synthesized on a custom robotic synthesizer or a commercial Aapptec Apex 396 robotic synthesizer on 100 mg of Rink amide polystyrene resin (0.6 mmol/g, Novabiochem, San Diego). All primary amine monomers, solvents, and reagents described here were purchased from commercial sources and used without further purification. The synthesis procedure was a modified version of methods previously described²⁷. The Fmoc group on the resin was deprotected by adding 2 mL of 20% (v/v) piperidine /N,N-dimethylformamide (DMF), agitating for 20 minutes, draining, and washing with DMF. All DMF washes consisted of the addition of 1 mL of DMF, followed by agitation for 1 minute (repeated 5 times). An acylation reaction was then performed on the amino resin by the addition of 1.0 mL of 1.2 M bromoacetic acid in DMF, followed by 0.18 mL of N,N-diisopropylcarbodiimide (DIC, 1.15 mmol, neat). The mixture was agitated for 20 minutes at room temperature, drained, and washed with DMF. Nucleophilic displacement of the bromide with various primary amines (Table 2.1) occurred by a 1.0 mL addition of the primary amine monomer as a 1.0 – 1.5 M solution in N-methyl-2-pyrrolidone (NMP), followed by agitation for 60 minutes at room temperature. The monomer solution was drained from the resin, and the resin was washed with DMF as described above. The acylation and displacement steps were repeated until a polypeptoid of the desired length was synthesized. All reactions were performed at room temperature.

All polypeptoids were acetylated on the resin after synthesis using a mixture (4.0 mL per 100 mg of resin) of 0.4 M acetic anhydride and 0.4 M pyridine in DMF for 30 minutes, followed by washing with DMF. Peptoid chains were cleaved from the resin by addition of 4.0 mL of a trifluoroacetic acid (TFA) cleavage cocktail for 20 minutes, which was then evaporated off under a stream of nitrogen gas. The composition of the TFA cleavage cocktail was 10% TFA in dichloromethane for pNbu15, pNhx15, and pNia15. All other peptoids were cleaved with 95% TFA in water. Following cleavage, peptoids were dissolved in 4.0 mL of either glacial acetic acid or appropriate acetonitrile/water mixtures and lyophilized twice to obtain a fluffy white powder.

Each polypeptoid was characterized by analytical reverse-phase HPLC using a C4 column (Vydac 214TP, 5 μ m, 4.6 x 150 mm) on a Varian ProStar system (Palo Alto, CA). The column was maintained at 60°C while a 30 minute linear gradient of 5-95% solvent B in solvent A was used (solvent A = 0.1% TFA in water, solvent B = 0.1% TFA in acetonitrile). Electrospray mass spectrometry was performed on an Agilent 1100 series LC/MSD Trap system (Agilent Technologies, Santa Clara, CA). All peptoids were purified by reverse-phase prep HPLC on a Varian ProStar system equipped with a Varian Model 345 UV-Vis Dual Wavelength detector (214 and 260 nm) and a C4 column (Vydac HPLC Protein C4 column, 10-15 μ m, 22 x 250 mm). pNpe15 required a linear gradient of 50-100% solvent B in solvent A over 40 minutes at a flow rate of 10 ml/min (solvent A = 0.1% TFA in water, solvent B = 0.1% TFA in 50:50 isopropanol:acetonitrile). All other peptoids used the same gradient but the same solvent system as that described for the analytical HPLC. pNoc15 was precipitated from acetonitrile and water.

Thermogravimetric Analysis Samples were characterized using a TGA Q50 (TA Instruments, New Castle, DE) to investigate degradation temperatures by mass loss. Approximately 5.0 mg of lyophilized peptoid powder were placed on a 100 μ L platinum sample pan. Samples were equilibrated at 30°C for 20 minutes and then heated to 500°C at 5°C/min under a nitrogen atmosphere.

Differential Scanning Calorimetry Differential Scanning Calorimetry (DSC) was carried out using a 2920 Modulated DSC equipped with a DSC Refrigerated Cooling System (both TA Instruments, New Castle, DE). 4-10 mg of lyophilized peptoid powder were hermetically sealed into aluminum pans. Each sample was taken through three temperature cycles at heating and cooling rates of 5°C/min. The first cycle from each sample was discarded in order to erase the thermal history.

Polarized Optical Microscopy Approximately 1-2 mg of lyophilized peptoid powder samples were placed between two glass slides secured to an Instec HCS302 heating stage (Boulder, CO) controlled by an Instec STC 200 temperature controller. The heating stage was further equipped with recirculating cooling water from a Neslab Coolflow CFT-25 (Thermo Scientific, Waltham, MA), and argon was continuously flowed over the sample to prevent burning. The sample apparatus was placed in an Olympus BX51 microscope, and data was

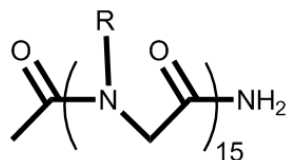


Figure 2.1. Model Acetylated Peptoid 15-mer. R denotes side chain.

Table 2.1. N-substituted glycine side chains.

Side Chain (R=)	Designator
	Nbu = N-(butyl)glycine
	Nhx = N-(hexyl)glycine
	Noc = N-(octyl)glycine
	Nia = N-(isoamyl)glycine
	Npe = N-(1-phenylethyl)glycine
	Nme = N-(2-methoxyethyl)glycine
	Npp = N-(3-phenyl-1-propyl)glycine

Table 2.2. Analytical data for a series of peptoid 15-mers.

Polypeptoid	Monomer sequence	X _n	Molar Mass (Calc/Obs)	Purity (%)*
pNbu15	Ac-(Nbu) ₁₅	15	1755.3/1755.8	78
pNhx15	Ac-(Nhx) ₁₅	15	2177.2/2178.4	94
pNoc15	Ac-(Noc) ₁₅	15	2598.0/2597.1	ND
pNia15	Ac-(Nia) ₁₅	15	1965.5	ND
pNpe15	Ac-(Npe) ₁₅	15	2477.1/2477.6	ND
pNme15	Ac-(Nme) ₁₅	15	1785.0/1788.6	78
pNpe-co-Npp2	Ac-(Npe) ₅ Npp(Npe) ₃ Npp(Npe) ₃	15	2505.1/2505.0	96
pNpe-co-Npp4	Ac-(Npe) ₂ Npp(Npe) ₂ Npp(Npe) ₃ Npp(Npe) ₂ Npp(Npe) ₂	15	2533.2/2533.2	99
pNia-co-Nh2	Ac-(Nia) ₅ Nh(Nia) ₃ Nh(Nia) ₅	15	1994.9/1994.2	ND
pNia-co-Nh4	Ac-(Nia) ₂ Nh(Nia) ₂ Nh(Nia) ₃ Nh(Nia) ₂ Nh(Nia) ₂	15	2022.9/2022.2	99
pNia-co-Nme2a	Ac-(Nia) ₂ Nme(Nia) ₉ Nme(Nia) ₂	15	1942.7/1945.2	96
pNia-co-Nme2b	Ac-(Nia) ₃ Nme(Nia) ₇ Nme(Nia) ₃	15	1942.7/1943.4	97
pNia-co-Nme2c	Ac-(Nia) ₄ Nme(Nia) ₅ Nme(Nia) ₄	15	1942.7/1943.4	96
pNia-co-Nme2d	Ac-(Nia) ₅ Nme(Nia) ₃ Nme(Nia) ₅	15	1942.7/1942.2	93
pNia-co-Nme2e	Ac-(Nia) ₆ NmeNiaNme(Nia) ₆	15	1942.7/1943.2	99
pNia-co-Nme4	Ac-(Nia) ₂ Nme(Nia) ₂ Nme(Nia) ₃ Nme(Nia) ₂ Nme(Nia) ₂	15	1918.6/1918.0	89
pNle15	Ac-(Norleucine) ₁₅	15	1713.3/1713.5	ND

* As determined by analytical HPLC of purified product. Ac = acetyl group, ND = not determined.

collected using a 50X lens. Polarizers were placed over the lens to view the birefringence of the sample. Heating and cooling passes were executed at 5°C/min to mimic the conditions of the DSC experiments.

X-Ray Diffraction X-Ray Diffraction (XRD) was performed at beamline [8.3.1](#) at the Advanced Light Source at Lawrence Berkeley National Laboratory. Samples were thermally annealed in a vacuum oven below their melting temperatures for 1-2 hours and 1-2 mg of the sample were then loaded onto a sample ring. X-rays of 11.11 keV were focused onto the sample and a two dimensional CCD array was used to collect the scattered x-rays after transmission through the sample. The signal was then radially integrated to obtain a 1D plot of intensity versus scattering angle.

2.3 Results and Discussion

2.3.1 Thermal Stability and Processability

Peptoid homopolymers are determined to be thermally stable to temperatures approaching 300°C with thermal behavior that can be tuned by altering the monomer sequence within the chain. Furthermore, many of the monodisperse, 15-mer peptoids crystallize with experimentally accessible thermal melting transitions. Figure 2.2 shows a representative XRD trace of a crystalline peptoid, pNbu15, as well as its DSC heating curve. X-ray powder diffraction obtained from the annealed peptoid shows two reflections in the ratio 1:2 at 44.35 Å and 22.09 Å respectively. These reflections could suggest chain-folded lamellae with thicknesses that measure roughly three-fourths of the fully extended peptoid chain length, 58.1 Å, but this is difficult to imagine given the implied non-integral folding. It is more likely that the peptoid chains are crystallizing such that one axis (the *c*-axis) of the unit cell is defined by the molecular length. XRD of three peptoids of various lengths supports this idea (see Appendix, Figure 2.13). The fact that the *c* axis is shorter than the length of a fully extended peptoid chain indicates the chain conformation may not be completely *trans* zig-zag. 2D NMR of achiral peptoid hexamers in solution has shown that the three types of rotamers in which the backbone amide bonds are *cis*-dominated, *trans*-dominated, or a mixture are all equally likely.²⁸ If crystallization in the solid state does lead the chain to prefer a *trans* zig-zag conformation, then the molecular axis would have to be tilted about 40° relative to the normal to the *c*-axis in the crystal to give dimensions consistent with the XRD.

Four additional wide angle reflections are seen at *q* ratios of 1:2:3:4 at 13.4 Å, 6.7 Å, 4.5 Å, and 3.5 Å respectively. These peaks come from side chain organization (as inferred from Figure 2.13 in the Appendix), with the multiple reflections indicating that they are well-ordered. In addition, the broadening at the base of the 3*q* peak indicates overlap with another peak ~4.5 Å. Reflections at this spacing are common for every peptoid investigated, and it is thought that this corresponds to the spacing between peptoid chains.²⁹ Previously, Cui et al. indexed polypeptide single crystals to a hexagonal unit cell,³⁰ and while it is possible that the peptoid XRD peaks

represent the 100, 200, 300, and 400 *hkl* reflections from such a unit cell, more reflections are necessary to confirm the assigned indices. In addition, diffraction of hexagonal packing usually shows a strong (110) reflection, which is not consistent with the data shown here.

pNbu15 melts over a narrow temperature range with a peak temperature of 168°C, and upon cooling (not shown), recrystallizes at 150°C. The transition is highly reversible for at least three temperature cycles.

Compared to other synthetic polyamides,^{31, 32} polypeptoids have much lower melting transitions, most likely due to the lack of hydrogen bonding in the N-substituted glycine backbone. By putting a side group on the backbone nitrogen, the main chain becomes devoid of hydrogen bond donors, whereas the amide linkages in nylons, aramids, or polypeptides allow hydrogen bonding to occur between adjacent chains. Such hydrogen bonding usually stabilizes the crystals and raises T_m . Hydrogen bonding interactions also dominate the thermal properties of polypeptides.³³ Polyglycine, which can be thought of as a peptoid without a side chain on the backbone nitrogen, has been shown to degrade before melting.^{33, 34} A direct comparison of a polypeptoid and a polypeptide can be made between pNbu15 and pNle15. pNle15 has a side chain identical to that of pNbu15, but the side chain is covalently bonded to the backbone alpha-carbon instead of the amide nitrogen, thereby allowing the backbone hydrogen bonding characteristic of all polypeptides. Figure 2.2a illustrates that no melting transition was observed over the experimental temperature range for this peptide, indicating that its crystal structure is likely stabilized by strong intermolecular interactions. In contrast, pNbu15 melts easily, as explained above. XRD (Figure 2.2b) indicates that thermal annealing does not enhance the crystal structure of pNle15, presumably because the chains do not have enough mobility to reorganize, while those of pNbu15 thermally anneal into well organized crystals. Furthermore, thermogravimetric analysis (Figure 2.2c) confirms that pNle15 starts degrading at approximately 320°C before ever melting. Conversely, thermogravimetric analysis has confirmed the stability of all of the 15mer polypeptoids synthesized up to approximately 260°C, leaving a region of thermal processability between the melting and degradation temperatures. The absence of strong intermolecular interactions suggests that polypeptoids may be suitable biologically inspired polymers for materials applications where processability and stability are necessary.

2.3.2 Controlling T_m by Varying Sidechains

Since the side chain functionality is introduced via a primary amine submonomer, there are hundreds of moieties that can be incorporated into a polypeptoid. Such chemical diversity potentially enables one to design a polypeptoid with specifically tailored properties. Here, a series of polypeptoids with various alkyl side chain lengths are compared to observe the effect of side chain chemistry on crystallization. Figure 2.3a presents the endotherms for polypeptoids with alkyl side chains 4 (pNbu15), 6 (pNhx15), and 8 (pNoc15) carbons long. Compared to pNbu15, which has a 4-carbon chain as a side group, longer alkyl chains lower the melting point. Adding 2 carbons to the side chain depresses the melting transition by almost 15°C, while adding

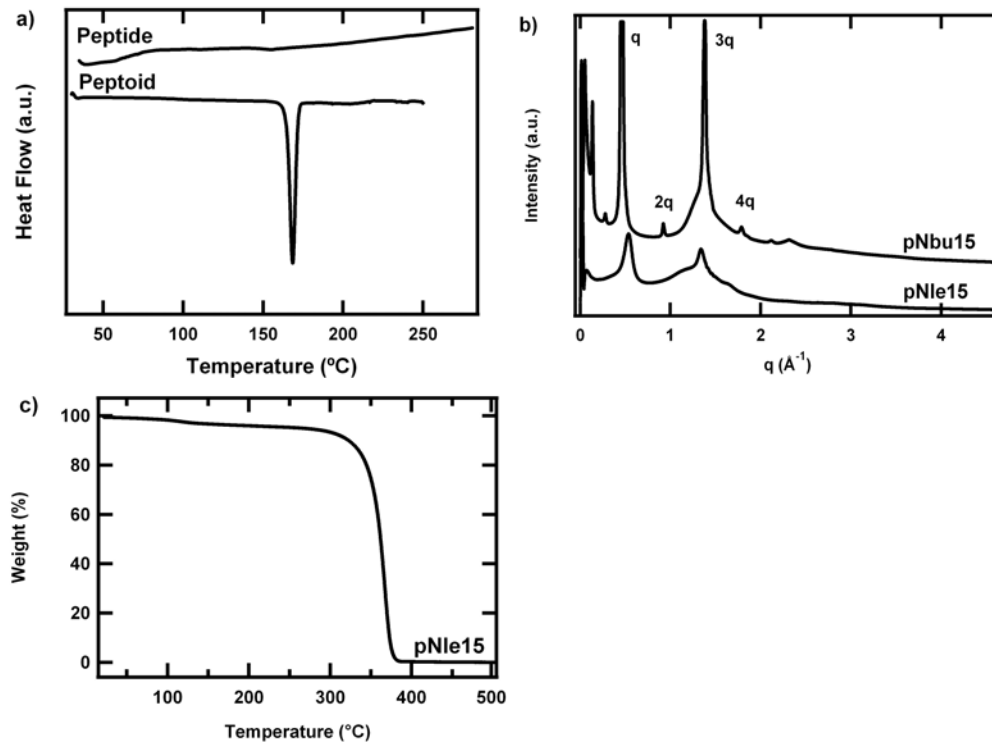


Figure 2.2. Thermal Properties of a Model Peptide vs. a Model Peptoid. a) DSC endotherms for a 15-mer polypeptoid (Nbu15) and its analogous polypeptide (pNle15). pNbu15 melts at a peak temperature of 168°C, while pNle15 clearly shows no melting transitions over the experimental temperature range. b) XRD spectra for pNbu15 and pNle15 indicate that the polypeptide does not anneal as easily as the polypeptoid due to decreased chain mobility from hydrogen bonding effects c) TGA of pNle15 proves the polypeptide degrades before melting.

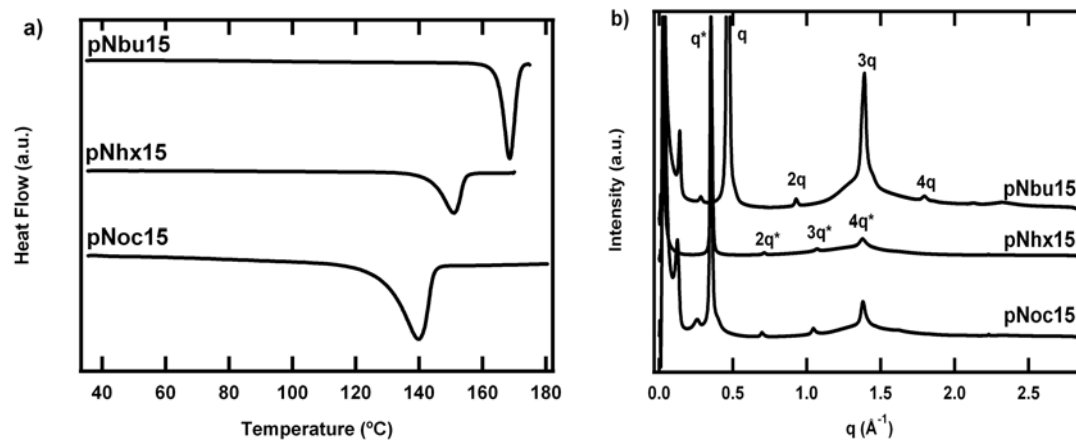


Figure 2.3. Tuning Melting Transition with Side Chain Length. a) DSC endotherms for three 15-mer peptides with increasingly longer alkyl side chains: butyl (pNbu15), hexyl (pNhx15), and octyl (pNoc15). As side chain length increases, the melting temperature decreases. b) XRD indicates that side chain length affects the spacings of the crystal lattice.

4 carbons shifts the melting transition down by approximately 30°C. The latent heat of melting appears to also depend on sidechain length, though it is unclear how the sidechains are affecting the enthalpic contribution to the free energy of crystallization. It is likely that longer, more flexible side chains prevent close crystalline packing of the molecules, thus making it easier to melt the material.

Except for pNhx15, the polypeptoids each show diffraction peaks at q and $2q$ in the small angle region (Figure 2.3b). These peaks show a difference in location: 0.141 \AA^{-1} (44.4 Å) for pNbu15 and 0.123 \AA^{-1} (50.85 Å) for pNoc15. The small increase in d -spacing for pNoc15 may reflect that longer side chains push the polypeptoid chain into a more extended configuration or that they allow a crystal structure where the chain axis is not as tilted relative to the c axis. The absence of the small angle peaks in pNhx15 is an effect of the thermal history of the sample. Moving into the wide angle region, each of these polypeptoids show peaks with q ratios of 1:2:3:4 (Figure 2.3b), but both pNhx15 and pNoc15 have larger spacings than pNbu15. The major reflection at 0.353 \AA^{-1} (17.8 Å) for pNoc15 represents a shift of about 4 Å relative to the same reflection seen for pNbu15 at 0.468 \AA^{-1} (13.4 Å). The increase in d -spacing further confirms that these reflections come from side chain crystallization and indicate that the longer side chains do indeed alter the spacing of the polypeptoid chains within the unit cell. Finally, both pNhx15 and pNoc15 show broadening and an increase in intensity around $4q$, suggestive of overlap with another peak centered around 4.5 Å as was discussed for pNbu15.

Conversely, the addition of bulkier side chains tends to drive the thermal transitions upwards. Adding one carbon to pNbu15 to introduce a branch in pNia15 shifts the melting peak up to 178°C. Whereas the addition of carbons in an n -alkyl conformation previously lowered the melting transition, the branched structure has the opposite effect, perhaps because the bulkier side group increases the overall stiffness of the polypeptoid chain. Introduction of an aromatic group in the side-chain (pNpe15) has a more dramatic effect - the melting transition is driven up to 225°C. The (001) spacing for pNpe15 is located at a q of 0.129 \AA^{-1} (48.4 Å, Figure 2.4), which is extended relative to pNbu15 but still shorter than pNoc15. Unlike pNbu15, there is no second order (002) reflection present, but there is an extraneous peak at 0.356 \AA^{-1} whose origin is unclear. Because the extraneous peak is close to the major reflection at 0.37 \AA^{-1} , which we believe stems from organization of the side chains, it may reflect the presence of two competing side chain structures within the crystalline domains. In addition to the wide-angle diffraction peaks seen at the q ratios of 1:2:3:4, pNpe15 also diffracts at the additional spacings of 4.5 Å and 3.7 Å (Figure 2.4), which are approximately $\sqrt{12} q$ and $\sqrt{19} q$, respectively. Both of these reflections are allowed in a hexagonal unit cell (among others), and so unfortunately do not contribute any additional information about the crystalline lattice of the peptoid. However, it should be noted that diffraction at similar spacings were seen by Nam et al. in a crystalline, two-dimensional peptoid sheet.²⁹ The spacing at 4.5 Å was attributed to chain-chain spacing (as previously mentioned), while the spacing at 3.7 Å corresponds to the spacing between each monomer residue along the peptoid chain in an extended conformation. The diffraction could

therefore be further evidence of an extended chain conformation for pNpe15. Besides the sharp diffraction pattern and the narrow and well-defined melting peak, strongly birefringent patterns in POM (Figure 2.5) confirm that pNpe15 is strongly crystalline at room temperature. This crystalline phase is present until melting into an isotropic phase at 225°C, a high temperature relative to the melting points of the other polypeptoids synthesized.

The kinetics of crystallization have a significant effect on the thermal behavior of pNpe15. At faster cooling rates, the material is locked into a solid conformation before it is able to fully crystallize. This is evidenced by the lack of a definitive crystallization peak in the cooling trace of the DSC (not shown). However, upon heating, the chains become mobile again and crystallize before melting at 225°C (Figure 2.6). Slower temperature ramps allow the material to crystallize fully upon cooling and there is no subsequent further crystallization upon reheating. The cold crystallization exotherm is different from a glass transition temperature which can also be seen in DSC traces upon heating. A glass transition reflects the increased motion of the chains relative to each other and is seen as an inflection point in the DSC trace. Recrystallization, however, is seen as an exothermal peak and indicates the reordering of the chains into an organized lattice. The passage of the T_g in this case allows the recrystallization to occur.

2.3.3 Controlling T_m with Sequence Defects

Sequence control provides an additional handle for tuning the thermal transitions of polypeptoids. It is well known that increasing comonomer content decreases the melting temperature for classical polymers such as polylactides^{13, 35} and polyethylenes.² In general, the comonomer content is related to the average length of a crystallizable sequence in the polymer, and the shorter that length, the lower the melting temperature of the copolymer. However, in most synthetic polymers this average sequence length can be difficult to control since it is dependent upon the molar ratio of the two monomers and their reactivity ratio, as described by Mayo and Lewis.³⁶ The stepwise synthesis of polypeptoids enables the average sequence length to be specified by inserting an exact number of defects per chain.

We have designed two symmetric yet arbitrary monomer sequences to investigate the effect of comonomer units on crystallinity for two polypeptoids: pNia15 and pNpe15, which as previously discussed have very different thermal behavior. To these two homopolymers, defects consisting of monomers with slight differences, particularly in terms of sidechain bulk, were added. Chains with two defects contained monomer substitutions at positions 6 and 10, while chains with four defects contained substitutions at positions 3, 6, 10, and 13 (Figure 2.7). In the case of the pNia15 polymer, two defects were made: an unbranched alkyl sidechain two carbons longer than the homopolymer side chain, and a methoxyethyl side chain. Sequences are tabulated in Table 2.2. In the case of pNpe15, the defect sidechain is virtually identical to the homopolymer side chain, but the phenyl ring is spaced one more alkyl unit away from the chain. Thus, the side chain imparts not a chemical defect but rather a spatial one.

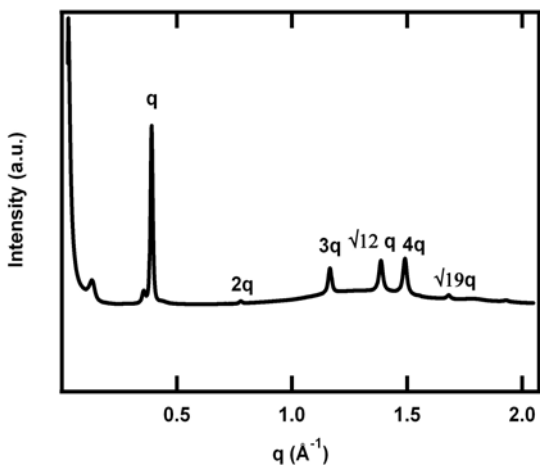


Figure 2.4. XRD of pNpe15. XRD pattern for pNpe15 shows several peaks, indicating a highly crystalline order.

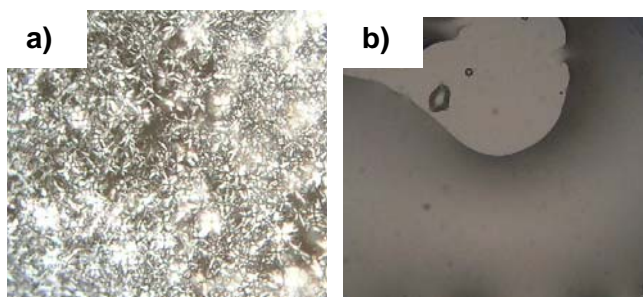


Figure 2.5. POM of pNpe15. a) Polarized optical microscopy for pNpe15 exhibits strongly birefringent patterns at room temperature. b) Upon heating past the melting transition, all birefringence is lost and an isotropic melt is observed.

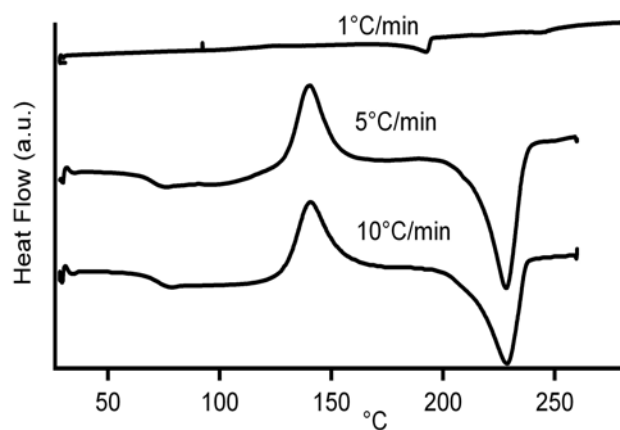
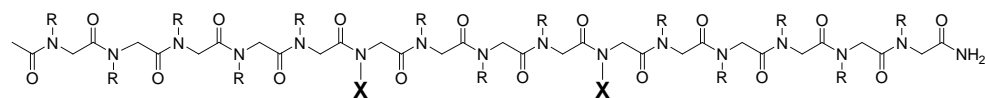
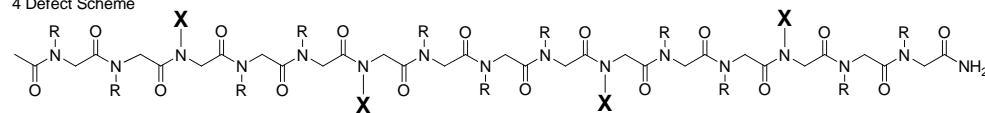


Figure 2.6. Heat Rate Dependence of Crystallization for pNpe15. After cooling from an isotropic melt at both 5°C/min and 10°C/min, the corresponding endotherms show that the peptoid continues to crystallize above its T_g before melting at 225°C. For 1°C/min, no further crystallization occurs upon heating.

2 Defect Scheme



4 Defect Scheme



No. defects	R=	X=	Name
2			pNia-co-Nme2d
2			pNia-co-Nha2
2			pNpe-co-Npp2
4			pNia-co-Nme4
4			pNia-co-Nha4
4			pNpe-co-Npp4

Figure 2.7. Defect Scheme for Peptoids. “Defects” were inserted along a 15-mer peptoid chain according to 2 schemes. X denotes defects; R denotes side chains, as listed in the table.

In agreement with the work done on random copolymers, we have found that the introduction of defects at precise locations in the polymer sequence (as a side chain substitution) allows crystallization and hence the melting temperature to be reduced for pNia15 when the defect is N-hexylglycine. N-hexylglycine defects introduced to pNia15 homopolymer depress the melting transition by up to 20°C (Figure 2.8a). Increasing the number of defects drives the melting temperature down further, indicating that the substitutions disrupt the thermodynamics of polypeptoid crystallization. In addition, the disappearance of higher order XRD reflections for both q^* (the low angle reflection, Figure 2.8b inset) and q (Figure 2.8b) suggests that the copolymers' crystal organization is disrupted relative to the pNia15 homopolymer. The peak just past $3q$ at 1.36 \AA^{-1} , however, persists for all polypeptoids. This peak corresponds to a spacing of 4.6 \AA , which may be the chain-chain spacing, as previously mentioned in the discussion above. It is worthy to note that all variations of the pNia15 copolypeptoid crystallized, even for an average sequence length of 2.2 pNia15 units. This number is low compared to a more traditional system such as ethylene copolymers, where the critical sequence length for crystallization lies between 6-25³⁷. Even for polyethylenes with a short chain branch introduced at precisely every fifth carbon (yielding an ethylene run length of four carbons), the resulting copolymer is amorphous.²² The possibility of defect co-crystallization within the peptoid chain may be one reason that such short lengths of pNia15 units can still crystallize.

N-2-methoxyethylglycine defects were also inserted into the pNia15 homopolymer. The methoxyethyl branch is chemically different from the isoamyl side chain of the homopolymer.. N-2-methoxyethylglycine monomer substitutions inserted at the same positions (Figure 2.7) altered the thermodynamics of crystallization in a similar way to the N-hexylglycine defects. XRD spectra (Figure 2.9b) for these copolymers once again show fewer higher order reflections than the spectrum of the homopolymer, though the peak at 1.36 \AA still persists. The DSC endotherms (Figure 2.9a) show that the depression of the melting temperature is approximately the same order of magnitude as that of the N-hexylglycine copolymers.

The thermal behavior of the pNia15 copolymers differs from the behavior predicted by Flory's theory of crystallization¹⁰ (previously shown as equation 2.1). The melting temperatures calculated from this equation are higher than the observed values, as shown graphically in Figure 2.10a. The main difference between the predicted melting temperatures and the observed melting temperatures is that the topographic defects used to suppress crystallization in this polypeptoid experiment are not randomly placed and as a result, may actually participate in and affect the crystal packing, while Flory's theory assumes exclusion of the defect from the crystal lattice. In addition, Flory's theory takes the crystal structures to be at total equilibrium, a situation that is difficult to achieve even with extremely slow crystallization conditions. The enthalpy of melting of these polypeptoids increases when a greater number of defects are present in the chain (Figure 2.10b). It is interesting to note that if these are equilibrium melting temperatures, then the entropy of melting must also increase in order for the melting temperature to decrease with respect to the homopolymer. However, since the entropy of melting is not measurable, we can

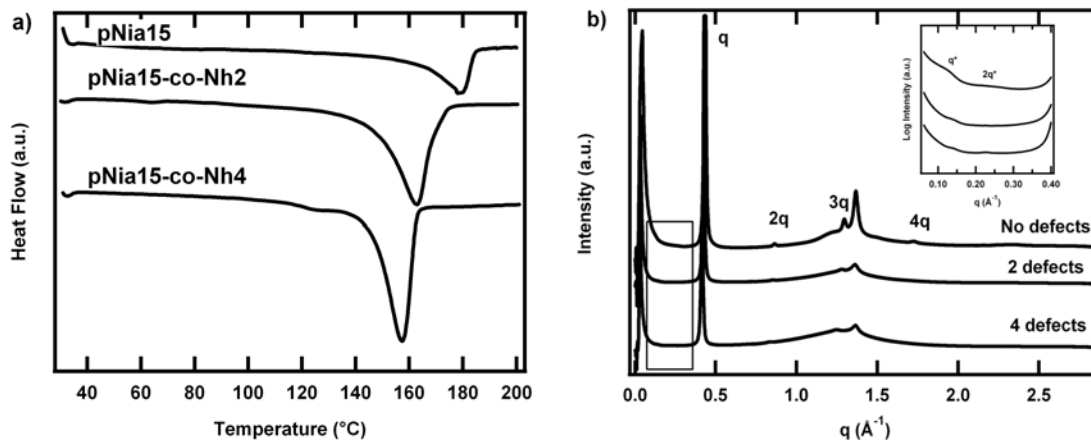


Figure 2.8. Thermal Behavior of Peptoids with Nhx Defects. a) DSC traces for pNia15, containing 0, 2, and 4 defects of Nhx. Increasing the number of defects disrupts crystallization and suppresses the melting point. b) XRD patterns for pNia15 homopolymers with 0, 2, and 4 defects. All three samples show nearly identical spectra.

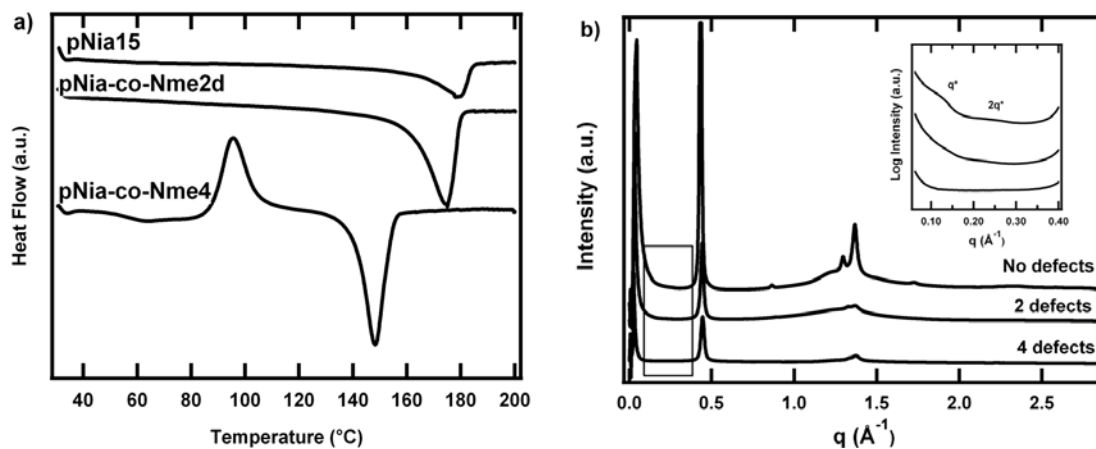


Figure 2.9. Thermal Behavior of Peptoids with Nme Defects. a) DSC endotherms for pNia15 with 0, 2, and 4 defects of Nme. The exothermic peak in pNia-co-Nme4 is due to cold crystallization of the polypeptoid. b) XRD patterns for pNia15 homopolymers with 0, 2, and 4 Nme defects. It is obvious that the Nme defects suppress crystallization.

only postulate its increase. Although our peptoid system is markedly different from that derived for Flory's treatment, it is interesting for comparison's sake that the basic form of Flory's theory still holds for the peptoid copolymers: increasing defect content depresses the melting temperature.

Interestingly, defects introduced into pNpe15 homopolymer disrupted the crystal structure nearly completely. No birefringent patterns were seen in POM for any of the copolymers and the DSC traces show a drastic reduction in the peak size for melting and recrystallization to the point of complete disappearance, as shown in Figure 2.11a. Furthermore, the XRD patterns (Figure 2.11b) show broad, diffuse scattering consistent with a lack of crystalline order. Both defected polypeptoids show two peaks, one centered around 0.4 \AA^{-1} and one centered around 1.3 \AA^{-1} . It is possible that there may be some weak ordering of the side chains and the chain-chain spacings at 0.4 \AA^{-1} and 1.3 \AA^{-1} , respectively. The lack of sharp diffraction peaks suggests that the crystalline packing of the pNpe15 homopolymer is strongly sensitive to the placement of the aromatic rings, and the addition of defects with an additional chemical moiety prevents the chains from aligning in any ordered way. It remains to be seen whether a less bulky defect (i.e. one without an aromatic ring) would still allow the pNpe copolymer to crystallize.

2.3.4 Controlling the Distribution of Sequence Defects

Not only can one exert exact control over the amount of defects per chain, but one can also control the pattern of defects within the peptoid monomer sequence. Unlike random copolymerizations, polypeptoids are synthesized such that a monodisperse batch of uniform sequence is obtained, therefore enabling direct comparisons between various distributions for peptoids with exactly the same number of defects. Recent progress has been made in the sequence control of polyethylene copolymers containing chlorines such that the chlorine atoms can be precisely limited to every *n*th carbon.²⁴ While this is a significant achievement for polymers of high molecular weight, polypeptoids offer greater freedom over the distribution of the "comonomer." A series of defected pNia15 polymers, all with exactly 2 defects of Nme each are shown in Table 2.3. The position of these 2 defects varies within the peptoid chain between each polymer, giving each copolymer different run lengths of Nia monomers or different "degrees of blockiness."³⁸ The exact sequences are tabulated in Table 2.2; the sequences have been reproduced pictorially in Table 2.3.

Although all pNia15 copolymers in this series have the same average Nia length (since all copolymers have exactly 2 defects for 15 monomer spaces), there are significant differences in the enthalpy of melting. It appears that the polymers with the defects located toward the center of the chain have the lowest enthalpies of melting, though their melting temperatures are not significantly different from those of the other copolymers. The XRD spectra (Figure 2.12) for all copolymers are extremely similar, though there are subtle differences in the location of the (001) peak and in the broadness of the peak at a *q* of 1.4 \AA^{-1} . The copolymers with the most asymmetric blocks of Nia side chains have sharper (001) reflections at spacings of 44.9 \AA , 45 \AA ,

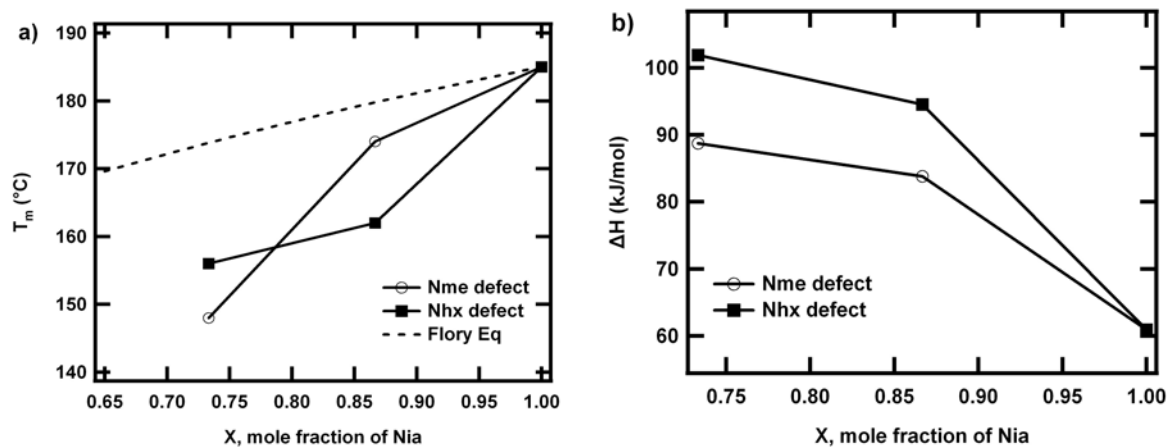


Figure 2.10. Melting Point Comparison of Peptoids with Defects. a) Melting point comparison for pNia15 defected with Nhx and Nme graphed by mole fraction. Dotted line represents the melting points predicted by the Flory equation. b) Enthalpies of melting for the same defected pNia15 polymers. As the defect content increases, the heat of melting also increases.

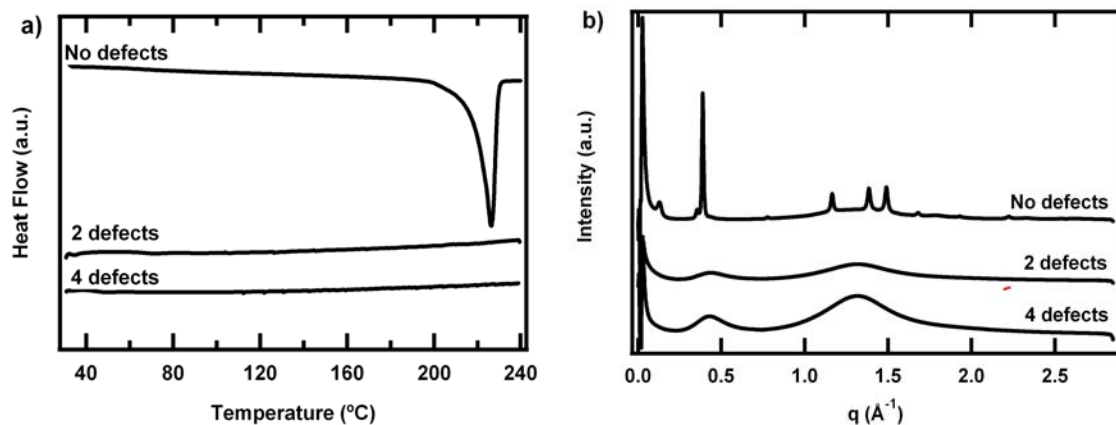


Figure 2.11. Thermal Behavior of pNpe15 Peptoids with Defects. a) DSC traces for pNpe15 containing 0, 2, and 4 defects. Increasing the number of defects disrupts crystallization completely. b) XRD patterns for pNpe15 homopolymers with 0, 2, and 4 defects. The traces for samples with defects indicate an amorphous solid.

Table 2.3. pNia15 copolymers with various sequence distributions of 2 defects. O denotes a defect; X denotes an Nia monomer.

Polypeptoid	$T_m(^{\circ}\text{C})$	ΔH (J/g)	Avg Nia Length	Sequence
pNia-co-Nme2a	174	58.3	4.3	X X O X X X X X X X X O X X
pNia-co-Nme2b	166	48.9	4.3	X X X O X X X X X X O X X X
pNia-co-Nme2c	174	51.5	4.3	X X X X O X X X X X O X X X X
pNia-co-Nme2d	170	41.9	4.3	X X X X X O X X X O X X X X X
pNia-co-Nme2e	173	35.5	4.3	X X X X X X O X O X X X X X X

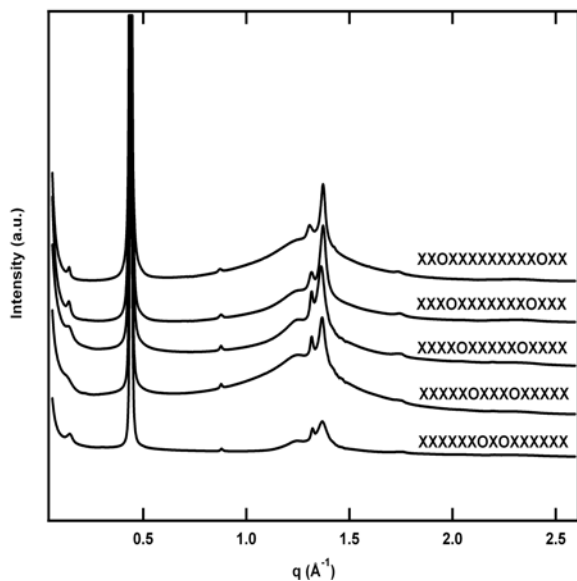


Figure 2.12. XRD patterns for pNia15 copolymers with 2 defects each. The location of the defects does not appear to affect the crystalline packing of the polymer in a qualitative way, though the location of the (001) peak at low q shifts slightly and broadens for the third and fourth spectra.

44.2 Å (the first, second, and fifth spectra in Figure 2.12), while the copolymers with more evenly spaced blocks of Nia side chains have broader (001) reflections at spacings of 46.1 Å and 48.3 Å. It is possible that in the more asymmetric copolymers, only the longest blocks of Nia are participating in crystallization (and leaving out the ends or the middle in the fifth case), whereas in the more evenly spaced copolymers, it is more energetically favorable for the entire chain to crystallize. In general, however, all of the reflections after the (001) are extremely similar for the copolymers. These preliminary experiments raise several questions, such as whether a more asymmetric distribution would have a larger effect on thermal behavior (all sequences investigated are symmetric). The peptoid system promises to be ideal for exploring the effects of sequence distribution on physical properties.

2.4 Conclusions

The thermal behavior of various polypeptoids exactly 15 monomers in length has been investigated. In contrast to polypeptides, several polypeptoids were found to melt and recrystallize at experimentally accessible temperatures, most likely due to the lack of intermolecular hydrogen bonding. Polypeptoid crystallization was controlled by changing the side chain, as well as by introducing sequence specific defects into polypeptoid homopolymers (via side chain substitutions). As expected, increasing the number of defects depresses the melting temperature, though in some cases, it suppresses crystallization completely. The location of these defects can be specified *exactly*, and a series of polypeptoid copolymers with exactly 2 defects in various distributions was synthesized. While the crystal structure and melting temperatures were slightly affected by the defect distribution, the enthalpies of melting varied significantly among the polypeptoids investigated. The sequence specificity and thermal stability of polypeptoids demonstrated in this work lay the foundation for polypeptoids as novel, biologically inspired polymers for materials applications.

2.5 Acknowledgements

This work was supported by the Office of Naval Research in the form of a Presidential Early Career Award in Science and Engineering (PECASE) for RAS. AMR gratefully acknowledges the National Science Foundation for a graduate fellowship, and HKM acknowledges the Department of Defense for a NDSEG fellowship. Polypeptoid synthesis and associated chemical characterization were performed at the Molecular Foundry, and XRD experiments were performed at the Advanced Light Source (ALS). Both are Lawrence Berkeley National Laboratory user facilities supported by the Office of Science, Office of Basic Energy Sciences, U.S. Department of Energy, under Contract No. DE-AC02-05CH11231. The authors thank Dr. James Holton and Dr. Alexander Hexemer for experimental assistance at the ALS. We also gratefully acknowledge Dr. Nitash Balsara for use of equipment.

2.6 Appendix

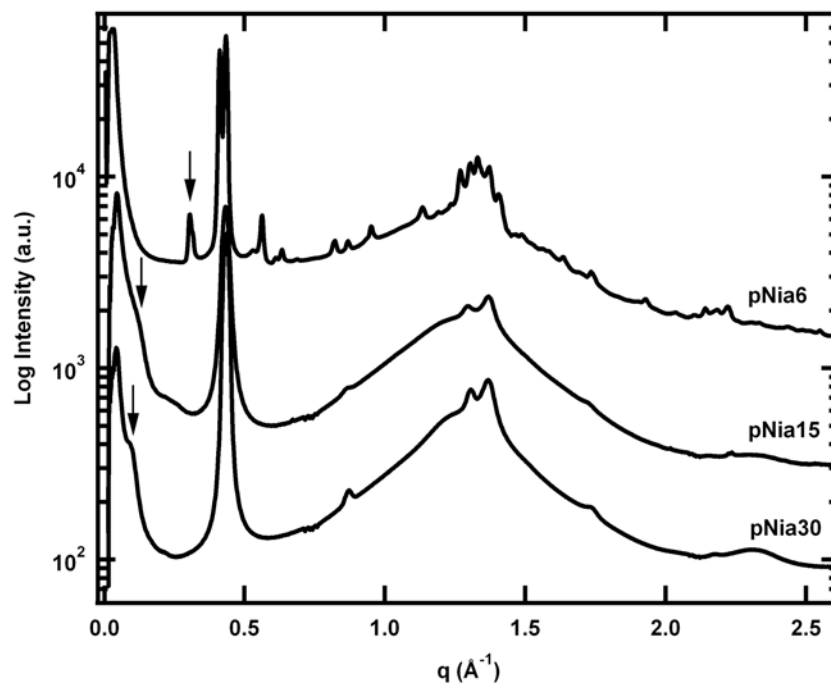


Figure 2.13. X-Ray Diffraction of Polypeptoids of Various Molecular Lengths. XRD traces for polypeptoids 6, 15, and 30 monomers in length. The arrow denotes the (001) spacing, which changes to lower q (higher d -spacing) as the molecular length increases. As the molecular length increases from 6 to 15 to 30 monomers, the d -spacing increases from 20.4 \AA to 45.5 \AA to 67.2 \AA , respectively. The major reflection at a q of 0.43 \AA^{-1} and its higher order reflections do not change as the molecular length changes, implying that these peaks correspond to side chain organization (as all three polypeptoids here have the same side chain).

2.7 References

1. Kint, D. P. R.; Munoz-Guerra, S. *Polymer International* 2003, 52, (3), 321-336.
2. Alamo, R. G.; Mandelkern, L. *Thermochimica Acta* 1994, 238, 155-201.
3. Zhang, M.; Lynch, D. T.; Wanke, S. E. *Polymer* 2001, 42, (7), 3067-3075.
4. Baratian, S.; Hall, E. S.; Lin, J. S.; Xu, R.; Runt, J. *Macromolecules* 2001, 34, (14), 4857-4864.
5. Crist, B.; Howard, P. R. *Macromolecules* 1999, 32, (9), 3057-3067.
6. Hauser, G.; Schmidtke, J.; Strobl, G. *Macromolecules* 1998, 31, (18), 6250-6258.
7. Boz, E.; Nemeth, A. J.; Wagener, K. B.; Jeon, K.; Smith, R.; Nazirov, F.; Bockstaller, M. R.; Alamo, R. G. *Macromolecules* 2008, 41, (5), 1647-1653.
8. Sfatos, C. D.; Shakhnovich, E. I. *Physics Reports-Review Section of Physics Letters* 1997, 288, (1-6), 77-108.
9. Madkour, T. M.; Azzam, R. A.; Mark, J. E. *Journal of Polymer Science Part B-Polymer Physics* 2006, 44, (18), 2524-2541.
10. Flory, P. J. *Transactions of the Faraday Society* 1955, 51, (6), 848-857.
11. Paul, J. F. *The Journal of Chemical Physics* 1949, 17, (3), 223-240.
12. Burfield, D. R. *Macromolecules* 1987, 20, (12), 3020-3023.
13. Sarasua, J. R.; Prud'homme, R. E.; Wisniewski, M.; Le Borgne, A.; Spassky, N. *Macromolecules* 1998, 31, (12), 3895-3905.
14. Richardson, M. J.; Flory, P. J.; Jackson, J. B. *Polymer* 1963, 4, (2), 221-236.
15. Alizadeh, A.; Richardson, L.; Xu, J.; McCartney, S.; Marand, H.; Cheung, Y. W.; Chum, S. *Macromolecules* 1999, 32, (19), 6221-6235.
16. Cheng, S. Z. D.; Janimak, J. J.; Zhang, A. Q.; Hsieh, E. T. *Polymer* 1991, 32, (4), 648-655.
17. Hosoda, S. *Polymer Journal* 1988, 20, (5), 383-397.
18. Paul, S. *Polymer International* 1996, 40, (2), 111-122.
19. Sanchez, I. C.; Eby, R. K. *Macromolecules* 1975, 8, (5), 638-641.
20. Adisson, E.; Ribeiro, M.; Deffieux, A.; Fontanille, M. *Polymer* 1992, 33, (20), 4337-4342.
21. Baughman, T. W.; Wagener, K. B., Recent advances in ADMET polymerization. In *Metathesis Polymerization*, Springer-Verlag Berlin: Berlin, 2005; Vol. 176, pp 1-42.
22. Rojas, G.; Berda, E. B.; Wagener, K. B. *Polymer* 2008, 49, (13-14), 2985-2995.
23. Sworen, J. C.; Smith, J. A.; Berg, J. M.; Wagener, K. B. *Journal of the American Chemical Society* 2004, 126, (36), 11238-11246.
24. Alamo, R. G.; Jeon, K.; Smith, R. L.; Boz, E.; Wagener, K. B.; Bockstaller, M. R. *Macromolecules* 2008, 41, (19), 7141-7151.
25. Kirshenbaum, K.; Zuckermann, R. N.; Dill, K. A. *Current Opinion in Structural Biology* 1999, 9, (4), 530-535.
26. Simon, R. J.; Kania, R. S.; Zuckermann, R. N.; Huebner, V. D.; Jewell, D. A.; Banville, S.; Ng, S.; Wang, L.; Rosenberg, S.; Marlowe, C. K.; Spellmeyer, D. C.; Tan, R. Y.; Frankel, A. D.; Santi, D. V.; Cohen, F. E.; Bartlett, P. A. *Proceedings of the National Academy of Sciences of the United States of America* 1992, 89, (20), 9367-9371.
27. Figliozzi, G. M.; Goldsmith, R.; Ng, S. C.; Banville, S. C.; Zuckermann, R. N. *Combinatorial Chemistry* 1996, 267, 437-447.
28. Wu, C. W.; Sanborn, T. J.; Huang, K.; Zuckermann, R. N.; Barron, A. E. *Journal of the American Chemical Society* 2001, 123, (28), 6778-6784.
29. Nam, K. T.; Shelby, S. A.; Choi, P. H.; Marciel, A. B.; Chen, R.; Tan, L.; Chu, T. K.; Mesch, R. A.; Lee, B.-C.; Connolly, M. D.; Kisielowski, C.; Zuckermann, R. N. *Nat Mater* 9, (5), 454-460.
30. Cui, H. G.; Krikorian, V.; Thompson, J.; Nowak, A. P.; Deming, T. J.; Pochan, D. J. *Macromolecules* 2005, 38, (17), 7371-7377.
31. Ke, B.; Sisko, A. W. *Journal of Polymer Science* 1961, 50, (153), 87-&.

32. Xenopoulos, A.; Wunderlich, B.; Subirana, J. A. *European Polymer Journal* 1993, 29, (7), 927-935.
33. Lotz, B. *Journal of Molecular Biology* 1974, 87, (2), 169-&.
34. Franco, L.; Xenopoulos, A.; Subirana, J. A.; Puiggali, J. *Journal of Polymer Science Part a-Polymer Chemistry* 1995, 33, (4), 727-741.
35. Sodergard, A.; Stolt, M. *Progress in Polymer Science* 2002, 27, (6), 1123-1163.
36. Mayo, F. R.; Lewis, F. M. *Journal of the American Chemical Society* 1944, 66, 1594-1601.
37. Chen, Q.; Luo, H. J.; Yang, G. A.; Xu, D. F. *Polymer* 1997, 38, (5), 1203-1205.
38. Khokhlov, A. R.; Khalatur, P. G. *Physica A* 1998, 249, (1-4), 253-261.

Chapter 3. Determination of the Persistence Length of Helical and Non-helical Polypeptoids in Solution

Adrienne M. Rosales, Hannah K. Murnen, Steven R. Kline, Ronald N. Zuckermann, and Rachel A. Segalman, *Soft Matter*, 2012, 8(13), pp. 3673-3680. Reproduced by permission of The Royal Society of Chemistry. <http://pubs.rsc.org/en/Content/ArticleLanding/2012/SM/c2sm07092h>

Control over the shape of a polymer chain is desirable from a materials perspective because polymer stiffness is directly related to chain characteristics such as liquid crystallinity and entanglement, which in turn are related to mechanical properties. However, the relationship between main chain helicity in novel biologically derived and inspired polymers and chain stiffness (persistence length) is relatively poorly understood. Polypeptoids, or poly(N-substituted glycines), constitute a modular, biomimetic system that enables precise tuning of chain sequence and are therefore a good model system for understanding the interrelationship between monomer structure, helicity, and persistence length. The incorporation of bulky chiral monomers is known to cause main chain helicity in polypeptoids. Here, we show that helical polypeptoid chains have flexibility nearly identical to an analogous random coil polypeptoid as observed via small angle neutron scattering (SANS). Additionally, our findings show that polypeptoids with aromatic phenyl side chains are inherently flexible with persistence lengths ranging from 0.5 to 1 nm.

3.1 Introduction

The shape of a polymer chain is a reflection of its intramolecular interactions and can directly influence a large number of characteristics, including mechanical properties and self-assembly behavior. These intramolecular interactions include sterics, hydrogen bonding, hydrophobic interactions, and aromatic interactions, among others. The chain conformation in turn affects how the polymer can interact with the other chains around it, which influences both the mechanical properties of the polymer and its self-assembly into various structures. Classical polymers self-assemble via a balance of enthalpic interactions and entropic chain stretching penalties, which can both be complicated by the conformation of the polymer chain. In polymers with more complicated chemical interactions, such as polyelectrolytes and conjugated polymers, chains are often significantly stiffer (have a longer persistence length) than classical materials. The polymer backbone itself plays a large role in intramolecular interactions leading to chain shape, and polymers with highly conjugated or sterically hindered backbones, such as polyphenylene vinylene, have longer persistence lengths in solution (6-40 nm)¹ than those with backbones composed of more aliphatic linkages, such as polystyrene (1 nm).² Side chains can also play a significant role in the rigidity of a polymer chain. For example, a subtle difference of one carbon in a polysilylene side chain can increase the persistence length from 6.2 nm up to 85 nm.³ Charged side chains introduce another level of complexity due to the ionic interactions between groups that can lead to chain stiffening.⁴

Secondary structure can also have a large impact on the persistence length of a chain. Helical secondary structure in particular correlates with increasing persistence lengths in polymers. Helical polyisocyanates⁵ have a persistence length of 40 nm to 50 nm, and α -helical poly(γ -benzyl-L-glutamate)⁶ (PBLG) has a persistence length up to approximately 200 nm at high molecular weights. Several design methods exist for the formation of a polymer helix; in particular, designing side chain interactions is an interesting route to controlling chain shape. Side chain interactions have a large influence on the formation of secondary structures in biological polymers and thus directly influence the persistence length of these polymers as well. For example, the addition of long stretches of prolines in a polypeptide induces the formation of a helix. Using FRET experiments, the persistence length of a polyproline type II helix was estimated to range from 9 nm to 13 nm⁷ using a chain that was 20 monomers long in the *all-trans* form.

Here, we evaluate the effect of subtle changes in side chain size and chirality on the persistence length of N-substituted glycine polymers, also known as polypeptoids. Although polypeptoids are a relatively new material, they have recently attracted much attention in polymeric studies,⁸⁻¹¹ meaning there is a need to quantify their properties. Quantifying polymer properties, such as flexibility and persistence length, is important for modeling these systems and further understanding their self-assembly.¹²

Polypeptoids are sequence-specific, biomimetic polymers that have been shown to form stable secondary structures in solution depending upon the types of side chains incorporated into the polymer^{9, 13-15}. In particular, polypeptoids with bulky α -chiral side chains form a polyproline type I-like helix in solution. Unlike the α -helices of polypeptides, the polypeptoid helices are stabilized by steric interactions, rather than hydrogen bonding. Both theoretical¹⁶ and experimental¹⁷⁻²⁰ studies have shown that the preferred conformation of the peptoid helix is entirely composed of *cis*-amide bonds with a periodicity of three residues per turn and a pitch of approximately 6 Å. These studies showed that a polypeptoid with α -chiral aromatic side chains prefers the all *cis* conformation to a *trans* conformation in the ratio of 2:1. In addition, the handedness of the helix is determined by the handedness of the α -chiral side chains, as the peptoid backbone is devoid of chirality. The presence of a helical fold would lead one to expect a stiffening of the polymer chain. However, our small angle neutron scattering (SANS) measurements have shown that helical polypeptoids have persistence lengths much smaller than expected. In fact, they are nearly as flexible as polypeptoids without any secondary structure.

3.2 Experimental Methods

Materials Compounds **1** and **2** (Figure 3.1) were synthesized using a step-wise solid-phase submonomer synthesis method²¹ on a custom robotic synthesizer or a commercial Aapptec Apex 396 robotic synthesizer. All polypeptoids were acetylated on the resin, cleaved from the resin using 95% v/v trifluoroacetic acid in water, and purified using reverse-phase HPLC, as previously described.^{8, 10} The synthesis was confirmed by electrospray mass spectrometry on an

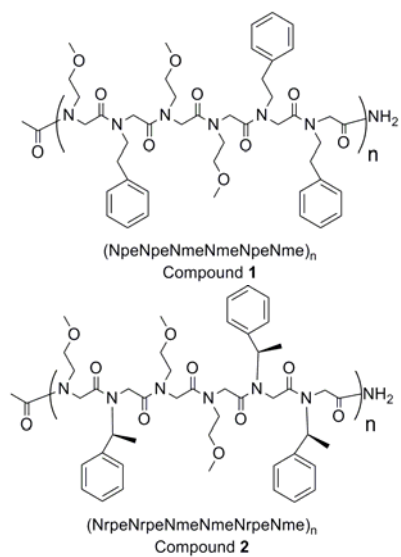


Figure 3.2. Structure of Helical and Non-Helical Peptoids. **1** contains achiral aromatic side chains, while **2**, a helix-forming polypeptoid, contains alpha-chiral side chains. The value of n ranges from 3 to 8 for chains of varying lengths.

Agilent 1100 series LC/MSD trap system (Agilent Technologies, Santa Clara, CA) and by matrix-assisted laser desorption/ionization-time of flight (MALDI-TOF) mass spectrometry on a 4800 series MALDI-TOF (Applied Biosystems, Carlsbad, CA) with a laser power of 5000. MALDI samples were prepared using a 1:1 ratio of polypeptoid in acetonitrile (1 mg/mL) and 1,8,9-anthracenetriol (10 mg/mL in tetrahydrofuran). The monomer sequences for the polypeptoids studied here are denoted in Figure 3.1, with *Nme* = *N*-(2-methoxyethyl)glycine, *Npe* = *N*-(2-phenylethyl)glycine, and *Nrpe* = (*R*)-*N*-(1-phenylethyl)glycine. Several polymers were made with *n* (the number of repeat units as designated in Figure 3.1) varying from 3 to 8. The majority of this publication will discuss the polymers where *n* is equal to 6, forming a polypeptoid with 36 total monomers.

Circular Dichroism (CD) CD measurements were performed on a J-185 CD spectrometer (Jasco Inc., Easton, MD). Stock solutions of the polypeptoids were made in tared vials using 5 mg/mL of peptoid powder in acetonitrile. The stock solutions were then diluted to a concentration of 0.08 mg/mL before acquiring CD spectra. CD spectra were acquired using a quartz cell (Hellma USA, Plainview, NY) with a path length of 1 mm. A scan rate of 50 nm/min was used, and 3 measurements were averaged for each compound.

Small Angle Neutron Scattering (SANS) SANS studies were conducted at the NG3 SANS line at the National Institute of Standards and Technology (NIST) Center for Neutron Research in Gaithersburg, Maryland and at the CG-3 Bio-SANS line at the High Flux Isotope Reactor at Oak Ridge National Laboratory (ORNL) in Oak Ridge, Tennessee. Samples were prepared at a concentration of 10 mg/mL in deuterated acetonitrile to enhance the contrast between the polypeptoids and the solvent. Quartz banjo cells (Hellma USA, Plainview, NY) with a path length of 1 mm and 2 mm were used at NIST and ORNL, respectively, in a temperature controlled multiple position sample holder. A neutron wavelength of 6 Å was used at both beamlines, and data were collected at two different instrument configurations (1.3 m and 4 m at NIST, and 1.7 m and 14.5 m at ORNL). The data were reduced using the NCNR SANS reduction macros²² and the Spice SANS reduction program in Igor Pro.

3.3 Results and Discussion

3.3.1 Circular Dichroism

Compounds **1** and **2** were designed to be non-structured and helical, respectively, through the incorporation of aromatic side chains with tunable chirality. Compound **2** contains 50% α -chiral aromatic side chains while compound **1** contains 50% achiral aromatic side chains instead. Previous literature has shown that **2** forms a polyproline type I-like helix in solution with all *cis* amide bonds¹⁴ as described above. However, **1** was designed to be minimally structured by removing the α -chiral substituent that provides the steric influence for secondary structure formation. Indeed, circular dichroism (Figure 3.2) in acetonitrile shows that there is helix formation of **2** as demonstrated by the characteristic peaks at 192 nm, 202 nm, and 218 nm. This

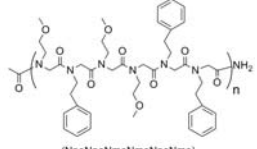
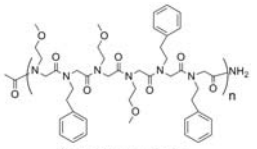
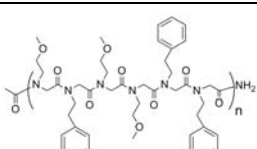
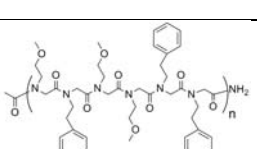
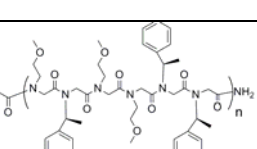
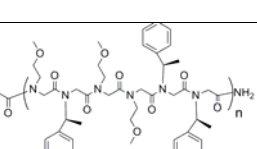
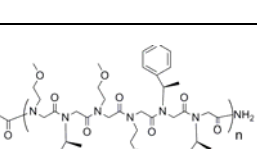
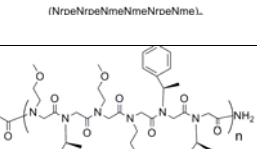
Compound	Repeat Unit	n (number of repeat units)	N (total number of monomers)	M_{obs}/M_{theo}	Structure
Compound 1a	 (NpeNpeNmeNmeNpeNme) _n	3	18	2548.5 / 2546	Non-helical
Compound 1b	 (NpeNpeNmeNmeNpeNme) _n	4	24	3379.4 / 3375	Non-helical
Compound 1c	 (NpeNpeNmeNmeNpeNme) _n	6	36	5033.2 / 5033	Non-helical
Compound 1d	 (NpeNpeNmeNmeNpeNme) _n	8	48	6701.6 / 6691.1	Non-helical
Compound 2a	 (NrpeNrpeNmeNmeNrpeNme) _n	3	18	2549.2 / 2546	Helical
Compound 2b	 (NrpeNrpeNmeNmeNrpeNme) _n	4	24	3377.5 / 3375	Helical
Compound 2c	 (NrpeNrpeNmeNmeNrpeNme) _n	6	36	5028.2 / 5033	Helical
Compound 2d	 (NrpeNrpeNmeNmeNrpeNme) _n	8	48	6604.4 / 6691.1	Helical

Table 3.1. Molecular design of non-helical and helical polypeptoids.

helix formation is constant across several polymers of varying molecular weights (**2a** through **2d**) with little deviation in the per-residue molar ellipticity. Previously, it was shown that as the chain length of a polypeptoid containing 100% Nrpe residues increases, the per-residue molar ellipticity also increases until a chain length of 13 residues is reached. After 13 residues, the ellipticity remains approximately constant for longer chain lengths, suggesting that the overall fraction of helical isomers is stabilized.²⁰ A similar trend was also observed for peptoid helices consisting of bulky *N*-1-naphthylethyl side chains, except in that case, the per-residue molar ellipticity reached a maximum after only 5 monomer units.¹⁷

It would be helpful to gain some quantitative insight about the helical content of these molecules using CD, as is often done for proteins. However, CD is a quantitative technique for proteins because there is a vast number of known protein structures, allowing the development of algorithms that can compute a reliable estimate of the fraction of α -helices, β -sheets, and random coils by comparing new CD data to that of the known structures.²³ There are few X-ray solved structures of polypeptoids, meaning that it is not possible to reliably calculate the fraction of helicity for polypeptoids from CD.

Because CD does not yield information about the population of conformers for polypeptoids, polypeptoid secondary structure has previously been established using a combination of 2D NMR, X-ray crystallography, and molecular modeling studies. These studies first confirmed the presence of a helical conformation in a very short polypeptoid (5 monomers in length) containing bulky chiral, aromatic residues ((*S*)-*N*-(1-phenylethyl)glycine, Nspe).¹⁶ However, the 2D NMR studies for Nspe₅ also show the presence of other isomers and conformations in the amount of approximately 40% in methanol solution.^{17, 18} Thus, the α -helix-like CD signature observed for (Nspe)₅ and other peptoid helices is from an ensemble of closely related conformations in rapid equilibrium with one another.

The presence of these other polypeptoid conformers is most likely due to the *cis/trans* isomerization of the backbone amide bonds, which may enable the polypeptoid backbone to sample many conformations. To probe whether the fraction of helices can be controlled, the effect of temperature and solvent on the per-residue molar ellipticity was examined. As **2c** is heated from 20°C to 70°C in acetonitrile (Figure 3.3a), there is no change in the spectrum shape and only a slight decrease in the peak intensity at 218 nm from 19,200 degcm²dmol⁻¹ to 15,300 degcm²dmol⁻¹. This result is consistent with the observation by Wu et. al that Nrpe₆, Nrpe₁₂, and Nrpe₁₈ all retain their helical CD signature at increased temperature, suggesting that the peptoid helices are stable to thermal unfolding because they are sterically constrained rather than hydrogen bond-stabilized.²⁰ This is the case for all of the helical polypeptoids investigated here, as shown in the Appendix. In addition, changing the solvent from acetonitrile to methanol has a minimal effect on the spectrum shape and intensity at increased temperature (Figure 3.3b). This result is also consistent with previous studies: Armand et. al previously observed a peptoid helix in methanol using 2D NMR. These results indicate that the peptoid helices are stable to both temperature and solvent.

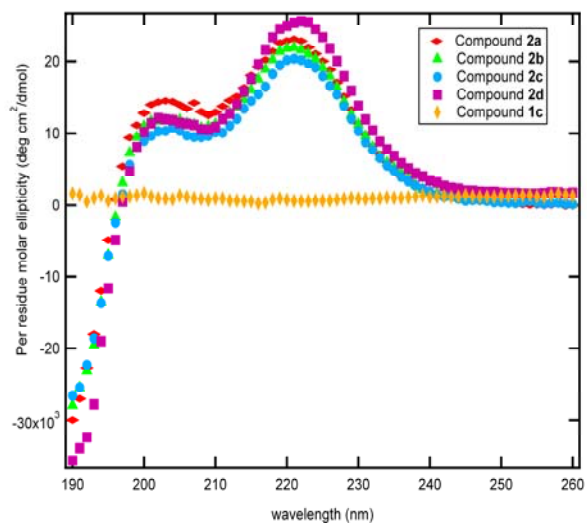


Figure 3.2. CD of Helical Peptoids. CD spectra for different chain lengths of a helical polypeptoid as well as a nonhelical polypeptoid.

All of the achiral polypeptoids studied here (**1a** to **1d**) show no net ellipticity because they do not contain chiral residues. Hence, little information about their structure can be gained using CD. Small angle neutron scattering (SANS) is thus used to probe the difference in chain statistics.

3.3.2 Small Angle Neutron Scattering

Because **2** forms a helix in solution, it was anticipated that its chain would be stiffer than the corresponding analog **1**; however, the SANS experiments detailed here show that the difference in chain stiffness is not as large as expected. Plotting the scattering intensity, I , versus the scattering angle, q , (Figure 3.3a) for the two 36-mer compounds yielded several insights about the polypeptoid chains. First, the two sequences both have typical scattering patterns for a single chain in dilute solution. It is expected that the intensity should scale with q as -2 for a random coil conformation and scale as -1 for a rod-like conformation. For a single chain, one should see the change in scaling behavior provided the appropriate q -range. For both polypeptoids, there was an exponential decrease over the q -range from 0.07 \AA^{-1} to 0.22 \AA^{-1} with a scaling of approximately -1.5 . Around $q \approx 0.22 \text{ \AA}^{-1}$, the intensity scales as $0.6 - 0.8$. The deviation from -2 scaling indicates that the polypeptoids are not forming Gaussian coils in solution, while the deviation from -1 scaling is most likely a result of noise in the data at high q .

To see the change in scaling better, a Kratky plot was used (Figure 3.3b), which plots Iq^2 vs. q . This has the effect of making the intensity data in the Gaussian regime tend toward a horizontal asymptote. The q -value at which the data deviate from this asymptote and begin to increase linearly (with an intercept coinciding with the origin) is inversely related to the persistence length. Because the intensity does not quite scale as -2 with q , it is difficult to pinpoint the exact transition. However, a good approximation was made by selecting the point at which Iq^2 deviates from a straight line passing through the origin (the red line in Figure 3.3b). A straight line passing through the origin on a Kratky plot corresponds to the scattering function for a rod; thus, the departure from this behavior indicates scattering from a molecule above its persistence length. The approximate q -value for this transition is marked by the dashed line in Figure 3.3b, and it is clear that it is quite similar for both sequences. To determine the persistence length, the equation $L_p = \frac{k}{q^*}$ was used, where k is a proportionality constant and q^* is the q -value for the transition in the Kratky plot. The value of the constant k given in literature is $6/\pi$ by Kratky²⁴ and Koyama²⁵, or 2.87 , according to Burchard and Kajiwara²⁶. The proportionality constants available indicate that the persistence length for both **1** and **2** is on the order of 0.8 nm to 1.3 nm . Thus, both **1** and **2** are more flexible than other helical polymers, including helical polypeptides. In fact, these polypeptoids have a flexibility very similar to that of polystyrene² ($\sim 1 \text{ nm}$).

Because the determination of the inflection point on the Kratky plot can be somewhat subjective, a more precise determination of the persistence length can be obtained by modeling and comparison to experimental data. The NIST NCNR analysis macro has been used to model these molecules as semi-flexible cylinders with excluded volume,²⁷ according to the Kratky and Porod

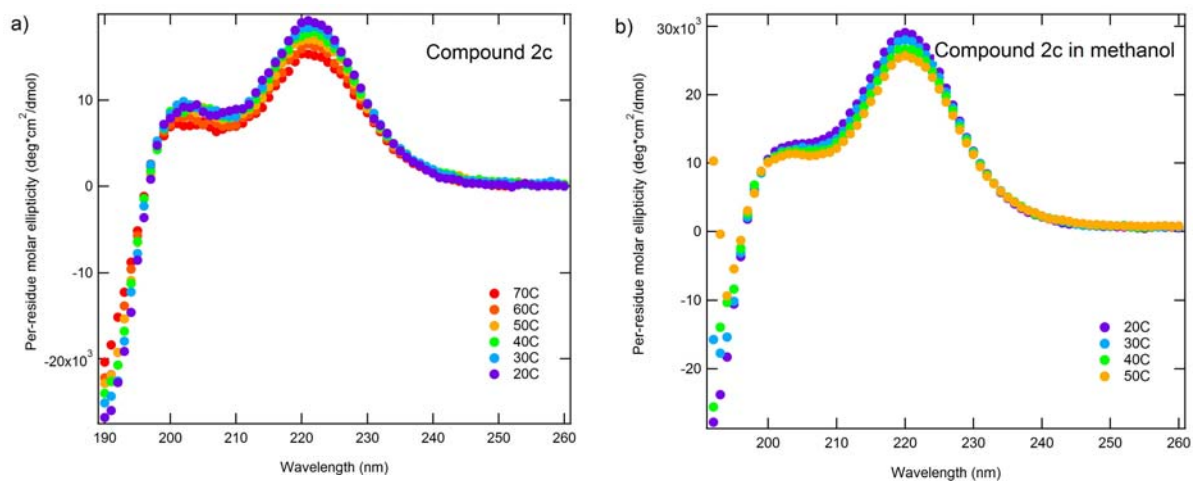


Figure 3.3. CD at Various Temperatures and in Methanol. Heating (a) and solvent (b) do not significantly affect the CD spectra of 2c.

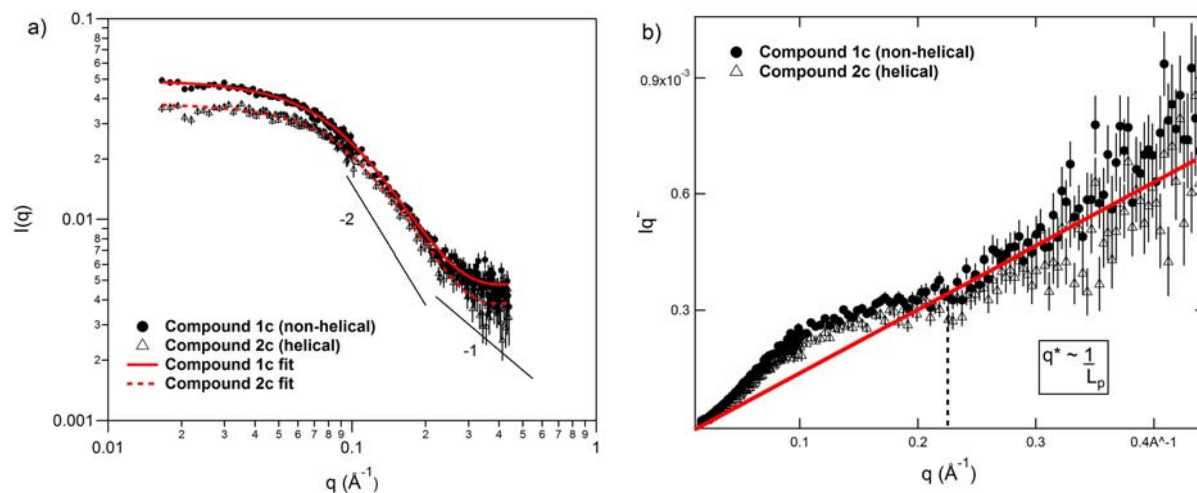


Figure 3.4. SANS of Polypeptoids. Small angle neutron scattering (SANS) shows the relatively short persistence length of both polypeptoids. The model fits are shown in (a), demonstrating good fits for the data. In addition, lines with scalings of -1 (rigid rod) and -2 (Gaussian coil) have been added as references. The intensity presented here is absolute intensity in units of cm^{-1} . The Kratky plot in (b) emphasizes the change in scaling behavior. Incoherent background has been subtracted from the data before the fits.

model of a wormlike chain. In this model, the cylinder of the chain is assumed to be composed of a series of connected locally stiff chain segments. The length of these segments is called the Kuhn length and is calculated by holding the scattering length densities and the contour length constant and fitting a Kuhn length and a radius to the semi-flexible cylinder. The equations for this model are described in the Appendix. Previously, 2D solution NMR was used to estimate a pitch of approximately 0.6 nm for a similar peptoid helix¹⁸. Based on this value for the pitch and the number of turns expected in **2c** (12, as there are 3 residues per turn), it is expected that the peptoid helix will have a contour length of approximately 7.2 nm. This value was used as the contour length for **2c**. For compound **1c**, the contour length was held at 13.0 nm, which corresponds to the distance along the peptoid backbone if all of the amide bonds are in the *trans* configuration. Table 3.2 shows the results of the fit. Interestingly, the persistence lengths are found to be quite similar: approximately 0.5 nm for **1c** and 1.0 nm for **2c**. Compound **2c** has a longer persistence length than **1c**, but it clearly is not stiff relative to other polymers containing secondary structure, such as PBLG molecules.⁶ The persistence lengths calculated from this semiflexible cylinder model match relatively well with the range estimated from the Kratky plot. Additionally, if the contour lengths are allowed to be fit by the semiflexible cylinder model, the same trend holds; compound **2c** has a shorter contour length and a larger persistence length than **1c**. These results are presented in the Appendix (Table 3.3).

The model fit indicates that the helical conformation of **2c** most likely imparts some rigidity to the polymer. However, **2c** still has a relatively short persistence length when compared to other helical polymers. Although the circular dichroism implies that the helical conformation is favored, the short persistence length indicates that the polymer can sample many different conformations and only a portion of the polymer chains adopt a full helical conformation at any given point in time. In addition, the helix observed here may simply be quite flexible. Previous intrinsic viscosity measurements of polymeric helical (*S*)-*N*-(1-phenylethyl)glycines (from 4 – 40 kg/mol) in DMF were consistent with random coil behavior such that Guo et al. concluded the persistence length of these chains must be less than 9 nm.¹¹ Flexible helical polymers have also previously been seen, such as in the case of chiral poly(2-oxazoline)s²⁸ where the polymer showed CD signal, indicating helix formation, but scattering indicated a random coil chain conformation.

Polyproline helices have also been observed to be flexible; in this case, the proline group creates a tertiary amide similar to those in the polypeptoid backbone. For tertiary amides, the energy barrier to rotation about the C-N bond is much lower than for the secondary amides that dominate proteins (REF). In addition, the *cis/trans* configurations are much closer in energy for tertiary amides,²⁹⁻³¹ and thus the isomerization can occur much more readily. Previously, the activation energy for the *cis/trans* isomerization in dimer peptoids was measured to be on the order of 17 – 20 kcal/mol,³² which is similar to the energies measured for prolyl peptide bonds.^{29, 33, 34} It is well known that prolyl peptide bonds are expected to have much higher *cis:trans* ratios (1:3) compared to planar peptide bonds (~1:1000)^{35, 36} and that the polyproline I helix, which

Table 3.2. Fitted parameters for Compounds 1 and 2 with $n = 6$. Compound 2 has a shorter contour length and a longer persistence length than 1, indicating its helical conformation imparts some stiffness to the chain.

Polypeptoid	Contour Length (nm)	Persistence Length* (nm)	Persistence Length** (nm)	Radius (nm)*
1c	13.0	0.51 ± 0.04	0.56	0.93 ± 0.2
2c	7.2	1.05 ± 0.08	1.12	0.99 ± 0.3

*As fitted by the flexible cylinder model

**As fitted by the wormlike chain model

consists of all *cis* bonds, has a much shorter persistence length than that of a traditional peptide α -helix such as PBLG.⁷ Because the peptoid helices studied here were also shown to have a relatively high *cis:trans* ratio ($\sim 2\text{-}3\text{:}1$),¹⁶⁻¹⁸ it should not be entirely unexpected that they are quite flexible. Recently, the introduction of much bulkier side groups (*N*-1-naphthylethyl) has been shown to raise the *cis:trans* ratio to $>19\text{:}1$,¹⁷ suggesting that even larger substituents can increase the energy barrier of backbone rotation and therefore increase chain stiffness.

Further information about the chain conformation and the persistence length can be obtained by evaluating the radius of gyration over a series of chain lengths and fitting the wormlike chain formula. To obtain the radius of gyration (R_g), a line was fit to the scattering data in a Guinier plot ($\ln I(q)$ vs. q^2). For compounds **1c** and **2c**, the R_g 's differ slightly, yielding a value of $14.7 \pm 0.1 \text{ \AA}$ and $13.3 \pm 0.1 \text{ \AA}$, respectively. This small decrease in R_g is most likely due to the more compact packing of the helical compound that stems from its secondary structure.

The wormlike chain formula³⁷ relates R_g to L_p :

$$R_g^2 = \frac{LL_p}{3} - L_p^2 + \frac{2L_p^3}{L} \left[1 - \frac{L_p}{L} \left(1 - e^{-L/L_p} \right) \right] \quad 3.1$$

where L is the contour length as calculated using the geometry of the molecule and the previous 2D NMR studies. Using this value and the measured R_g , it is possible to solve the equation for the persistence length. Table 3.1 shows the values for the persistence length as determined by this method. This analysis supports the conclusions drawn from the semiflexible cylinder model. The persistence length for **2c** is slightly longer than that of **1c** (1.12 nm vs. 0.56 nm), but they are both short on an absolute scale.

As calculated by the wormlike chain model, the persistence length is plotted against the number of monomers for chains of 18, 24, 36, and 48 residues. The first conclusion from this plot is that **2** consistently has a higher persistence length than **1**. Additionally, the shorter molecules have higher fitted persistence lengths, especially in the case of the helical molecule. The helical chain of 18 monomers could not fit the wormlike chain model with any reasonable value of the persistence length, indicating that the 18-mers are too short to be treated using this analysis. This is probably not due to actual differences in the number of residues present in the helical conformation as CD has shown that all of the different length polymers have very similar per-residue molar ellipticities. It is more likely that the wormlike chain model is not valid for short chains where the persistence length is not sufficiently shorter than the contour length. However, the chains of 36 and 48 monomers have reached an asymptote in their persistence length, suggesting that these polymers are of sufficient length to treat using the wormlike chain model. It is possible to fit the wormlike chain simultaneously to the polymers of different lengths and obtain a persistence length for each type of polymer. This analysis is presented in the Appendix

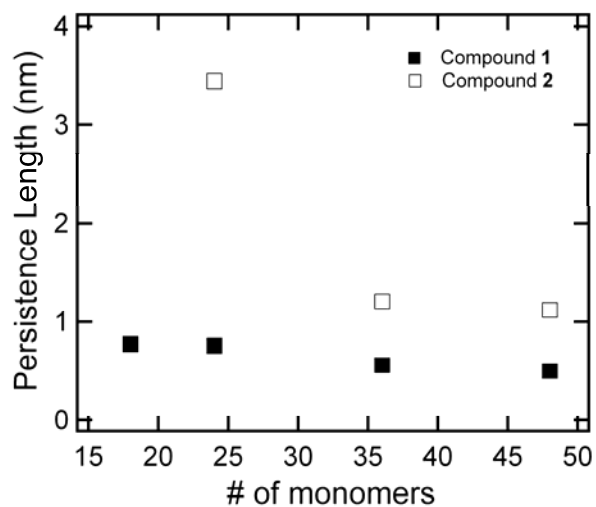


Figure 3.5. Persistence Length as a Function of Chain Length. The persistence length of polypeptoids ranging in length from 18 to 48 monomers as determined from the wormlike chain model is plotted versus the number of monomers. The shorter chains have significantly higher persistence lengths, indicating that the molecules are too short to be treated using this method.

and yields similar values for the persistence lengths.

3.4 Conclusions

In conclusion, the SANS study presented here yields two main insights into the chain conformation of polypeptoids. First, the polypeptoids studied here are inherently flexible in solution with persistence lengths ranging from 0.5 nm to 1.0 nm. Second, both the semiflexible cylinder model and the wormlike chain model indicate that inducing helicity by introducing bulky α -chiral side chains into a 36-mer polypeptoid results in a small increase in the persistence length or rigidity of the molecule. However, the fitted persistence length is still quite short in comparison to other helical polymers, suggesting that the polymer retains considerable conformational freedom. In agreement with previous 2D solution NMR studies and intrinsic viscosity measurements, the SANS data presented here indicates that helical polypeptoids with α -chiral, bulky phenyl side chains prefer an all *cis*-amide bond configuration in solution but can readily isomerize to sample other conformations as well.

3.5 Acknowledgements

We gratefully acknowledge funding from the Office of Naval Research via a Presidential Early Career Award in Science and Engineering. A.M.R. and H.K.M also gratefully acknowledge the National Science Foundation and the Department of Defense for graduate fellowships (respectively). Polypeptoid synthesis and associated chemical characterization were performed at the Molecular Foundry, a Lawrence Berkeley National Laboratory user facility supported by the Office of Science, Office of Basic Energy Sciences, U.S. Department of Energy, under Contract DE-AC02-05CH11231. The neutron scattering in this work is based on activities at the NIST Center for Neutron Research, which is supported in part by the National Science Foundation under Agreement No. DMR-0454672. Certain trade names and company products are identified to adequately specify the experimental procedure. In no case does such identification imply recommendation or endorsement by the National Institute of Standards and Technology, nor does it imply that the products are necessarily best for the purpose. A portion of this research was also performed at Oak Ridge National Laboratory. The authors thank Dr. Volker S. Urban at Oak Ridge National Laboratory for assistance on SANS data collection. The SANS studies at Oak Ridge National Laboratory's Center for Structural Molecular Biology were supported by the Office of Biological and Environmental Research, using facilities supported by the DOE, managed by UT-Battelle, LLC, under Contract No. DE-AC05-00OR22725.

3.6 Appendix

Semi-flexible Cylinder Model Equations

The following equations are used to fit the scattering data and calculate a persistence length.

$$S_{SB}(q, L, b) = S_{exv}(q, L, b) + \left[\frac{4}{15} + \frac{7}{15u} - \left(\frac{11}{15} + \frac{7}{15u} \right) \exp(-u) \right] b / L$$

$$S_{exv}(q) = w(qR_g) S_{Debye}(q, L, b) + [w(qR_g)] [C_1 (qR_g)^{-1/9} + C_2 (qR_g)^{-2/9} + C_3 (qR_g)^{-3/9}]$$

$$w(qR_g) = \left[1 + \left(\frac{qR_g}{3.12} \right)^2 + \left(\frac{qR_g}{8.67} \right)^3 \right]^{\frac{0.176}{3}}$$

$$S_{Debye}(q, L, b) = 2[\exp(-u) + u - 1] / u^2$$

$$u = R_g^2 q^2$$

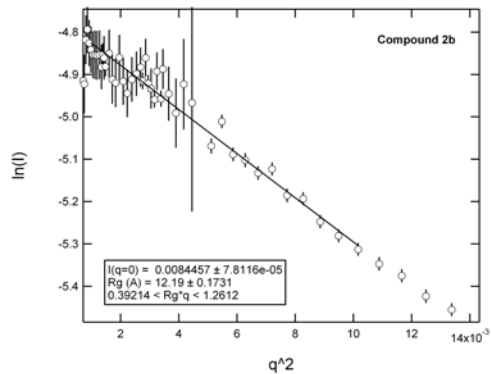
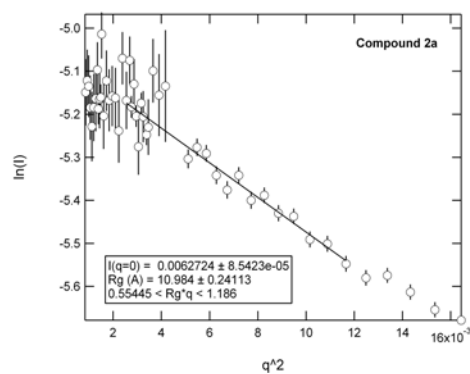
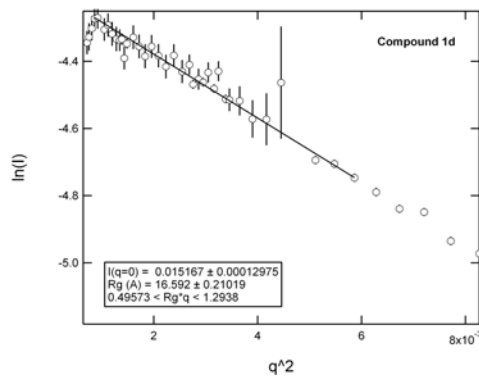
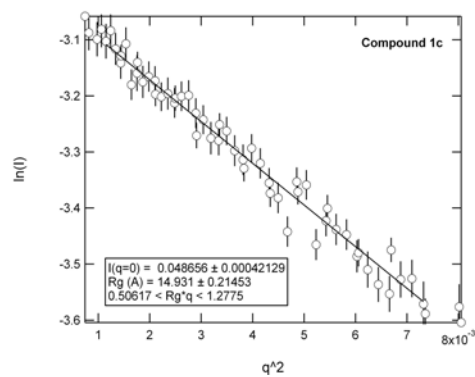
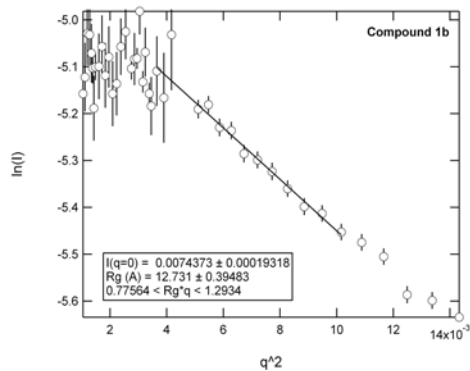
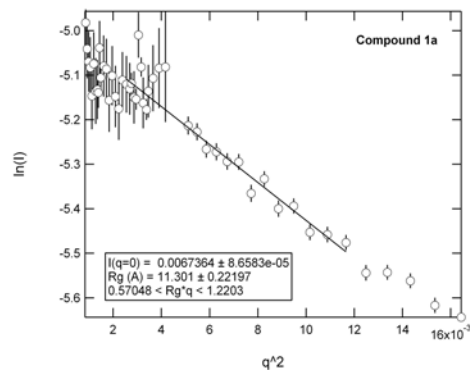
$$\theta = 0.585$$

$$b = \text{statistical segment (Kuhn) length} = 2l_p$$

$$l_p = \text{persistence length}$$

$$L = \text{contour length}$$

Guinier Plots



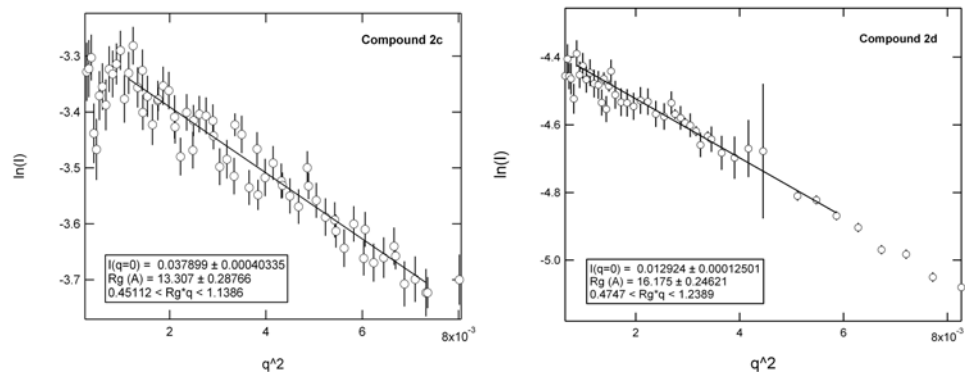


Figure 3.6. Guinier Plots of Polypeptoids. The Guinier plots were used to deduce the R_g s of Compounds 1 and 2.

Wormlike Chain Analysis for Different Polypeptoid Chain Lengths

The radius of gyration (R_g) for polypeptoids 18, 24, 36, and 48 monomers long were obtained using a Guinier analysis on the SANS scattering curves for each polypeptoid (above). This molecular weight series was measured for both the non-helical (**1**) and the helical (**2**) compound. For compound **1**, the contour length was calculated as product of the number of monomers and the length of each monomer, and the wormlike chain equation was fit to the data by changing the persistence length, L_p . For compound **2**, the contour length was calculated using the helical pitch (0.6 nm) previously measured by 2D solution NMR experiments in acetonitrile. The fitted L_p was 0.6 nm for **1** and 1.1 nm for **2**, which agrees well with the values obtained from the semiflexible cylinder model fit.

Despite the good agreement, the wormlike chain equation does not quite fit the data, especially at lower polypeptoid chain lengths for both **1** and **2**. As stated in the manuscript, this error is due to the 18 and 24-mers simply being too short to be modeled by this equation.

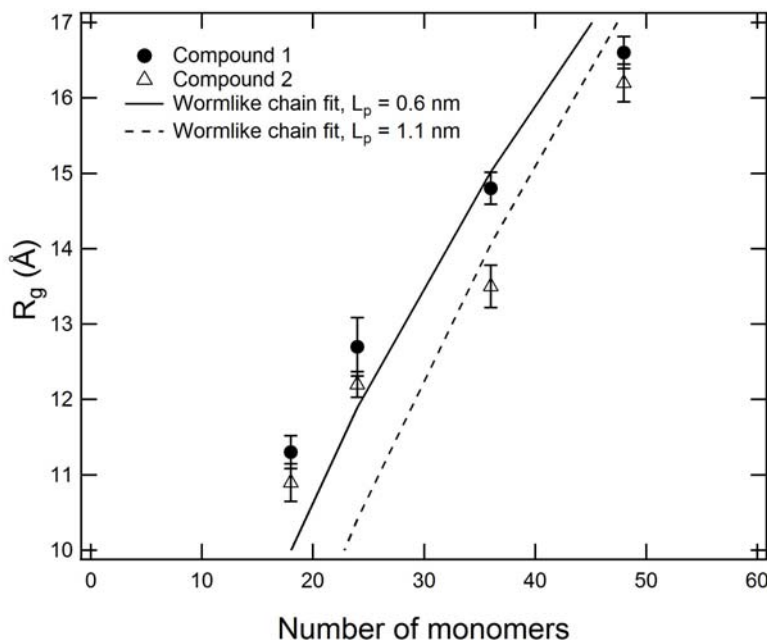


Figure 3.7. Persistence Length Fits. Fitted persistence lengths using the wormlike chain equation over a series of polypeptoid chain lengths. The fitted L_p of **2** is longer than that of **1**, indicating it is indeed stiffer.

Persistence Length of a Polypeptoid with a Racemic Mixture of Monomers

As another point of comparison, a 36-mer polypeptoid was synthesized using the same monomers as **2** but with a racemic mixture instead of an enantiomerically pure mixture of the α -methylbenzyl side chain. The structure for this compound (compound **3**) is given in Figure 3.8. Circular dichroism data is provided in Figure 3.9, showing that **3** is truly racemic and that there is no net ellipticity due to an equal mixture of *R* and *S* enantiomers. The helical structure of **2** results from the steric hindrance of the bulky side chains with the same chirality; thus, the racemic nature of **3** should disrupt any helical structure.

SANS measurements probed the structure of **3** in the same way as for **1** and **2**. A Guinier analysis of the scattering curve yields an R_g of $14.5 \pm 0.1 \text{ \AA}$, which is closer to the value of the R_g for **1** (14.7 \AA) than **2** (13.3 \AA). In addition, using the wormlike chain formula and the semiflexible cylinder model to calculate a persistence length for **3** yields a value of 0.62 nm and 0.39 nm , respectively. These results indicate that **3** is quite flexible, which is similar to **1** and **2**.

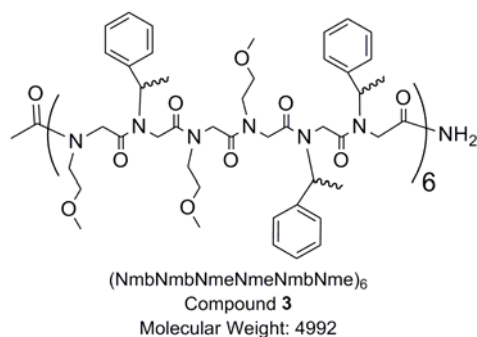


Figure 3.8. Structure of Racemic Peptoid. **3** contains a racemic mixture of α -chiral side chains and is proposed to be non-helical.

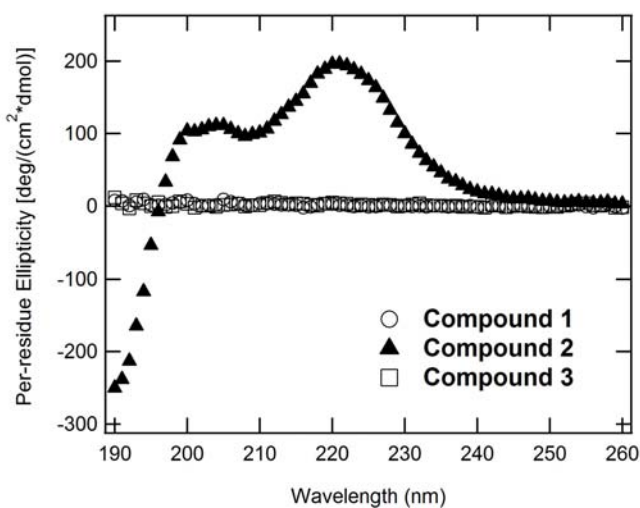


Figure 3.9. CD of Racemic Peptoid. Compound **3** shows no net ellipticity, confirming its racemic nature.

Semiflexible Cylinder Model of the 36-mer Polypeptoids Using a Fitted Contour Length

The semiflexible cylinder model was allowed to fit the contour length, persistence length, and cylinder radius simultaneously. Using this model, the non-helical sequence, **1**, has a much longer contour length than the chiral sequence, **2**. The secondary structure of **2c** is thought to cause the contour length to be much shorter as the polymer is adopting a helix conformation with the majority of the amide bonds in the *cis* geometry. This fitted value is less than the value estimated by NMR (7.2 nm) by about 2 nm. The fitted contour length for **1c** is less than the calculated fully extended (all-*trans*) chain length (13 nm), which is reasonable given that the flexible polypeptoid backbone chain likely exists with both *cis* and *trans* amide bonds at any given moment. Furthermore, a contour length of 8.5 ± 0.6 nm is obtained for compound **3**, suggesting that **3** is not as compact as **2c**. The fitted persistence length is also smaller for **3** (0.9 ± 0.02 nm) than **2c** (1.97 ± 0.17 nm), supporting the idea that the racemic nature of **3** results in a more flexible molecule. The results of this model fit are consistent with the trends identified from the semiflexible cylinder fit with a fixed contour length and the wormlike chain equation fit, but there is a larger error in the persistence length.

Table 3.3. Fitted Peptoid Parameters allowing Contour Length to Fluctuate. The contour length and the persistence length have been fitted using the semiflexible cylinder model. Consistent with other analyses explored in this paper, the helical compound has a slightly higher persistence length than the non-helical version.

Polypeptoid	Contour Length (nm)*	Persistence Length* (nm)	Radius (nm)*
1	10.58 ± 4.8	0.66 ± 0.03	0.93 ± 0.2
2	4.93 ± 2.8	1.97 ± 0.17	0.99 ± 0.3
3	8.5 ± 0.6	0.9 ± 0.02	0.96 ± 0.2

Circular Dichroism Measurements

Extensive CD measurements have been taken at various temperatures and solvents. The most relevant graphs have been included in the manuscript. The remaining data is summarized here.

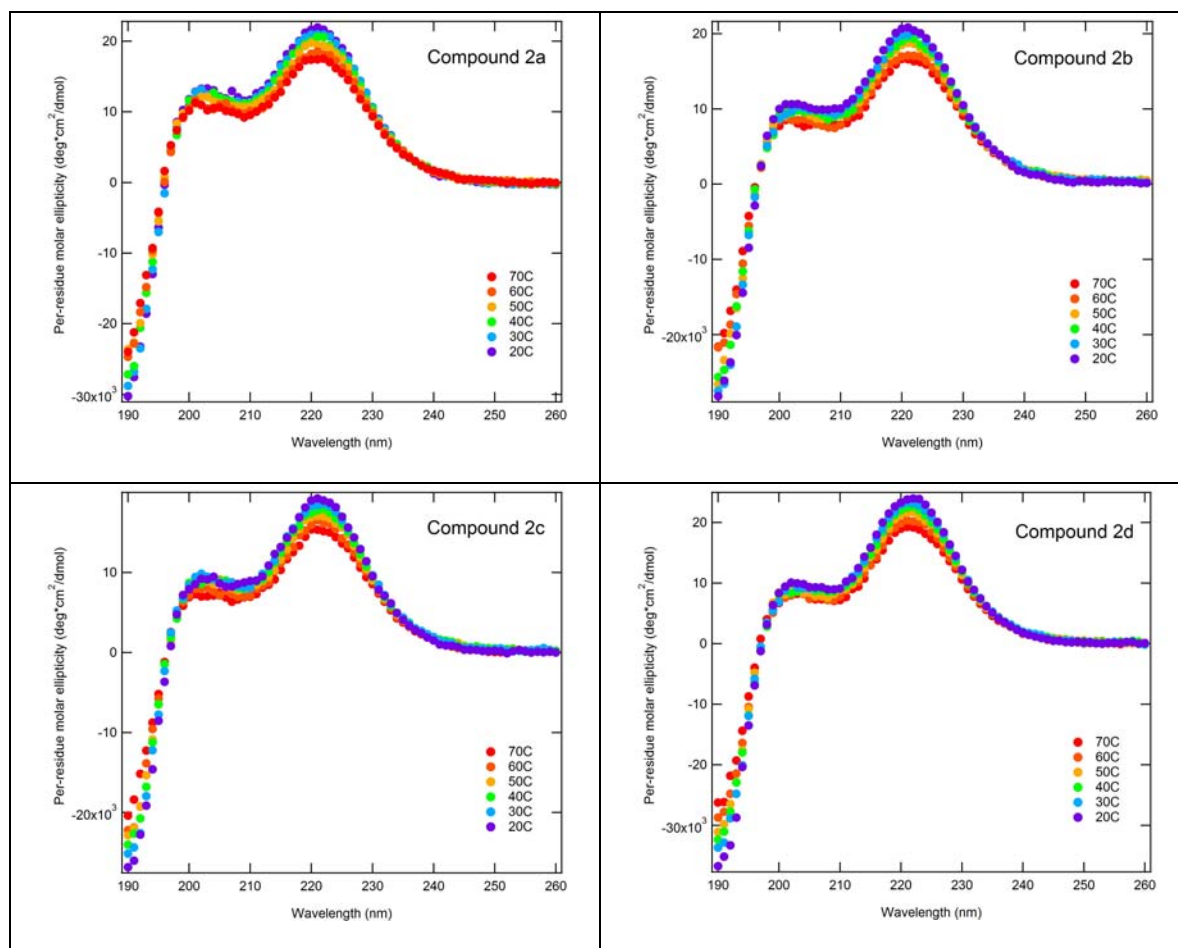


Figure 3.10. Variable Temperature CD. Circular dichroism at varying temperatures for each helical polypeptoid.

3.7 References

1. Gettinger, C. L.; Heeger, A. J.; Drake, J. M.; Pine, D. J., A Photoluminescence Study of Poly(phenylene vinylene) Derivatives - The Effect of Intrinsic Persistence Length. *J. Chem. Phys.* **1994**, *101* (2), 1673-1678.
2. Brulet, A.; Boue, F.; Cotton, J. P., About the experimental determination of the persistence length of wormlike chains of polystyrene. *Journal De Physique Ii* **1996**, *6* (6), 885-891.
3. Terao, K.; Terao, Y.; Teramoto, A.; Nakamura, N.; Terakawa, I.; Sato, T., Stiffness of polysilylenes depending remarkably on a subtle difference in chiral side chain structure: Poly{n-hexyl-[(S)-2-methylbutyl]silylene} and poly{n-hexyl-[(S)-3-methylpentyl]silylene}. *Macromolecules* **2001**, *34* (8), 2682-2685.
4. Muller-Spath, S.; Soranno, A.; Hirschfeld, V.; Hofmann, H.; Ruegger, S.; Reymond, L.; Nettels, D.; Schuler, B., Charge interactions can dominate the dimensions of intrinsically disordered proteins. *Proc. Natl. Acad. Sci. U. S. A.* **2010**, *107* (33), 14609-14614.
5. Gu, H.; Nakamura, Y.; Sato, T.; Teramoto, A.; Green, M. M.; Andreola, C., Global conformations of chiral polyisocyanates in dilute solution. *Polymer* **1999**, *40* (4), 849-856.
6. Temyanko, E.; Russo, P. S.; Ricks, H., Study of rodlike homopolypeptides by gel permeation chromatography with light scattering detection: Validity of universal calibration and stiffness assessment. *Macromolecules* **2001**, *34* (3), 582-586.
7. Best, R. B.; Merchant, K. A.; Gopich, I. V.; Schuler, B.; Bax, A.; Eaton, W. A., Effect of flexibility and cis residues in single-molecule FRET studies of polyproline. *Proc. Natl. Acad. Sci. U. S. A.* **2007**, *104* (48), 18964-18969.
8. Murnen, H. K.; Rosales, A. M.; Jaworsk, J. N.; Segalman, R. A.; Zuckermann, R. N., Hierarchical Self-Assembly of a Biomimetic Diblock Copolypeptoid into Homochiral Superhelices. *J. Am. Chem. Soc.* **2010**, *132* (45), 16112-16119.
9. Nam, K. T.; Shelby, S. A.; Choi, P. H.; Marciel, A. B.; Chen, R.; Tan, L.; Chu, T. K.; Mesch, R. A.; Lee, B. C.; Connolly, M. D.; Kisielowski, C.; Zuckermann, R. N., Free-floating ultrathin two-dimensional crystals from sequence-specific peptoid polymers. *Nat. Mater.* **2010**, *9* (5), 454-460.
10. Rosales, A. M.; Murnen, H. K.; Zuckermann, R. N.; Segalman, R. A., Control of Crystallization and Melting Behavior in Sequence Specific Polypeptoids. *Macromolecules* **2010**, *43* (13), 5627-5636.
11. Guo, L.; Li, J. H.; Brown, Z.; Ghale, K.; Zhang, D. H., Synthesis and Characterization of Cyclic and Linear Helical Poly(alpha-peptoid)s by N-Heterocyclic Carbene-Mediated Ring-Opening Polymerizations of N-Substituted N-Carboxyanhydrides. *Biopolymers* **2011**, *96* (5), 596-603.
12. "Thermodynamics of Polymer Blends", N. P. B., H.B. Eitouni, Physical Properties of Polymers Handbook, Second Edition, Chapter 19, p. 339-356, J.E. Mark, editor, Springer, New York, 2007.
13. Fowler, S. A.; Blackwell, H. E., Structure-function relationships in peptoids: Recent advances toward deciphering the structural requirements for biological function. *Organic & Biomolecular Chemistry* **2009**, *7* (8), 1508-1524.
14. Kirshenbaum, K.; Barron, A. E.; Goldsmith, R. A.; Armand, P.; Bradley, E. K.; Truong, K. T. V.; Dill, K. A.; Cohen, F. E.; Zuckermann, R. N., Sequence-specific polypeptoids: A diverse family of heteropolymers with stable secondary structure. *Proc. Natl. Acad. Sci. U. S. A.* **1998**, *95* (8), 4303-4308.
15. Yoo, B.; Kirshenbaum, K., Peptoid architectures: elaboration, actuation, and application. *Current Opinion in Chemical Biology* **2008**, *12* (6), 714-721.
16. Armand, P.; Kirshenbaum, K.; Falicov, A.; Dunbrack, R. L.; Dill, K. A.; Zuckermann, R. N.; Cohen, F. E., Chiral N-substituted glycines can form stable helical conformations. *Folding & Design* **1997**, *2* (6), 369-375.
17. Stringer, J. R.; Crapster, J. A.; Guzei, I. A.; Blackwell, H. E., Extraordinarily Robust Polyproline Type I Peptoid Helices Generated via the Incorporation of $\hat{I}\pm$ -Chiral Aromatic N-1-Naphthylethyl Side Chains. *Journal of the American Chemical Society* **2011**.
18. Armand, P.; Kirshenbaum, K.; Goldsmith, R. A.; Farr-Jones, S.; Barron, A. E.; Truong, K. T. V.; Dill, K. A.; Mierke, D. F.; Cohen, F. E.; Zuckermann, R. N.; Bradley, E. K., NMR determination of the

- major solution conformation of a peptoid pentamer with chiral side chains. *Proc. Natl. Acad. Sci. U. S. A.* **1998**, *95* (8), 4309-4314.
19. Wu, C. W.; Sanborn, T. J.; Huang, K.; Zuckermann, R. N.; Barron, A. E., Peptoid oligomers with alpha-chiral, aromatic side chains: Sequence requirements for the formation of stable peptoid helices. *J. Am. Chem. Soc.* **2001**, *123* (28), 6778-6784.
 20. Wu, C. W.; Sanborn, T. J.; Zuckermann, R. N.; Barron, A. E., Peptoid oligomers with alpha-chiral, aromatic side chains: Effects of chain length on secondary structure. *J. Am. Chem. Soc.* **2001**, *123* (13), 2958-2963.
 21. Figliozzi, G. M.; Goldsmith, R.; Ng, S. C.; Banville, S. C.; Zuckermann, R. N., Synthesis of N-substituted glycine peptoid libraries. *Combinatorial Chemistry* **1996**, *267*, 437-447.
 22. Kline, S. R., Reduction and analysis of SANS and USANS data using IGOR Pro. *J. Appl. Crystallogr.* **2006**, *39*, 895-900.
 23. Kelly, S. M.; Jess, T. J.; Price, N. C., How to study proteins by circular dichroism. *BBA-Proteins Proteomics* **2005**, *1751* (2), 119-139.
 24. Kratky, O., Das Studium Geloster Fadenmolekule Mittels Der Rontgenkleinwinkelmethode. *Kolloid-Zeitschrift and Zeitschrift Fur Polymere* **1962**, *182* (1-2), 7-&.
 25. Koyama, R., Light-Scattering of Stiff Chain Polymers. *Journal of the Physical Society of Japan* **1973**, *34* (4), 1029-1038.
 26. Burchard, W.; Kajiwara, K., Statistics of Stiff Chain Molecules. 1. Particle Scattering Factor. *Proceedings of the Royal Society of London Series a-Mathematical and Physical Sciences* **1970**, *316* (1525), 185-&.
 27. Pedersen, J. S.; Schurtenberger, P., Scattering functions of semiflexible polymers with and without excluded volume effects. *Macromolecules* **1996**, *29* (23), 7602-7612.
 28. Bloksma, M. M.; Rogers, S.; Schubert, U. S.; Hoogenboom, R., Secondary structure formation of main-chain chiral poly(2-oxazoline)s in solution. *Soft Matter* **2010**, *6* (5), 994-1003.
 29. Wedemeyer, W. J.; Welker, E.; Scheraga, H. A., Proline cis-trans isomerization and protein folding. *Biochemistry* **2002**, *41* (50), 14637-14644.
 30. Zimmerman, S. S.; Scheraga, H. A., Stability of Cis, Trans, and Nonplanar Peptide Groups. *Macromolecules* **1976**, *9* (3), 408-416.
 31. Maigret, B.; Perahia, D.; Pullman, B., Molecular Orbital Calculations on Conformation of Polypeptides and Proteins. 4. Conformation of Prolyl and Hydroxyprolyl Residues. *J. Theor. Biol.* **1970**, *29* (2), 275-&.
 32. Sui, Q.; Borchardt, D.; Rabenstein, D. L., Kinetics and equilibria of cis/trans isomerization of backbone amide bonds in peptoids. *J. Am. Chem. Soc.* **2007**, *129* (39), 12042-12048.
 33. Fischer, S.; Dunbrack, R. L.; Karplus, M., Cis-Trans Imide Isomerization of the Proline Dipeptide. *J. Am. Chem. Soc.* **1994**, *116* (26), 11931-11937.
 34. Steinberg, I. Z.; Harrington, W. F.; Berger, A.; Sela, M.; Katchalski, E., The Configurational Changes of Poly-L-proline in Solution. *J. Am. Chem. Soc.* **1960**, *82* (20), 5263-5279.
 35. Weiss, M. S.; Jabs, A.; Hilgenfeld, R., Peptide bonds revisited. *Nat. Struct. Biol.* **1998**, *5* (8), 676-676.
 36. Chakrabarti, P.; Pal, D., The interrelationships of side-chain and main-chain conformations in proteins. *Prog. Biophys. Mol. Biol.* **2001**, *76* (1-2), 1-102.
 37. Benoit, H.; Doty, P., Light Scattering from Non-Gaussian Chains. *The Journal of Physical Chemistry* **1953**, *57* (9), 958-963.

Chapter 4. Tunable Phase Behavior of Polystyrene-Polypeptoid Block Copolymers

Reproduced with permission from Adrienne M. Rosales, Bryan L. McCulloch, Ronald N. Zuckermann, and Rachel A. Segalman, *Macromolecules*, 2012, 45(15), pp. 6027-6035. Copyright (2012), American Chemical Society.

Block copolymers with tunable compositions offer the ability to directly control the interaction strength between the two blocks and therefore polymer properties. The miscibility of an A-B block copolymer can be increased by introducing B or B-like comonomers into the A block, and literature has shown that both the amount and the distribution of these comonomers affect the compatibility of the two blocks. Sequence-defined block copolymers in which one can exactly control the composition and comonomer distribution provide a unique opportunity to control the overall strength of segregation. Here, sequence-defined block copolymers have been synthesized via azide-alkyne coupling using polystyrene and sequence-specific polypeptoids (N-substituted glycines) with 2-methoxyethyl side chains. These polystyrene-polypeptoid block copolymers readily self-assemble into hexagonally-packed and lamellar morphologies. N-(2-phenylethyl)glycine residues, which have a styrene-like side chain, were introduced throughout the polypeptoid block to increase the compatibility with the polystyrene block. As the compatibility increased, the strength of segregation and therefore the block copolymer order-disorder transitions decreased. The polystyrene-polypeptoid block copolymers provide a tunable platform for further studies on the effect of composition and sequence design on self-assembly and block copolymer properties.

4.1 Introduction

Well-defined polymers with tunable compositions are desirable because they offer control over polymer properties. In the case of block copolymers, where the volume fraction of the A or B monomer dictates the self-assembled morphology,¹ the introduction of B or B-like monomers into the A block (or vice versa) can allow the effective interaction parameter to be tuned by increasing the compatibility of the two blocks. The ability to directly control this interaction between the two blocks (or the strength of segregation of the block copolymer) has an important impact on the tunability of the order-disorder transition (ODT) temperature, which in turn relates to polymer processing temperatures and mechanical properties.

The introduction of both A and B-like monomers into one block requires a synthesis method with control over the comonomer distribution. It has been shown that gradient, blocky, and statistical distributions all affect the strength of segregation for a given composition.²⁻⁸ For instance, Beckingham and Register found that a block-random architecture (A-B/A) decreases the interaction energy density between styrene and isoprene by a factor of 8 compared to A-B block copolymers (for a composition of 0.5).² In addition, Hodrokoukes et al. found that increasing the size of a tapered interface for styrene-isoprene block copolymers systematically

increased the compatibility and that inversely tapered distributions further lowered the strength of segregation.⁸ Thus, in order to have a controlled effect on the strength of segregation, control over both composition and comonomer distribution is required.

Classical polymerization methods offer various levels of control over comonomer distribution. Radical and anionic polymerization methods are often sensitive to differences in the reactivity ratios of the monomers,^{9, 10} leading to the formation of gradient or blocky sequences, though completely statistical copolymers are more difficult. While previous research has shown that the addition of modifiers to anionic copolymerizations can effectively tune the randomness of the comonomers,^{2, 4, 11} the type and concentration of the modifier is system-dependent and does not affect all comonomer pairs equally. In addition, copolymerization leads to heterogeneous batches (not every polymer chain is the same), further complicating the characterization of the comonomer distribution. Sequence-defined syntheses, however, offer the freedom to completely control both polymer composition and comonomer distribution.

Despite recent advances in sequence control in polymerization chemistry,^{10, 12-17} the synthesis of biological and biomimetic polymers perhaps offers the most versatility and control over the composition of a polymer. Because monomer sequence is a fundamental attribute of the structure and function of biological polymers, monodisperse polymers are typically synthesized by solid-phase, step-by-step methods, although genetic engineering techniques have also been used.¹⁸⁻²⁰ Recently, there has been much interest in the self-assembly of block copolymers containing a sequence-defined biopolymer.²¹⁻²⁴ However, traditional biopolymers such as polypeptides often exhibit uncontrollable hydrogen bonding interactions or crystallinity in the solid state that can lead to rigid chain shapes and inhibit self-assembly. In this work, block copolymers with tunable compositions have been synthesized from polystyrene and a sequence-defined peptoid polymer.

Polypeptoids, or N-substituted glycines, are peptidomimetic polymers that offer several advantageous properties for materials studies in the solid state.²⁵ The N-substitution in the polypeptoid backbone removes intermolecular hydrogen bonding, and the achiral backbone leads to a flexible polymer chain (persistence length of approximately 0.5 – 1 nm).²⁶ These simplified interactions allow the design of polymer properties through the choice of side chains. Polypeptoids are sequence specific and have absolute monodispersity because they can be synthesized by solid-phase methods,^{27, 28} and this control over the exact placement and choice of monomers leads to further control over the thermal, mechanical, and conformational properties of the peptoid polymer chain.^{25, 26, 29} In addition, the chemical diversity of polypeptoids is vast because the side chain moiety is introduced via displacement with a primary amine (of which there are literally hundreds readily available), meaning that one can easily tune the interaction strength of the polypeptoid with neighboring polymer chains. For example, peptoid polymers have been shown to have interesting self-assembly properties in solution.³⁰⁻³⁴ All of these factors indicate that polypeptoids are ideally suited for exploring self-assembly in the solid state with composition and sequence control.

Here, it is shown that polypeptoids are an excellent system for designing block copolymers with tunable compositions and hence ODTs. Block copolymers were synthesized from polystyrene and polypeptoids using azide-alkyne coupling. The polypeptoids had methoxyethyl side chains and ranged from exactly 18 to 48 monomers in length. As homopolymers, these peptoids are amorphous with glass transitions below that of polystyrene, as shown by differential scanning calorimetry. Several of the block copolymers self-assembled in the solid state with morphologies similar to those expected from classical block copolymers with analogous volume fractions. Upon the introduction of a comonomer with a styrene-like side chain into the polypeptoid block, the strength of segregation was decreased, and the order-disorder transition for all block copolymers decreased. These block copolymers set the stage for the investigation of the effect of more complex interactions and monomer sequences on self-assembly through the manipulation of the polypeptoid block.

4.2 Experimental Methods

Synthesis of Chloride End-Functionalized Polystyrene. Nitroxide-mediated radical polymerization was used to synthesize polystyrene with a chloride end group. The alkoxyamine initiator, *N-tert-butyl-O-[1-(4-chloromethylphenyl)ethyl]-N-(2-methyl-1-phenylpropyl)hydroxylamine* (Cl-BzEt-TIPNO), was synthesized following a previously published procedure.³⁵ Styrene monomer (Sigma-Aldrich, St. Louis, MO) was filtered over basic alumina to remove the inhibitor. Depending on the desired molecular weight, calculated amounts of the filtered styrene and the Cl-BzEt-TIPNO initiator were added to the reaction flask and degassed by three freeze-pump-thaw cycles. The reaction mixture was heated in an oil bath at 115°C overnight. The reaction mixture was then precipitated in methanol to give a white powder.

Synthesis of Azide End-Functionalized Polystyrene. Chloride end-functionalized polystyrene (0.15 mmol) was dissolved in DMF (100 mL), and 25 molar equivalents of sodium azide were added. The reaction mixture was stirred overnight at 60°C. The polymer was then precipitated in methanol to yield a white powder.

Synthesis of Alkyne End-Functionalized Polypeptoids. Polypeptoids were synthesized on a custom robotic synthesizer or a commercial Aapptec Apex 396 robotic synthesizer according to previously published methods.^{25, 27} As previously described, all primary amine monomers were added in a stepwise fashion. The final monomer on the N-terminus of the polypeptoid was functionalized with an alkyne using propargylamine (Sigma-Aldrich, St. Louis, MO). All polypeptoids were acetylated on the resin and purified as previously described.²⁵ Molecular weights of the polypeptoids were determined using an Applied Biosystems 4800 series MALDI-TOF with a laser power of 5000. MALDI samples were prepared using a 1:1 ratio of polypeptoid in acetonitrile (1 mg/mL) to 1,8,9-anthracenetriol (10 mg/mL in THF). The polypeptoid sequences investigated in this work are shown in Figure 4.2, and details of the molecules synthesized are given in Table 4.1. Peptoid purities were determined by analytical HPLC and refer to the amount of exactly monodisperse peptoid of the desired length. The major observed

side products for the polypeptoids synthesized here do not contain the acetyl end group or the alkyne functional group and do not participate in the azide-alkyne coupling.

Synthesis of Polypeptoid-Polystyrene Block Copolymers. The block copolymers were synthesized by azide-alkyne coupling, as shown in Figure 4.1, using a modification of the procedure described by Holub et. al.³⁶ The azide end-functionalized polystyrene (1.8 mM) was allowed to react with 2 equivalents of the alkyne end-functionalized polypeptoid (3.7 mM), 5 equivalents of Cu(I)I (9.5 mM), 6 equivalents of ascorbic acid (10.8 mM), and 10 equivalents of DIPEA (18 mM) in DMF in a 20 mL scintillation vial. The vial was purged with nitrogen, capped, and sealed with Parafilm. To ensure that the reactants were dissolved, the vial was placed into a bath sonicator (Fisher Scientific, Solid State Ultrasonic FS-9) for 10 minutes. It was then shaken at room temperature overnight. Upon completion of the reaction, the polymer was precipitated in methanol if the polystyrene block was large (8800 g/mol) and washed with acetonitrile to remove excess polypeptoid homopolymer. If the polystyrene block was small (4800 g/mol and 3300 g/mol), the polymer was precipitated in water, redissolved in THF, and stirred with basic alumina for 30 min to remove the copper catalyst. Following filtration of the basic alumina, the block copolymer was purified using a Viscotek preparative GPC equipped with a UV wavelength detector (260 nm). Chloroform was used as the solvent. After purification, the polypeptoid-polystyrene block copolymers were dissolved in appropriate glacial acetic acid/acetonitrile/water mixtures and lyophilized twice to obtain a fluffy white powder. A comprehensive list of the block copolymers synthesized is given in Table 4.2.

Gel Permeation Chromatography (GPC). The molecular weights and polydispersities of the polystyrene homopolymers were measured on a Viscotek SEC using Viscotek GMH_{HR}-M columns. Refractive index was used for molecular weight determination with the use of polystyrene calibration standards (Polymer Laboratories). Using a flow rate of 1 mL/min, the mobile phase was DMF with 0.2% w/v LiCl at 70°C. Representative GPC traces for the synthesized block copolymers are shown in Figure 4.3.

Density. The density of the polypeptoids was measured to be 1.18 ± 0.02 g/cm³ using a density gradient column at room temperature with an aqueous sucrose gradient. The density gradient was built from a 20% w/v sucrose solution (1.08 g/cm³) and a 60% w/v sucrose solution (1.29 g/cm³) using a BioComp Gradient Master (BioComp Instruments Inc., Canada). The linearity of the density gradient column was confirmed using glass beads of known density. The measured density was used to calculate ϕ_{peptoid} , the volume fraction of the polypeptoid in the polystyrene-polypeptoid block copolymers.

Differential Scanning Calorimetry (DSC). DSC was performed on a Thermal Advantage Q20 calorimeter equipped with a Refrigerated Cooling System RCS40 (both TA Instruments, New Castle, DE). Homopolymer and block copolymer samples were hermetically sealed into aluminum pans. Each sample was taken through five temperature cycles. In each cycle, the

sample was equilibrated at -40°C, heated to 180°C at 10°C/min, then cooled back to -40°C at 10°C/min. The first cycle was discarded to erase the thermal history of the sample.

Small Angle X-Ray Scattering (SAXS). Samples were prepared by hot pressing the block copolymers into aluminum washers at 120°C - 150°C using a Carver Press at 5000 lbs. Samples were pressed until 1 mm thick polymer disks were formed in the interior of the washer. One side of the sample washer was glued to a Kapton window, and the entire sample cell was then annealed in a vacuum oven (10^{-9} torr, at various temperatures between 100°C and 150°C depending on the block copolymer) for 24 hours. After annealing, a second Kapton window was glued to the washer to seal the polymer sample completely.

SAXS was conducted at beamline 7.3.3 at the Advanced Light Source (ALS) and beamline 1-4 at the Stanford Synchrotron Radiation Lightsource (SSRL). At the ALS, the beamline was configured with an X-ray wavelength of $\lambda=1.240$ Å and focused to a spot size of 50 μm by 300 μm . Two-dimensional scattering patterns were collected on an ADSC CCD detector with an active area of 188 mm by 188 mm. The isotropic scattering patterns were radially averaged, and the scattering intensity was corrected with the post-ion chamber intensity using Nika³⁷ version 1.18. At SSRL, the beamline was configured with an X-ray wavelength of $\lambda=1.488$ Å and focused to a 0.5 mm diameter spot. A single quadrant of a two-dimensional scattering pattern was collected on a CCD detector with an active area of 25.4 by 25.4 mm. The two-dimensional profiles were radially averaged and corrected for detector null signal, dark current, and empty cell scattering.

Transmission Electron Microscopy (TEM). Bulk block copolymer samples were prepared by casting thick films (several microns) from THF onto molded epoxy resins and annealing in a vacuum oven overnight. After annealing, a thin layer of gold was evaporated onto the sample, which was then fully encapsulated in epoxy resin. The samples were microtomed and selectively stained with RuO₄ vapor for 45 minutes. TEM imaging was conducted on a JEOL JEM-2100 microscope at an operating voltage of 200 kV.

4.3 Results and Discussion

4.3.1 Synthesis of Polypeptoids and Polystyrene-Polypeptoid Block Copolymers

Two sets of polypeptoids ranging in length from 18 monomers to 48 monomers were successfully synthesized, as shown in Table 4.1. The first set of polypeptoids was designed to be amorphous and soluble in similar solvents to polystyrene. Thus, N-(2-methoxyethyl)glycine was chosen to incorporate a neutral, polar side chain into the peptoid polymer. The second set of polypeptoids was designed to contain similar side groups to polystyrene; to achieve this chemical similarity, 50% of the monomers were N-(2-phenylethyl)glycine residues. Figure 4.2 shows the chemical structures for both sets of these polypeptoids.

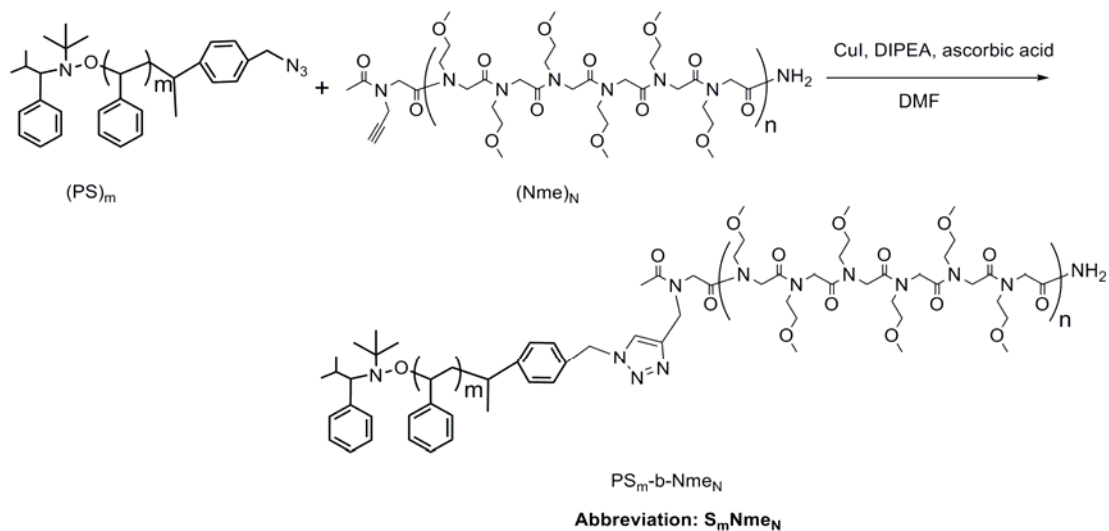


Figure 4.1. Conjugation reaction scheme for polystyrene and an example polypeptoid.

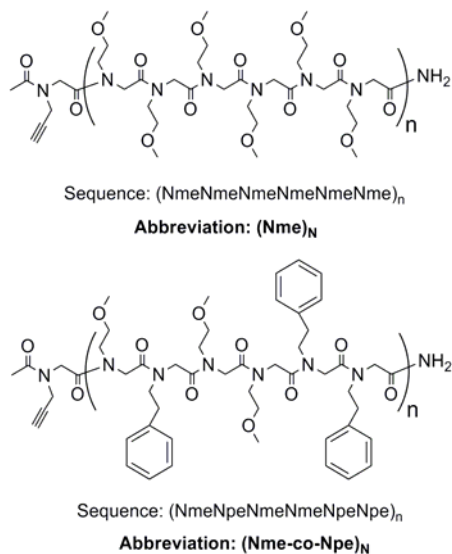


Figure 4.2. Peptoid structure with alkyne functionalization. Nme = N-(2-methoxyethyl)glycine, Npe = N-(2-phenylethyl)glycine. The hexapeptoid repeat unit is n, and N is the total number of repeat units.

Polystyrene was prepared using nitroxide-mediated radical polymerization with an alkoxyamine initiator.³⁵ All polystyrene polymers synthesized had low polydispersities of approximately 1.1 (Table 4.2). The polypeptoids were conjugated to polystyrene using azide-alkyne coupling, as shown in Figure 4.1. Various molecular weights of polystyrene were chosen to access a wide range of polypeptoid volume fractions. Details of the block copolymers are given in Table 4.2, and representative GPC traces for the synthesized block copolymers are given in Figure 4.3. The shifts in the GPC retention times indicate the successful conjugation of the polypeptoid blocks to the polystyrene blocks.

4.3.2 Thermal Properties of Polypeptoids.

The side chains in a given peptoid polymer have a large influence on the thermal properties of the chain.²⁵ Here, homopolymer peptoids of N-(2-methoxyethyl)glycine (Nme, Figure 4.2) and copolymers of Nme and N-(2-phenylethyl)glycine (Nme-co-Npe, Figure 4.2) were amorphous polymers with measurable glass transition temperatures (T_g). As shown in Figure 4.4, all Nme polypeptoids studied showed a T_g at approximately 45°C. Upon incorporation of 50% aromatic residues into the polypeptoid chain, the T_g increased for all chain lengths. The T_g increased from approximately 58°C for an Nme-co-Npe copolymer that was 18 monomers in length to approximately 70°C for an Nme-co-Npe copolymer 48 monomers in length. Previously, it was shown that a homopolymer peptoid containing 100% Npe residues crystallized readily with a melting transition at 225°C.²⁵ In addition, when only two (of fifteen) N-(3-phenylpropyl)glycine residues were inserted into that homopolypeptoid, the crystallinity was completely disrupted. Here, spacing the phenylethyl side chains with methoxyethyl residues prevents the aromatic side chains from crystallizing, although the aromatic side chains do contribute to the glassiness of the polypeptoid chain. As the total number of aromatic residues and the chain length increase, the T_g also increases slightly, whereas for the Nme homopolymers, all chain lengths showed about the same T_g .

4.3.3 Self-assembly of PS-*b*-Nme block copolymers

Block copolymers were synthesized from Nme blocks that were *exactly* 18, 24, 36, and 48 monomers long and polystyrene blocks that were *approximately* 32, 48, and 84 monomers long with a polydispersity of 1.1. DSC heating traces for a subset of these diblocks are presented in Figure 4.5 to show a representative sample of their thermal behavior. The derivative heat flow is plotted so that the glass transitions of the two blocks can be seen more clearly (as peaks rather than inflection points). For these PS-*b*-Nme block copolymers (hereafter denoted as S_mNme_N , where m is the approximate number of repeat units of the polystyrene block and N is the total number of repeat units of the polypeptoid block), the DSC endotherms can indicate the presence of microphase separation if two T_g s are present.

Table 4.1. Polypeptoids synthesized and their characteristics. Chemical structures of the polypeptoid blocks are given in Figure 4.2. Nme = N-(2-methoxyethyl)glycine, Npe = N-(2-phenylethyl)glycine.

Polymer	Sequence	$M_{n,theor/obs}$ (g/mol)	$N_{peptoid}$	Purity (%)*
(Nme) ₁₈	(NmeNmeNmeNmeNmeNme) ₃	2226 / 2227.7	18	97.1
(Nme) ₂₄	(NmeNmeNmeNmeNmeNme) ₄	2917 / 2916.4	24	93.8
(Nme) ₃₆	(NmeNmeNmeNmeNmeNme) ₆	4285 / 4286.1	36	90.7
(Nme) ₄₈	(NmeNmeNmeNmeNmeNme) ₈	5681 / 5684.0	48	95.7
(Nme-co-Npe) ₁₈	(NmeNpeNmeNmeNpeNpe) ₃	2641 / 2642.7	18	91.2
(Nme-co-Npe) ₂₄	(NmeNpeNmeNmeNpeNpe) ₄	3471 / 3471.4	24	97.6
(Nme-co-Npe) ₃₆	(NmeNpeNmeNmeNpeNpe) ₆	5129 / 5128.3	36	89.7
(Nme-co-Npe) ₄₈	(NmeNpeNmeNmeNpeNpe) ₈	6787 / 6786.2	48	77.1

*After HPLC purification, determined by analytical HPLC.

Table 4.2. Polystyrene-polypeptoid block copolymers. “S” denotes polystyrene. Peptoid abbreviations are given in Table 4.1.

Polymer Abbreviation	PS M_n (g/mol)	PS PDI	Peptoid M_n (g/mol)	Φ_{peptoid}	Morphology	Domain Spacing (nm)
S ₈₄ Nme ₁₈	8800	1.09	2226	0.18	DIS	
S ₈₄ Nme ₂₄	8800	1.09	2917	0.23	HEX	13.4
S ₈₄ Nme ₃₆	8800	1.09	4285	0.30	HEX	14.6
S ₈₄ (Nme-co-Npe) ₁₈	8800	1.09	2641	0.21	DIS	
S ₈₄ (Nme-co-Npe) ₂₄	8800	1.09	3471	0.26	DIS	
S ₈₄ (Nme-co-Npe) ₃₆	8800	1.09	5129	0.34	HEX	15.6
S ₈₄ (Nme-co-Npe) ₄₈	8800	1.09	6787	0.41	LAM	15.9
S ₄₈ Nme ₃₆	4800	1.1	4285	0.44	LAM	14.0
S ₄₈ (Nme-co-Npe) ₃₆	4800	1.1	5129	0.49	LAM	14.8
S ₃₂ Nme ₁₈	3300	1.08	2226	0.38	DIS	
S ₃₂ Nme ₂₄	3300	1.08	2917	0.44	LAM	11.1
S ₃₂ Nme ₃₆	3300	1.08	4285	0.54	LAM	12.6
S ₃₂ Nme ₄₈	3300	1.08	5681	0.61	LAM	13.1
S ₃₂ (Nme-co-Npe) ₁₈	3300	1.08	2641	0.42	DIS	
S ₃₂ (Nme-co-Npe) ₂₄	3300	1.08	3471	0.48	DIS	
S ₃₂ (Nme-co-Npe) ₃₆	3300	1.08	5129	0.58	DIS	
S ₃₂ (Nme-co-Npe) ₄₈	3300	1.08	6787	0.65	DIS	

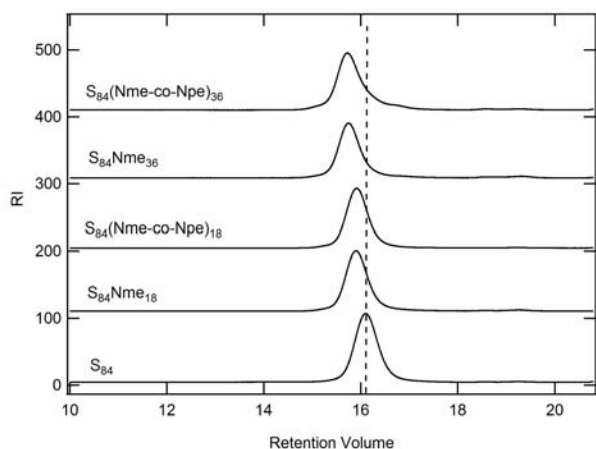


Figure 4.3. GPC for block copolymers containing Nme or (Nme-co-Npe) polypeptoids. The dashed vertical line is a guide to the eye so that the peak shifts can be seen more clearly.

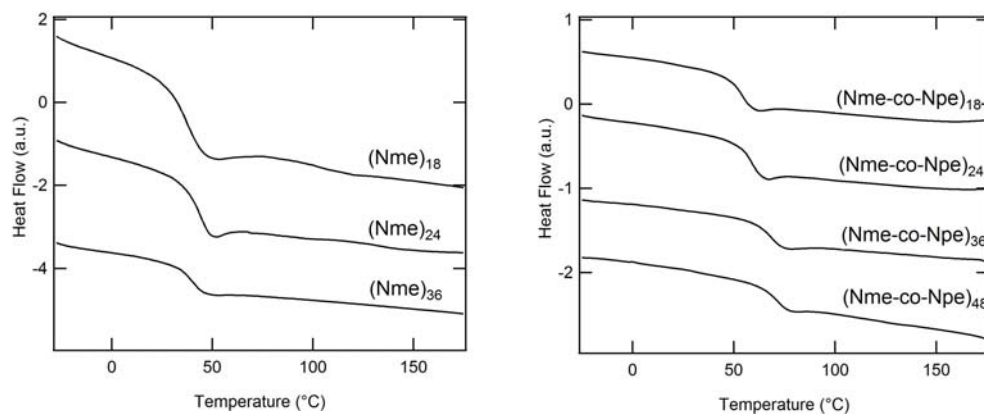


Figure 4.3. DSC thermograms of Nme and (Nme-co-Npe) peptoid copolymers. The addition of aromatic residues increases the glass transition of the polypeptoid chain.

For S₈₄Nme₃₆, two peaks can be seen: a relatively broad peak around 45°C corresponding to the peptoid Nme block and a sharper peak at approximately 100°C corresponding to the polystyrene block. The presence of these two peaks indicates microphase separation of the two blocks and therefore self-assembly, which is corroborated by SAXS and TEM (as will be discussed below). The DSC heating traces show that for S₈₄Nme₁₈ and S₈₄Nme₂₄, only the T_g of the polystyrene block can be clearly observed. For S₈₄Nme₁₈, this result indicates a lack of microphase separation. For S₈₄Nme₂₄, however, SAXS (Figure 4.6) shows microphase separation, meaning that the thermal behavior of the peptoid block may simply be difficult to see with DSC because it is relatively short compared to the polystyrene block.

As indicated by the SAXS data in Figure 4.6, the polypeptoid-based block copolymers with methoxyethyl side chains readily self-assemble into both lamellar and hexagonally-packed morphologies. As indicated by the integer spacing of peaks, q^* and $2q^*$, both S₃₂Nme₄₈ and S₄₈Nme₃₆ self-assemble into a lamellar morphology. It is well known that classical block copolymers with a volume fraction ratio in the range of 40:60 – 60:40 (roughly symmetric) of the two blocks form lamellar morphologies.¹ With respective peptoid volume fractions of 0.61 and 0.44, S₃₂Nme₄₈ and S₄₈Nme₃₆ fall into this volume fraction range. As the volume fraction of polypeptoid is decreased, a hexagonal morphology is accessed, as indicated by the $1:\sqrt{3}:\sqrt{7}$ spacing of the SAXS peaks for both S₈₄Nme₃₆ and S₈₄Nme₂₄ (peptoid volume fractions of 0.30 and 0.23, respectively). This result is again in good agreement with the classical block copolymer phase diagram in which block copolymers with 70:30 – 80:20 compositions of the two blocks form hexagonal morphologies.¹ For hexagonally packed cylinders, a reflection at $\sqrt{4}q^*$ is also usually seen. In the case of S₈₄Nme₂₄, this reflection is quite small (shown in the Appendix); however, for S₈₄Nme₃₆, this reflection is completely suppressed as a result of destructive interference between the form factor and the structure factor for cylinders at this volume fraction of polypeptoid.³⁸ Below 20% volume fraction of polypeptoid, the SNme block copolymers show no higher order peaks and a relatively broad primary peak, indicating a disordered phase.

Previous studies on the self-assembly of block copolymers containing a peptide block (which has the same backbone and side chain spacing as polypeptoids) have observed both lamellar³⁹⁻⁴² and hexagonal⁴³⁻⁴⁶ structures. However, it is not unusual for the lamellar phases to persist to unusually asymmetric block copolymer compositions due to factors that rigidify the peptide chain such as crystallinity, hydrogen bonding, and helicity.⁴² For a polypeptoid, all of these types of interactions are controlled via careful choice of the side chain moieties, as the N-substitution in polypeptoids precludes the presence of hydrogen bonding or chirality in the backbone. The choice of amorphous, methoxyethyl side chains here yields a flexible polymer chain, leading to a phase behavior containing morphologies with curved interfaces (cylinders), as shown by TEM in Figure 4.7a.

Although the SNme block copolymers follow the classical block copolymer phase diagram qualitatively, these short block copolymers do not follow the polymeric scaling laws

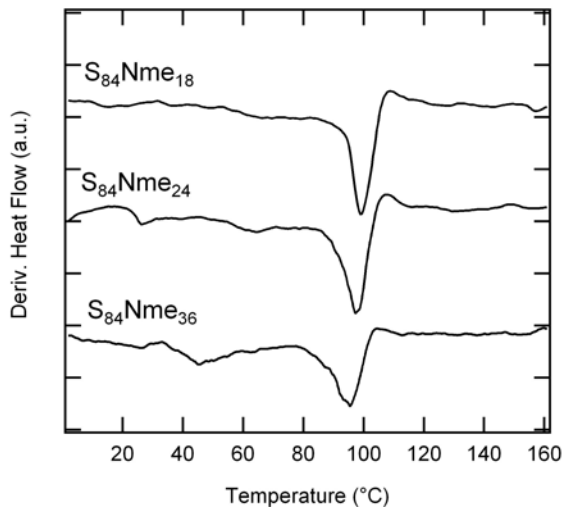


Figure 4.4. DSC traces for SNme block copolymers. The presence of two peaks for $S_{84}Nme_{36}$ indicates microphase separation.

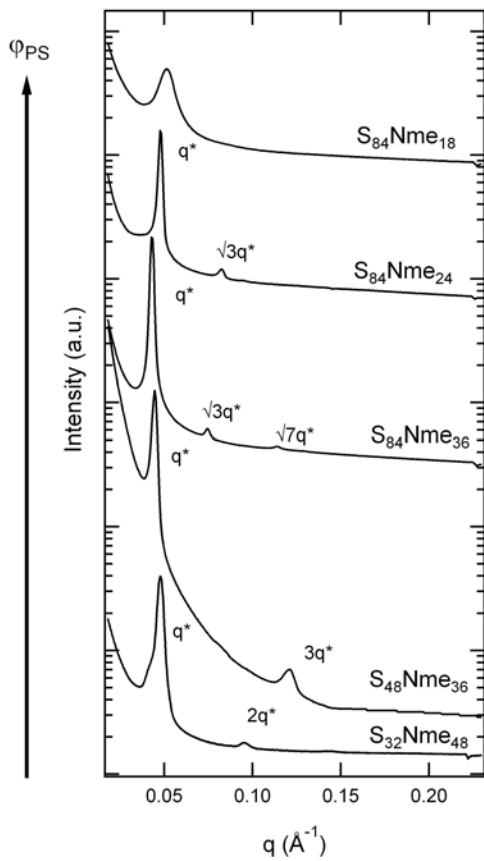


Figure 4.6. SAXS of SNme Block Copolymers. SAXS data indicates that SNme block copolymers readily self-assemble into both lamellar and hexagonally-packed morphologies.

largely due to their relatively short length. For strongly-segregated Gaussian block copolymers, the domain spacing scales as $N^{2/3}$ (where N is the number of volumetric repeat units) as molecular weight is increased.⁴⁷ A comparison of the lamellar SNme block copolymers synthesized here (Table 4.2) indicates that these polymers do not scale in this way. It is clear, however, that the polypeptoid blocks are not fully extended, as evidenced by the change in domain spacing between $S_{32}Nme_{24}$ (11.1 nm) and $S_{32}Nme_{48}$ (13.1 nm). For all of the block copolymers in this paper, the contour length of the polypeptoid is approximately two orders of magnitude larger than the persistence length,²⁶ meaning that the polypeptoid block is likely somewhat flexible.

As some of the ordered block copolymers are heated, there is a transition from their ordered phase to a disordered phase, as shown for a typical example in Figure 4.8. This order-disorder transition (ODT) is indicated by the disappearance of higher order peaks, a drop in the intensity of the primary peak, and an increase in the breadth of the primary peak. In a plot of the inverse primary peak intensity against inverse temperature, the ODT coincides with the discontinuity in scaling (see Appendix). For all ordered SNme diblocks containing a polystyrene block approximately 32 or 48 monomers long, the ODT could be accessed upon heating, and the self-assembled nanostructure was recovered upon cooling, thus showing that the self-assembly leads to equilibrium structures. Table 4.3 details the measured ODTs for these diblocks. However, for $S_{84}Nme_{36}$ and $S_{84}Nme_{24}$, which contained a larger polystyrene block, the disordered phase could not be accessed within the experimental temperature range (up to 250°C). The strength of segregation was high enough in these diblocks such that the hexagonal order persisted at very high temperature. It is well known that the strength of segregation increases with an increase in molecular weight; however, with the polypeptoid-polystyrene block copolymer system, we can directly manipulate the ODT with the introduction of styrene-like residues into the polypeptoid block.

4.3.4 Tuning Segregation Strength with the Introduction of *N*-(2-Phenylethyl)glycine Residues

The self-assembly and strength of segregation for the polypeptoid-polystyrene block copolymers can be tuned with the addition of styrene-like residues into the peptoid block. Derivative DSC heating traces for some of these PS-*b*-(Nme-co-Npe) diblocks (hereafter denoted as $S_m(Nme-co-Npe)_N$) are given in Figure 4.9. As the polypeptoid block grows in length, the emergence of a second T_g peak indicates microphase separation. $S_{84}Nme_{18}$ only shows a broad T_g slightly below 100°C, indicating that the sample is disordered and that the short peptoid block mixes with the polystyrene block. As the polypeptoid volume fraction increases to 0.26, a shoulder emerges around the T_g at approximately 84°C, which is significantly higher than the T_g of the corresponding (Nme-co-Npe)₂₄ copolymer (60°C). Diblocks with even higher volume fractions of polypeptoid, $S_{84}(Nme-co-Npe)_{36}$ and $S_{84}(Nme-co-Npe)_{48}$, exhibit two clear T_g 's at 75°C and 80°C, respectively. This result is a clear indication of microphase separation; however, the measured T_g 's are still significantly higher than those of the corresponding peptoids by

approximately 5-10°C (as given in Figure 4.4). This slight discrepancy may indicate that there is still some miscibility with the polystyrene domain despite the microphase separation.

The self-assembly behavior of the S(Nme-co-Npe) diblocks show a decreased strength of segregation compared to the SNme diblocks in two ways: the disordered phases of the S(Nme-co-Npe) diblocks persist over a larger range of block copolymer compositions, and the S(Nme-co-Npe) diblocks have lower ODTs for ordered phases. Room temperature SAXS scans are shown in Figure 4.10 for similar block copolymer compositions to the SNme block copolymers in Figure 4.6 such that they can be directly compared. For example, both $S_{84}Nme_{24}$ and $S_{84}(Nme-co-Npe)_{24}$ contain a peptoid block 24 monomers in length, but $S_{84}Nme_{24}$ is ordered, while $S_{84}(Nme-co-Npe)_{24}$ is not. When styrene-like residues are present in the peptoid block, an increase in molecular weight is required to compensate for the decrease in the Flory Huggins parameter. When the S(Nme-co-Npe) block copolymers are ordered, they exhibit the same morphology as their corresponding SNme diblocks, as illustrated by the following pairs: $S_{84}Nme_{36}$ and $S_{84}(Nme-co-Npe)_{36}$ (hexagonal) and $S_{48}Nme_{36}$ and $S_{48}(Nme-co-Npe)_{36}$ (lamellar). In both cases, the domain spacing of the S(Nme-co-Npe) diblock is larger by 0.8 – 1 nm, which likely reflects an increase in the polypeptoid domain to accommodate the bulkier N-(2-phenylethyl)glycine residues. Despite the increase in domain spacing, the S(Nme-co-Npe) block copolymer has a lower ODT than the analogous SNme block copolymer (Table 4.3). Thus, it is possible to tune the strength of segregation for these block copolymers without changing the self-assembled morphology. Additional experiments that vary the monomer sequence of the (Nme-co-Npe) block will yield further insight into the effect of sequence on the strength of segregation.

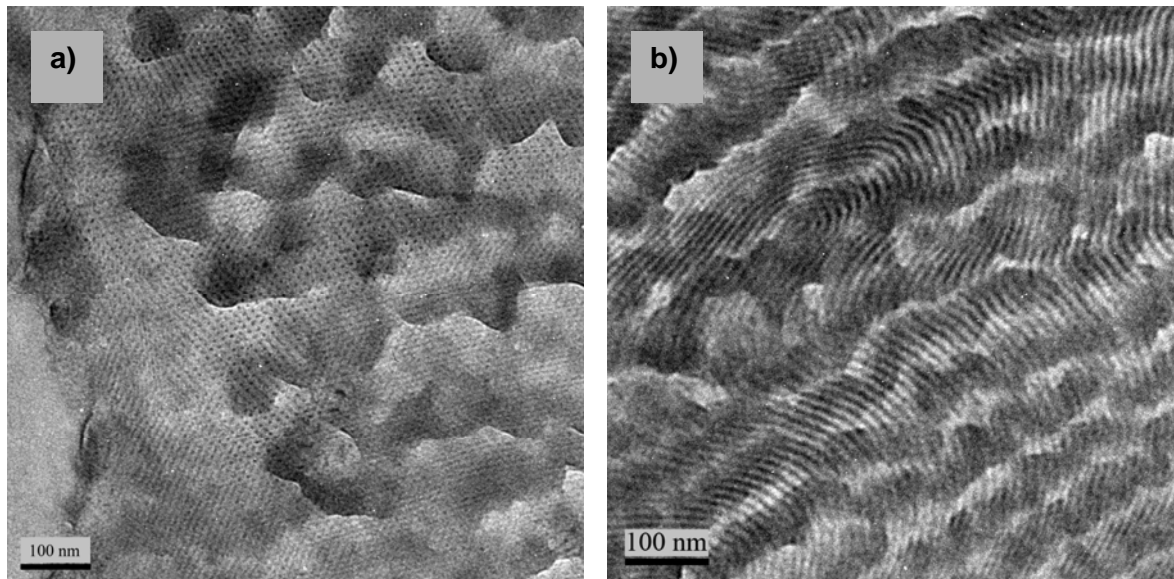


Figure 4.7. TEM of Block Copolymers. TEM analysis reveals the hexagonal structure of $S_{84}Nme_{24}$ (a) and the lamellar structure of $S_{84}(Nme-co-Npe)_{48}$ (b). Based on the asymmetric composition of $S_{84}Nme_{24}$, the peptoid block is dark due to RuO_4 staining.

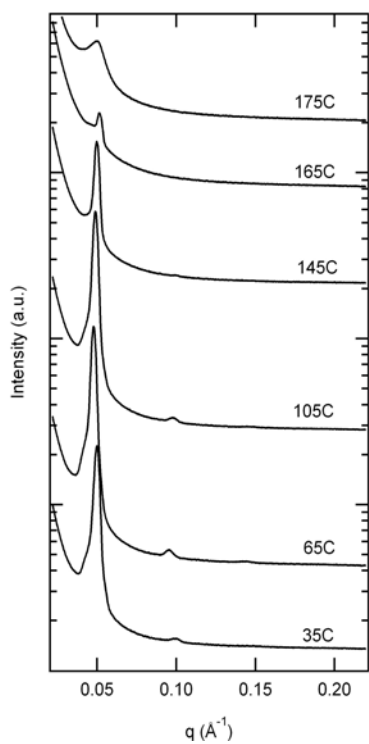


Figure 4.8. SAXS heating scan for $S_{32}Nme_{48}$. The disappearance of higher order peaks and the drop in intensity of the primary peak at 145°C indicates a transition to a disordered phase.

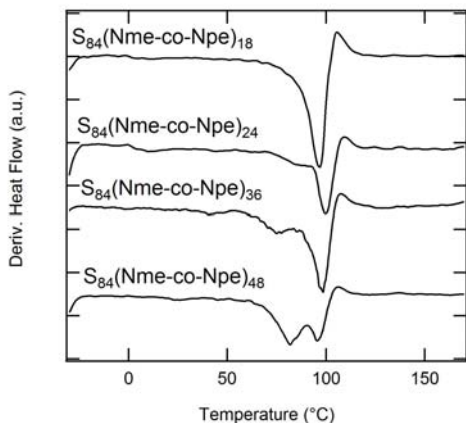


Figure 4.9. DSC heating traces for representative S(Nme-co-Npe) block copolymers. The emergence of two glass transition peaks indicates microphase separation at higher molecular weights.

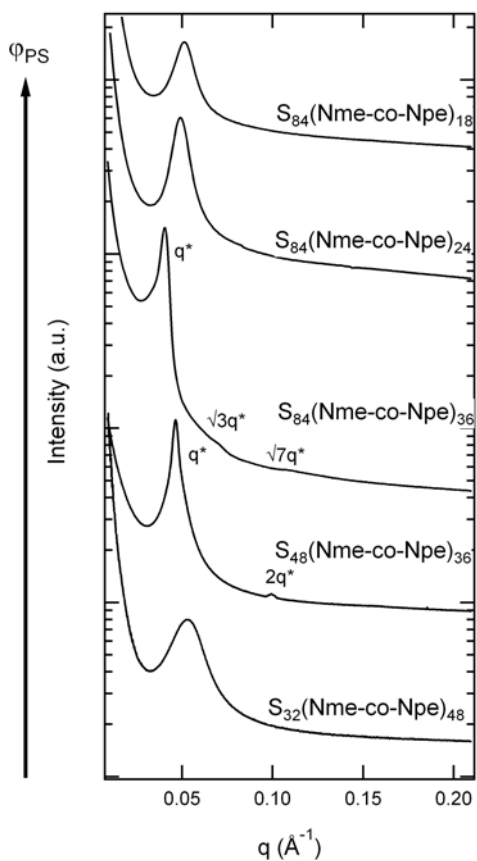


Figure 4.10. SAXS of S(Nme-co-Npe) Block Copolymers. SAXS curves for S(Nme-co-Npe) block copolymers indicates that the incorporation of styrene-like residues into the polypeptoid block decreases the strength of segregation.

Table 4.3. ODT Comparison for Analogous SNme and S(Nme-co-Npe) Block Copolymers.

Polymer	Peptoid Block	
	Nme _N ODT	(Nme-co-Npe) _N ODT
S ₈₄ -Peptoid ₁₈	DIS	DIS
S ₈₄ -Peptoid ₂₄	>250°C	DIS
S ₈₄ -Peptoid ₃₆	>250°C	190°C
S ₄₆ -Peptoid ₃₆	129°C	95°C
S ₃₂ -Peptoid ₁₈	DIS	DIS
S ₃₂ -Peptoid ₂₄	145°C	DIS
S ₃₂ -Peptoid ₃₆	145°C	DIS
S ₃₂ -Peptoid ₄₈	149°C	DIS

*DIS indicates disordered morphology.

4.4 Conclusions

Sequence-defined polystyrene-polypeptoid block copolymers were synthesized via azide-alkyne coupling for the first time and shown to readily self-assemble into morphologies with tunable segregation strengths. The glass transition of the polypeptoid block increases upon the incorporation of styrene-like residues, as well as upon an increase in chain length for the (Nme-co-Npe) copolypeptoids. SNme block copolymers self-assembled into both hexagonally packed and lamellar morphologies; some had accessible, reversible ODTs, indicating the ordered morphologies were equilibrium structures. For block copolymers with a styrene-like residue in the polypeptoid block, the segregation strength was significantly decreased. S(Nme-co-Npe) block copolymers showed decreased ODTs compared to analogous SNme block copolymers across all compositions. The polystyrene-polypeptoid block copolymers are thus an effective system for controlling the interaction between the two blocks, and their sequence definition will enable future studies on the effect of comonomer distribution on segregation strength in many types of block copolymer systems.

4.5 Acknowledgements

We gratefully acknowledge funding from the Office of Naval Research via a Presidential Early Career Award in Science and Engineering. A.M.R. also gratefully acknowledges the National Science Foundation for a graduate fellowship. Polypeptoid synthesis and associated chemical characterization were performed at the Molecular Foundry, a Lawrence Berkeley National Laboratory user facility supported by the Office of Science, Office of Basic Energy Sciences, U.S. Department of Energy, under Contract DE-AC02-05CH11231. SAXS studies at the Advanced Light Source (beamline 7.3.3) were supported by the U.S. Department of Energy under contract number DE-AC02-05CH11231, and SAXS studies at the Stanford Synchrotron Radiation Laboratory (beamline 1-4) were facilitated by Stanford University on behalf of the U.S. Department of Energy. A.M.R thanks Scott Mullin for the use of a multi-sample heating stage for the SAXS experiments and Bryan Boudouris for help with the synthesis of the alkoxyamine initiator.

4.6 Appendix

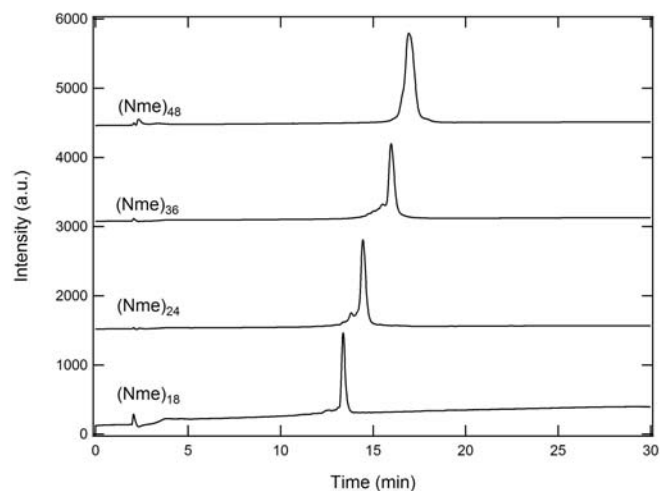


Figure 4.11. Analytical HPLC traces for (Nme)_N polypeptoids. The HPLC gradient was 5-95% acetonitrile (solvent B was water) over 30 minutes at 60°C.

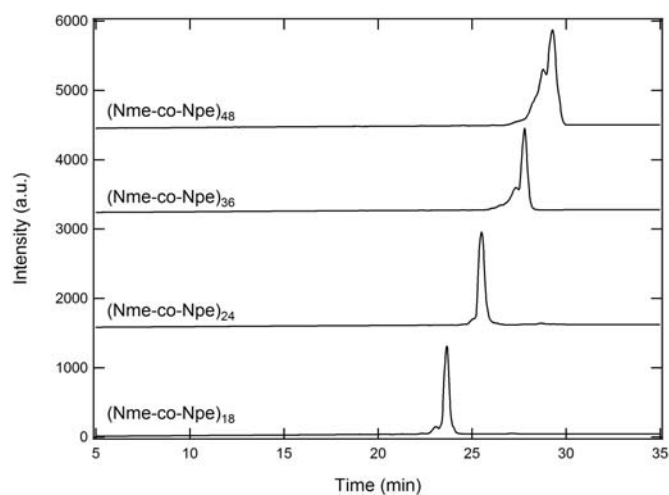


Figure 4.12. Analytical HPLC traces for (Nme-co-Npe)_N polypeptoids. The HPLC gradient was 5-95% acetonitrile (solvent B was water) over 30 minutes at 60°C.

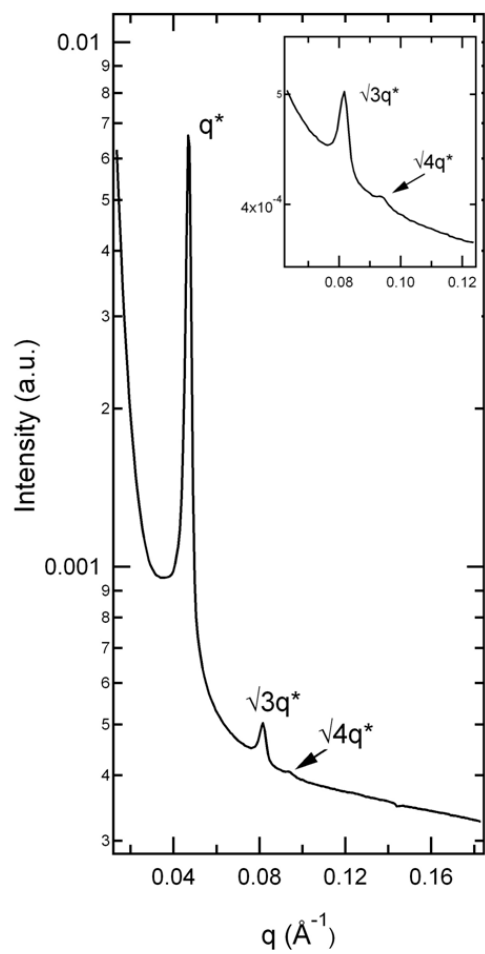


Figure 4.13. Magnified SAXS for $S_{84}Nme_{24}$. Magnified SAXS pattern for $S_{84}Nme_{24}$ allows one to see the $\sqrt{4}q^*$ peak more clearly.

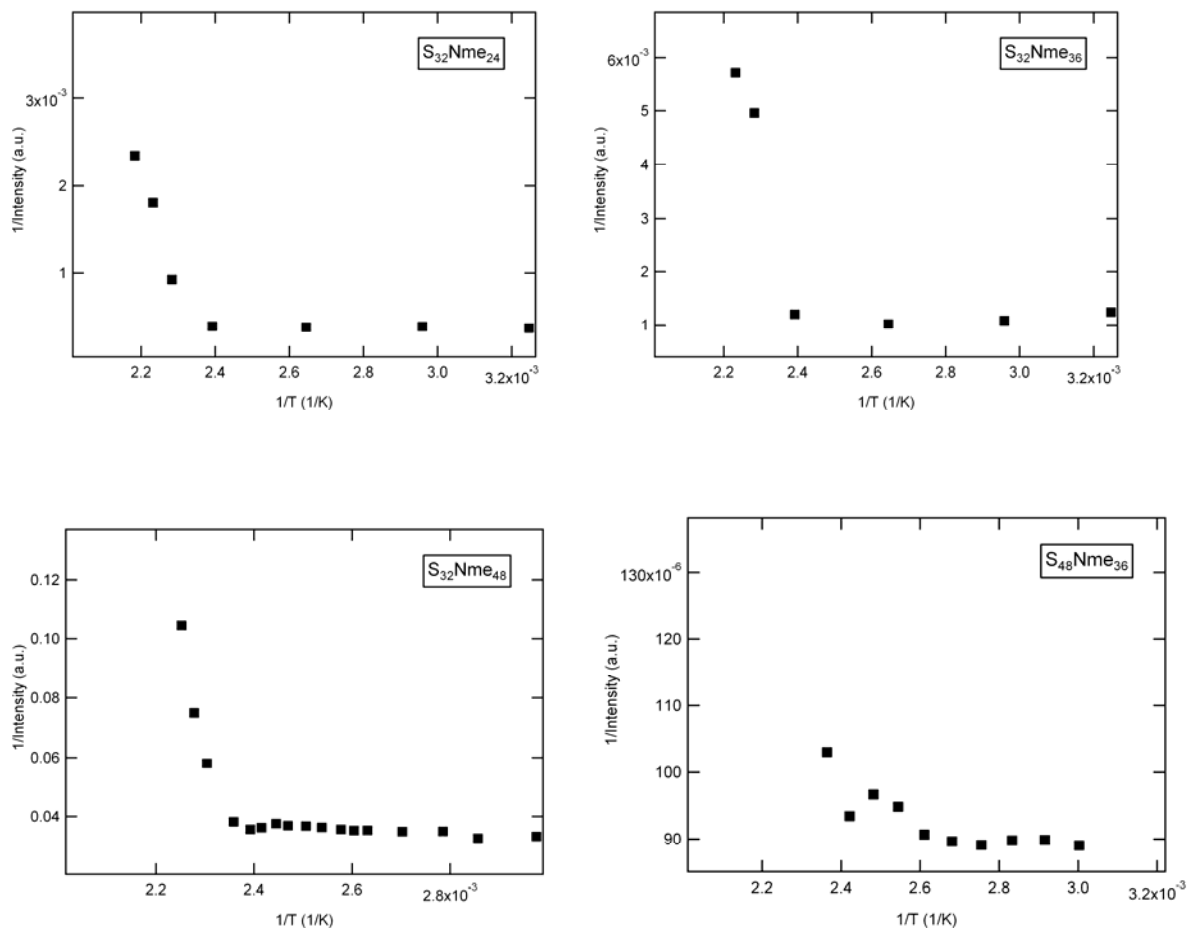
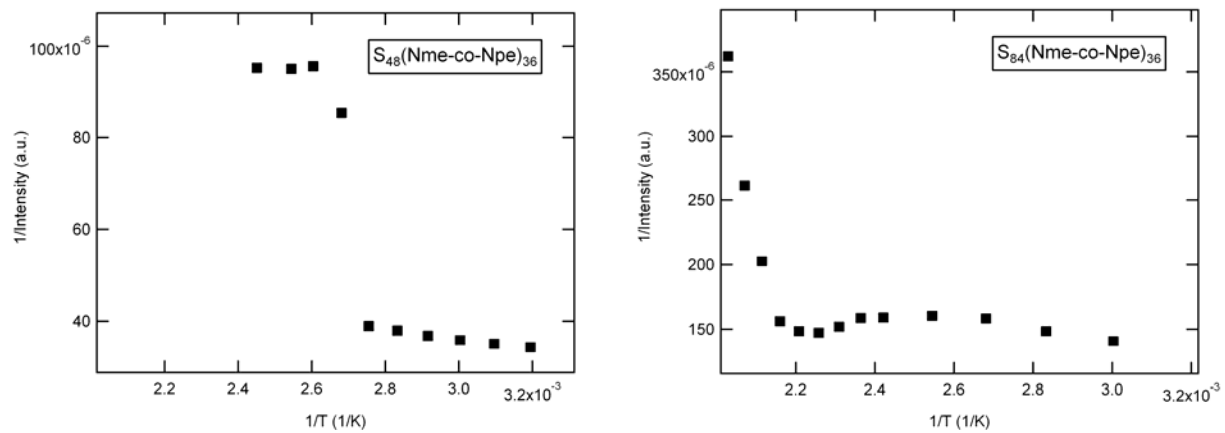


Figure 4.14. Inverse intensity vs. inverse temperature plots to determine ODTs for SNme block copolymers.



4.7 References

1. Bates, F. S.; Fredrickson, G. H., Block copolymers - Designer soft materials. *Phys. Today* **1999**, *52* (2), 32-38.
2. Beckingham, B. S.; Register, R. A., Synthesis and Phase Behavior of Block-Random Copolymers of Styrene and Hydrogenated Isoprene. *Macromolecules* **2011**, *44* (11), 4313-4319.
3. Mok, M. M.; Ellison, C. J.; Torkelson, J. M., Effect of Gradient Sequencing on Copolymer Order-Disorder Transitions: Phase Behavior of Styrene/n-Butyl Acrylate Block and Gradient Copolymers. *Macromolecules* **2011**, *44* (15), 6220-6226.
4. Quinn, J. D.; Register, R. A., Microphase Separation in Block-Random Copolymers of Styrene, 4-Acetoxystyrene, and 4-Hydroxystyrene. *J. Polym. Sci. Pt. B-Polym. Phys.* **2009**, *47* (21), 2106-2113.
5. Roy, R.; Park, J. K.; Young, W. S.; Mastroianni, S. E.; Tureau, M. S.; Epps, T. H., Double-Gyroid Network Morphology in Tapered Diblock Copolymers. *Macromolecules* **2011**, *44* (10), 3910-3915.
6. Samseth, J.; Spontak, R. J.; Smith, S. D.; Ashraf, A.; Mortensen, K., MICROPHASE-SEPARATED TAPERED TRIBLOCK COPOLYMERS. *J. Phys. IV* **1993**, *3* (C8), 59-62.
7. Singh, N.; Tureau, M. S.; Epps, T. H., Manipulating ordering transitions in interfacially modified block copolymers. *Soft Matter* **2009**, *5* (23), 4757-4762.
8. Hodrokoukes, P.; Floudas, G.; Pispas, S.; Hadjichristidis, N., Microphase separation in normal and inverse tapered block copolymers of polystyrene and polyisoprene. 1. Phase state. *Macromolecules* **2001**, *34* (3), 650-657.
9. Mayo, F. R.; Lewis, F. M., Copolymerization I A basis for comparing the behavior of monomers in copolymerization, the copolymerization of styrene and methyl methacrylate. *J. Am. Chem. Soc.* **1944**, *66*, 1594-1601.
10. Lutz, J. F.; Pakula, T.; Matyjaszewski, K., Synthesis and properties of copolymers with tailored sequence distribution by controlled/living radical polymerization. In *Advances in Controlled/Living Radical Polymerization*, Matyjaszewski, K., Ed. Amer Chemical Soc: Washington, 2003; Vol. 854, pp 268-282.
11. Antkowiak, T.; Tate, D. P.; Oberster, A. E.; Halasa, A. F., TEMPERATURE AND CONCENTRATION EFFECTS ON POLAR-MODIFIED ALKYL LITHIUM POLYMERIZATIONS AND COPOLYMERIZATIONS. *Journal of Polymer Science Part a-1-Polymer Chemistry* **1972**, *10* (5), 1319-&.
12. Badi, N.; Lutz, J. F., Sequence control in polymer synthesis. *Chem. Soc. Rev.* **2009**, *38* (12), 3383-3390.
13. Lutz, J. F., Sequence-controlled polymerizations: the next Holy Grail in polymer science? *Polym. Chem.* **2010**, *1* (1), 55-62.
14. Lutz, J. F.; Kirci, B.; Matyjaszewski, K., Synthesis of well-defined alternating copolymers by controlled/living radical polymerization in the presence of Lewis acids. *Macromolecules* **2003**, *36* (9), 3136-3145.
15. Ouchi, M.; Terashima, T.; Sawamoto, M., Transition Metal-Catalyzed Living Radical Polymerization: Toward Perfection in Catalysis and Precision Polymer Synthesis. *Chem. Rev.* **2009**, *109* (11), 4963-5050.
16. Smith, J. A.; Brzezinska, K. R.; Valenti, D. J.; Wagener, K. B., Precisely controlled methyl branching in polyethylene via acyclic diene metathesis (ADMET) polymerization. *Macromolecules* **2000**, *33* (10), 3781-3794.
17. Soeriyadi, A. H.; Boyer, C.; Nystrom, F.; Zetterlund, P. B.; Whittaker, M. R., High-Order Multiblock Copolymers via Iterative Cu(0)-Mediated Radical Polymerizations (SET-LRP): Toward Biological Precision. *J. Am. Chem. Soc.* **2011**, *133* (29), 11128-11131.
18. Link, A. J.; Mock, M. L.; Tirrell, D. A., Non-canonical amino acids in protein engineering. *Curr. Opin. Biotechnol.* **2003**, *14* (6), 603-609.

19. van Hest, J. C. M.; Tirrell, D. A., Protein-based materials, toward a new level of structural control. *Chem. Commun.* **2001**, (19), 1897-1904.
20. Barron, A. E.; Zuckermann, R. N., Bioinspired polymeric materials: in-between proteins and plastics. *Curr. Opin. Chem. Biol.* **1999**, 3 (6), 681-687.
21. Borner, H. G., Precision Polymers - Modern Tools to Understand and Program Macromolecular Interactions. *Macromol. Rapid Commun.* **2011**, 32 (2), 115-126.
22. Borner, H. G.; Schlaad, H., Bioinspired functional block copolymers. *Soft Matter* **2007**, 3 (4), 394-408.
23. Hartmann, L.; Borner, H. G., Precision Polymers: Monodisperse, Monomer-Sequence-Defined Segments to Target Future Demands of Polymers in Medicine. *Adv. Mater.* **2009**, 21 (32-33), 3425-3431.
24. Lutz, J. F.; Borner, H. G., Modern trends in polymer bioconjugates design. *Prog. Polym. Sci.* **2008**, 33 (1), 1-39.
25. Rosales, A. M.; Murnen, H. K.; Zuckermann, R. N.; Segalman, R. A., Control of Crystallization and Melting Behavior in Sequence Specific Polypeptoids. *Macromolecules* 43 (13), 5627-5636.
26. Rosales, A. M.; Murnen, H. K.; Kline, S. R.; Zuckermann, R. N.; Segalman, R. A., Determination of the persistence length of helical and non-helical polypeptoids in solution. *Soft Matter* **2012**, 8 (13), 3673-3680.
27. Figliozzi, G. M.; Goldsmith, R.; Ng, S. C.; Banville, S. C.; Zuckermann, R. N., Synthesis of N-substituted glycine peptoid libraries. *Methods Enzymol.* **1996**, 267, 437-447.
28. Zuckermann, R. N.; Kerr, J. M.; Kent, S. B. H.; Moos, W. H., EFFICIENT METHOD FOR THE PREPARATION OF PEPTOIDS [OLIGO(N-SUBSTITUTED GLYCINES)] BY SUBMONOMER SOLID-PHASE SYNTHESIS. *J. Am. Chem. Soc.* **1992**, 114 (26), 10646-10647.
29. Wu, C. W.; Sanborn, T. J.; Huang, K.; Zuckermann, R. N.; Barron, A. E., Peptoid oligomers with alpha-chiral, aromatic side chains: Sequence requirements for the formation of stable peptoid helices. *J. Am. Chem. Soc.* **2001**, 123 (28), 6778-6784.
30. Murnen, H. K.; Rosales, A. M.; Jaworski, J. N.; Segalman, R. A.; Zuckermann, R. N., Hierarchical Self-Assembly of a Biomimetic Diblock Copolypeptoid into Homochiral Superhelices. *J. Am. Chem. Soc.* **2010**, 132 (45), 16112-16119.
31. Nam, K. T.; Shelby, S. A.; Choi, P. H.; Marciel, A. B.; Chen, R.; Tan, L.; Chu, T. K.; Mesch, R. A.; Lee, B. C.; Connolly, M. D.; Kisielowski, C.; Zuckermann, R. N., Free-floating ultrathin two-dimensional crystals from sequence-specific peptoid polymers. *Nat. Mater.* **2010**, 9 (5), 454-460.
32. Lee, C.-U.; Smart, T. P.; Guo, L.; Epps, T. H.; Zhang, D., Synthesis and Characterization of Amphiphilic Cyclic Diblock Copolypeptoids from N-Heterocyclic Carbene-Mediated Zwitterionic Polymerization of N-Substituted N-Carboxyanhydride. *Macromolecules* **2011**.
33. Lee, B. C.; Chu, T. K.; Dill, K. A.; Zuckermann, R. N., Biomimetic nanostructures: Creating a high-affinity zinc-binding site in a folded nonbiological polymer. *J. Am. Chem. Soc.* **2008**, 130 (27), 8847-8855.
34. Kudirka, R.; Tran, H.; Sanii, B.; Nam, K. T.; Choi, P. H.; Venkateswaran, N.; Chen, R.; Whitelam, S.; Zuckermann, R. N., Folding of a Single-Chain, Information-Rich Polypeptoid Sequence into a Highly Ordered Nanosheet. *Biopolymers* **2011**, 96 (5), 586-595.
35. Bothe, M.; Schmidt-Naake, G., An improved catalytic method for alkoxyamine synthesis - Functionalized and biradical initiators for nitroxide-mediated radical polymerization. *Macromol. Rapid Commun.* **2003**, 24 (10), 609-613.
36. Holub, J. M.; Jang, H. J.; Kirshenbaum, K., Clickity-click: highly functionalized peptoid oligomers generated by sequential conjugation reactions on solid-phase support. *Org. Biomol. Chem.* **2006**, 4 (8), 1497-1502.
37. Ilavsky, J., Nika: software for two-dimensional data reduction. *Journal of Applied Crystallography* **2012**, 45 (2), 324-328.
38. Hashimoto, T.; Kawamura, T.; Harada, M.; Tanaka, H., Small-Angle Scattering from Hexagonally Packed Cylindrical Particles with Paracrystalline Distortion. *Macromolecules* **1994**, 27 (11), 3063-3072.

39. Billot, J. P.; Douy, A.; Gallot, B., SYNTHESIS AND STRUCTURAL STUDY OF BLOCK COPOLYMERS WITH A HYDROPHOBIC POLYVINYL BLOCK AND A HYDROPHILIC POLYPEPTIDE BLOCK - COPOLYMERS POLYSTYRENE-POLY(L-LYSINE) AND POLYBUTADIENE-POLY(L-LYSINE). *Makromolekulare Chemie-Macromolecular Chemistry and Physics* **1976**, *177* (6), 1889-1893.
40. Douy, A.; Gallot, B., BLOCK COPOLYMERS WITH A POLYVINYL AND A POLYPEPTIDE BLOCK - FACTORS GOVERNING THE FOLDING OF THE POLYPEPTIDE-CHAINS. *Polymer* **1982**, *23* (7), 1039-1044.
41. Perly, B.; Douy, A.; Gallot, B., BLOCK COPOLYMERS POLYBUTADIENE-POLY(BENZYL-L-GLUTAMATE) AND POLYBUTADIENE-POLY(N5-HYDROXYPROPYLGLUTAMINE) PREPARATION AND STRUCTURAL STUDY BY X-RAY AND ELECTRON-MICROSCOPY. *Makromolekulare Chemie-Macromolecular Chemistry and Physics* **1976**, *177* (9), 2569-2589.
42. Minich, E. A.; Nowak, A. P.; Deming, T. J.; Pochan, D. J., Rod-rod and rod-coil self-assembly and phase behavior of polypeptide diblock copolymers. *Polymer* **2004**, *45* (6), 1951-1957.
43. Babin, J.; Taton, D.; Brinkmann, M.; Lecommandoux, S., Synthesis and Self-Assembly in Bulk of Linear and Mikto-Arm Star Block Copolymers Based on Polystyrene and Poly(glutamic acid). *Macromolecules* **2008**, *41* (4), 1384-1392.
44. Klok, H. A.; Langenwaller, J. F.; Lecommandoux, S., Self-assembly of peptide-based diblock oligomers. *Macromolecules* **2000**, *33* (21), 7819-7826.
45. Klok, H. A.; Lecommandoux, S., Solid-state structure, organization and properties of peptide - Synthetic hybrid block copolymers. In *Peptide Hybrid Polymers*, Klok, H. A.; Schlaad, H., Eds. Springer-Verlag Berlin: Berlin, 2006; Vol. 202, pp 75-111.
46. Lecommandoux, S.; Achard, M. F.; Langenwaller, J. F.; Klok, H. A., Self-assembly of rod-coil diblock oligomers based on alpha-helical peptides. *Macromolecules* **2001**, *34* (26), 9100-9111.
47. Matsen, M. W.; Bates, F. S., Unifying weak- and strong-segregation block copolymer theories. *Macromolecules* **1996**, *29* (4), 1091-1098.

Chapter 5. Effect of Chain Shape on Peptoid Block Copolymer Self-Assembly

Reproduced with permission from Adrienne M. Rosales, Boris Russ, Ronald N. Zuckermann, and Rachel A. Segalman (2013). *In preparation*.

Polymer chain shape is well known to affect block copolymer self-assembly; however, it is difficult to control in a precise way. Polypeptoids are sequence-specific N-substituted glycine polymers for which the backbone can form a molecular helix upon the introduction of monomers with bulky, chiral side chains. Furthermore, sequence specificity enables the precise placement of those chiral monomers along the polymer chain, leading to controlled interactions. This work presents a systematic study of block copolymer self-assembly using chiral polypeptoids or their racemic analogs and poly(n-butyl acrylate). It is shown via SAXS measurements that the change in conformational asymmetry increases the morphological domain spacing. Increasing the number of chiral residues within a peptoid block also increases the domain spacing, although the sequence of the chiral residues is important. In particular, the effect of chiral residue location on domain spacing is probed by changing the position of the chiral monomers with respect to the block copolymer junction. Stabilizing the peptoid helix with chiral residues at the C-terminus of the chain leads to larger domain spacing. These results lend insight to the design of block copolymers with molecular structure.

5.1 Introduction

Polymer chain shape has important effects on both polymer properties and self-assembly. In nature, one of the most predominant chain shapes is the helix. Helical architectures are essential to the structure of proteins and DNA and are known to impact polymer material properties, as in the case of the helical fibrils of collagen.¹ Molecular helices are also found in synthetic polymers²⁻⁶; however, while biological polymers tend to form helices due to hydrogen bonding interactions, synthetic polymers tend to form helices as a result of chiral interactions.⁷

A number of helical polymers have the ability to sense chiral molecules and respond to certain chiralities by a change in conformation, therefore showing potential for use as molecular sensors.⁸ For instance, poly(phenylacetylenes) form dynamic racemic helices in which the left- and right-handed conformations interconvert.⁸ Upon complexation with chiral amines, a large shift in the population of helices occurs such that one conformation is preferred in large excess, leading to an induced circular dichroism signal. Functionalizing the poly(phenylacetylene) with bulky diisopropylaminomethyl groups increases the sensitivity of the polymer conformation to enantiomeric dopants due to changes in chain stiffness, and this also leads to significant changes in the self-assembly of the polymer.^{9,10} Concentrated solutions of the functionalized poly(phenylacetylene) in water form a nematic liquid crystalline phase; when just 0.001 equivalents of a chiral amine are introduced, the cholesteric phase results instead. Several synthetic helical polymers have shown similar responsiveness to chiral molecules with changes in chain shape and self-assembly.^{8,11-13}

Incorporating chiral helical polymers into block copolymers provides the opportunity to control higher order levels of structure with chirality both in solution and in bulk. The chirality provides a convenient handle to tune chain shape, as the racemic polymer is usually unstructured. In modified poly(L-lysine)-b-poly(L-leucine) diblock copolypeptides, racemic amino acids could be incorporated into the leucine block to disrupt α -helical structure, leading to a change in the self-assembly from sheets or fibrils to spherical micelles.¹⁴ Similarly, block copolymers composed of poly(2-oxazolines) with either *R*-2-butyl-4-ethyl-2-oxazoline (*R*-BuEtOx) or a racemic (*RS*-BuEtOx) block showed cylindrical and spherical micelles, respectively.¹⁵ Other block copolymers show chiral information transfer across multiple length scales, as in the case of polystyrene-b-poly(isocyno-L-alanine-L-alanine) (PS-PIAA) in which the molecular chirality of the isocyanodipeptide block informs the chirality of a self-assembled supramolecular helix in solution.¹⁶ Polystyrene-b-poly(L-lactide) (PS-PLLA) block copolymers show similar behavior in bulk systems, giving rise to a hexagonally-packed helical phase that is not observed in corresponding achiral systems and has not been previously observed in other block copolymer systems.^{17,18} While all of these studies present a nice demonstration of chiral information transfer across multiple length scales, further insight can be gained from systems in which the chiral moieties can be precisely placed.

In this study, the self-assembly is probed for poly(*n*-butyl acrylate)-b-polypeptoid block copolymers in which the peptoid block contains either 50% *R*- α -methylbenzylglycine or 50% racemic *RS*- α -methylbenzylglycine. The enantiomerically pure peptoid leads to a helical chain conformation, while the racemic peptoid has a disordered chain shape. In addition, polypeptoid sequences that contained both a helical domain and a disordered domain were studied and the location of the helical domain was tuned relative to the block copolymer junction. Because polypeptoids are synthesized using a solid phase synthesis method, the location of the chiral residues could be varied exactly and in a monodisperse fashion. Thus, a systematic study on the effect of chirality on block copolymer self-assembly could be explored.

5.2 Experimental Methods

Synthesis of Bromine-Terminated Poly(n-butyl acrylate) Atom transfer radical polymerization (ATRP) as used to synthesize poly(*n*-butyl acrylate) with a bromine end group. The initiator, methyl 2-bromo-propionate (Sigma-Aldrich, St. Louis, MO), solvent, anisole (anhydrous, Sigma-Aldrich), and catalyst, copper(I) bromide (Sigma-Aldrich), were used as received. Butyl acrylate monomer (Sigma-Aldrich) and *N,N,N',N',N''*-pentamethyldiethylenetriamine (PMDETA, Sigma-Aldrich) were filtered over basic alumina before use. In a reaction flask, the following were combined: 0.179 mmol initiator, 0.067 mmol PMDETA, 34.7 mmol butyl acrylate, 0.067 mmol Cu(I)Br, and 2 mL anisole. The reaction mixture was degassed by three freeze-pump-thaw cycles, then heated in an oil bath at 80°C for 6 h under N₂. The reaction mixture was precipitated

into cold methanol (over dry ice) to give a white product, and any residual copper was removed by filtering the product over basic alumina.

Synthesis of Azide-Terminated Poly(n-butyl acrylate) Bromine-terminated poly(n-butyl acrylate) (0.071 mmol) was dissolved in DMF (25 mL), and 25 mol equiv of sodium azide were added. The reaction mixture was stirred overnight at room temperature. The polymer was then precipitated in cold methanol to yield a white product.

Synthesis of Alkyne-Terminated Polypeptoids Polypeptoids were synthesized on a custom robotic synthesizer or a commercial Aapptec Apex 396 robotic synthesizer according to previously published methods.¹⁹ The N-terminus of all polypeptoids were functionalized with an alkyne using propargylamine, then acetylated on the resin and purified as previously described.²⁰ Molecular weights of the polypeptoids were determined using an Applied Biosystems 4800 series MALDI-TOF with a laser power of 5000. MALDI samples were prepared using a 1:1 ratio of polypeptoid in acetonitrile (0.5 mg/mL) to 1,8,9-anthracenetriol (10 mg/mL in THF). Polypeptoid purities were determined using analytical HPLC (Table 5.1) and refer to the amount of exactly monodisperse peptoid of the desired length. The major observed side products for the polypeptoids synthesized here do not contain the acetyl end group or the alkyne functional group and do not participate in the azide-alkyne coupling. The polypeptoid sequence investigated in this work is shown in Table 5.1 and for the enantiomeric peptoid, is known to form a helix according to Wu et. al.^{21,22}

Synthesis of Polypeptoid-Poly(n-butyl acrylate) Block Copolymers The block copolymers were synthesized by azide-alkyne coupling, as shown in Scheme 5.1, using the procedure described previously,²⁰ which was a modification of a procedure described by Holub et. al.²³ Upon completion of the reaction, the polymer was precipitated twice in cold methanol/water mixtures and centrifuged at 4°C to collect the product. Excess peptoid remained in the supernatant. The product was then re-precipitated from acetonitrile/water mixtures and lyophilized to recover the white product.

Gel Permeation Chromatography (GPC) The molecular weights and polydispersities of the poly(n-butyl acrylate) homopolymers were measured on a Viscotek SEC. Refractive index was used for molecular weight determination with the use of polystyrene calibration standards (Polymer Laboratories). Using a flow rate of 1 mL/min, the mobile phase was THF at 30°C. Representative GPC traces for the synthesized block copolymers are shown in the Appendix.

Table 5.1. Characterization of polypeptoids.

Sample	Peptoid block	Sequence ^a	M_n , theor/obs (g/mol)
R24	Helical	(NmeNRpeNmeNmeNRpeNRpe) ₄	3471/3474.4
R36	Helical	(NmeNRpeNmeNmeNRpeNRpe) ₆	5129/5129.6
R48	Helical	(NmeNRpeNmeNmeNRpeNRpe) ₈	6787/6793.2
R54	Helical	(NmeNRpeNmeNmeNRpeNRpe) ₉	7617/7614.1
N24	Racemic	(NmeNmbNmeNmeNmbNmb) ₄	3471/3477.2
N36	Racemic	(NmeNmbNmeNmeNmbNmb) ₆	5129/5130.3
N48	Racemic	(NmeNmbNmeNmeNmbNmb) ₈	6787/6783.3
N54	Racemic	(NmeNmbNmeNmeNmbNmb) ₉	7617/7610.1
RN36	Helical/Rac	(NmeNRpeNmeNmeNRpeNRpe) ₃ (NmeNmbNmeNmeNmbNmb) ₃	5129/5130.2
NR36	Rac/Helical	(NmeNmbNmeNmeNmbNmb) ₃ (NmeNRpeNmeNmeNRpeNRpe) ₃	5129/5129.6

^a Nme = *N*-(2-methoxyethyl)glycine; NRpe = *N*-(*R*- α -methylbenzyl)glycine; Nmb = *N*-(α -methylbenzyl)glycine.

Table 5.2. Characterization of poly(n-butyl acrylate-peptoid) block copolymers.

Sample	Peptoid block	M_n^{PnBA} (g/mol) ^a	P(nBA) PDI ^a	M_n^{peptoid} (g/mol)	f_{peptoid} ^b
P(nBA-R24)	Helical	14000	1.1	3471	0.18
P(nBA-R36)	Helical	14000	1.1	5129	0.25
P(nBA-R48)	Helical	14000	1.1	6787	0.31
P(nBA-R54)	Helical	14000	1.1	7617	0.33
P(nBA-N24)	Racemic	14000	1.1	3471	0.18
P(nBA-N36)	Racemic	14000	1.1	5129	0.25
P(nBA-N48)	Racemic	14000	1.1	6787	0.31
P(nBA-N54)	Racemic	14000	1.1	7617	0.33
P(nBA-RN36)	Helical/Rac	14000	1.1	5129	0.25
P(nBA-NR36)	Rac/Helical	14000	1.1	5129	0.25

^a As determined by GPC using polystyrene calibration standards. ^b $f_{\text{peptoid}} = M_n^{\text{peptoid}}/1.18/(M_n^{\text{peptoid}}/1.18 + M_n^{\text{PnBA}}/1.08)$.

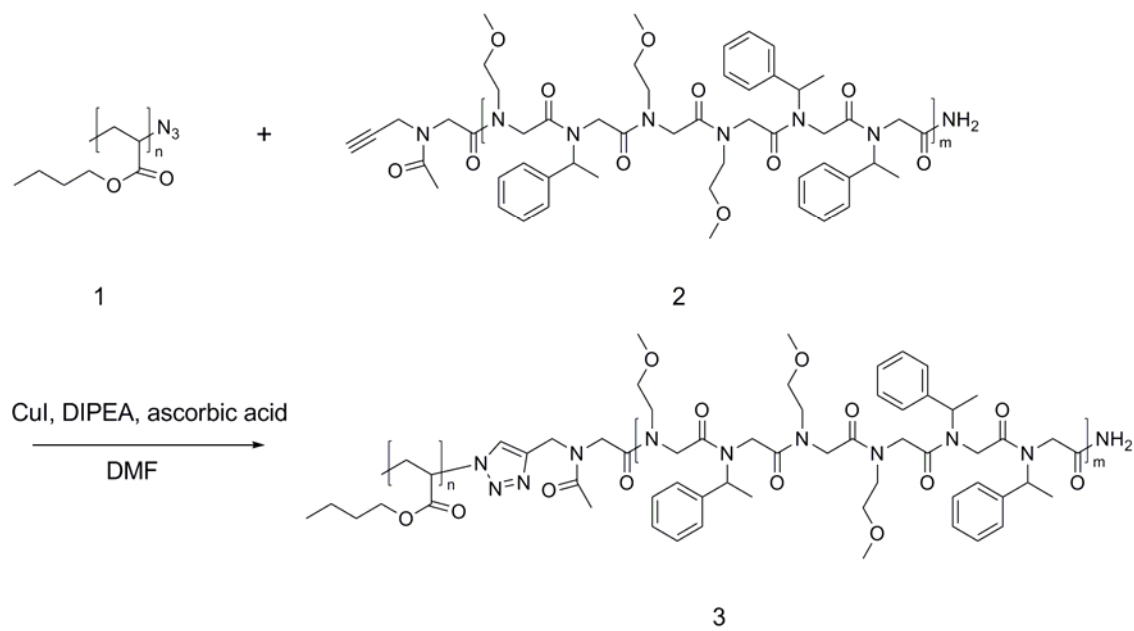
Circular Dichroism (CD) CD measurements were performed on a J-185 CD spectrometer (Jasco Inc., Easton, MD). Stock solutions of the polypeptoids were made in tared vials using 5 mg/mL of peptoid powder in acetonitrile. The stock solutions were then diluted to a concentration of 0.1 mg/mL before acquiring CD spectra. CD spectra were acquired using a quartz cell (Hellma USA, Plainview, NY) with a path length of 1 mm. A scan rate of 50 nm/min was used, and 3 measurements were averaged for each compound.

Small Angle X-Ray Scattering (SAXS) Because the block copolymers were very soft due to the poly(n-butyl acrylate) block, samples were prepared by filling 1 mm thick aluminum washers with the block copolymers using a spatula at room temperature. One side of the sample washer was glued to a Kapton window, and the entire sample cell was annealed in a vacuum oven (10^{-9} Torr) at 130°C for 24 h. After annealing, a second Kapton window was glued to the washer to seal the polymer sample completely. SAXS was conducted at the Advanced Light Source (ALS, beamline 7.3.3) and at the Stanford Synchrotron Radiation Lightsource (SSRL, beamline 1-4). At the ALS, the beamline was configured with an X-ray wavelength of $\lambda = 1.240 \text{ \AA}$ and focused to a spot size of 50 μm by 300 μm . Two-dimensional scattering patterns were collected on a Pilatus 100k detector. The isotropic scattering patterns were radially averaged, and the scattering intensity was corrected with the post-ion chamber intensity using Nika version 1.18. SAXS patterns were calibrated with a silver behenate standard. At SSRL, the beamline was configured with an X-ray wavelength of $\lambda = 1.488 \text{ \AA}$ and focused to a 0.5 mm diameter spot. A single quadrant of a two-dimensional scattering pattern was collected on a CCD detector with an active area of 25.4 mm by 25.4 mm. The two-dimensional profiles were radially averaged.

5.3 Results and Discussion

The effect of peptoid chain shape on self-assembly was probed with two series of block copolymers. The chain shape of peptoid polymers was controlled using molecular chirality as a handle (sequences shown in Table 5.1). Polypeptoids containing 50% of N-*R*- α -methylbenzylglycine monomers formed a helical chain conformation, while polypeptoids containing 50% of a racemic mixture of N- α -methylbenzylglycine monomers possessed a disordered chain shape. Previous neutron scattering experiments in dilute acetonitrile solution found that the persistence length of an unstructured polypeptoid chain is 0.6 nm, while the persistence length of a helical polypeptoid chain is approximately 1.1 nm for peptoid chains at least 36 monomers in length.²⁴ In this study, the length of the peptoid polymers was varied from 24 monomers to 54 monomers, and these polymers were combined with poly(n-butyl acrylate) ($M_n \sim 14,000 \text{ g/mol}$) to yield block copolymers (Table 5.2). The polypeptoid was the minority phase of all block copolymers investigated here; the peptoid volume fractions ranged from approximately 0.18 to 0.33.

Scheme 5.1. Synthetic Route of P(nBA-peptoid) block copolymers.



To probe whether conjugating the polypeptoid to the poly(*n*-butyl acrylate) disrupted the helical conformation of the polypeptoid, CD was used. Figure 5.1 shows the CD for the block copolymers in dilute acetonitrile solution. A CD signal for all block copolymers containing *N*-*R*- α -methylbenzylglycine monomers is found, including the characteristic peaks at 190 nm, 205 nm, and 220 nm that indicate the peptoid helical conformation. These peaks have been attributed to the perpendicularly polarized π - π^* transition, the parallel-polarized π - π^* transition, and the *n*- π^* transition of the amide groups.²⁵ In past studies,^{21,22} the intensity of the peak around 220 nm has been used to assess the degree of helical ordering in the peptoid samples. Relative to the peptoid homopolymers (data available in the Appendix), the intensity of this peak is approximately the same, indicating that attachment of the poly(*n*-butyl acrylate) block does not influence the amount of helicity in the peptoid block and the peptoid retains a helical conformation. All racemic block copolymers consistently show no CD signal.

The racemic P(*n*BA-*N*) block copolymers self-assemble into hexagonally packed cylinders at volume fractions ranging from 0.25 to 0.33, as indicated by the $1:\sqrt{3}:\sqrt{7}:\sqrt{9}$ peak spacing in the SAXS patterns (Figure 5.2). This lattice type usually shows a reflection at $\sqrt{4}q^*$ as well; however, destructive interference between the form factor and the structure factor of the block copolymer can suppress this peak. The structure formation agrees with the theoretically predicted phase diagram for block copolymers in the strongly segregated regime.²⁶ Furthermore, this result is also similar to the behavior previously observed for this range of volume fractions in polypeptoid-polystyrene block copolymers.²⁰ The change in volume fraction from 0.18 to 0.33 stems from an increase in the length of the peptoid block, and this yields an increase in the domain spacing of the self-assembled nanostructure as well (Figure 5.3).

Matsen and Bates previously described the change in domain spacing for strongly segregated block copolymers according to the conformational asymmetry between the two blocks, the molecular composition, and the geometry of the self-assembled structure (Equation 5.1).²⁷ Using the statistical segment length of the peptoid block as measured by small angle neutron scattering and allowing the Flory-Huggins parameter, χ , to be fit does not result in a good fit for the measured domain spacings of the block copolymers (Appendix). However, if the statistical segment length of the peptoid block is also allowed to be fit, the quality of the fit is greatly increased, suggesting there may be significant differences between the segment length of the polypeptoid in the solid state as compared to that measured in solution.

When the peptoid block contains enantiomerically pure *N*-*R*- α -methylbenzylglycine monomers, the block copolymers still self-assemble into hexagonally packed cylinders (Figure 5.2). However, the corresponding domain spacings are larger by a few nanometers (Figure 5.3),

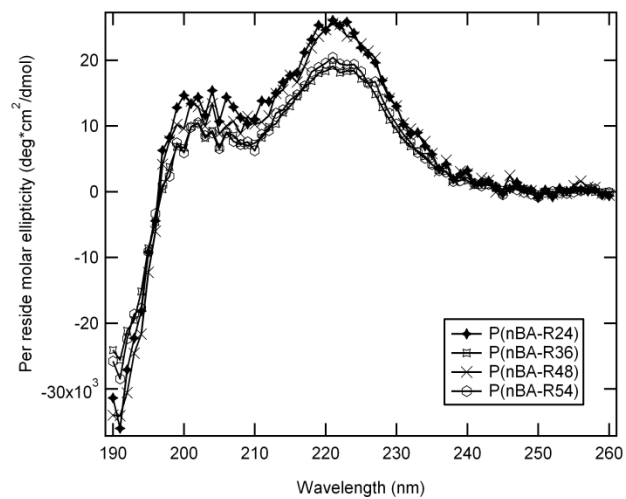


Figure 5.1. CD of P(nBA-peptoid) Block Copolymers. Circular dichroism of P(nBA-peptoid) block copolymers indicates the preservation of the peptoid helical conformation.

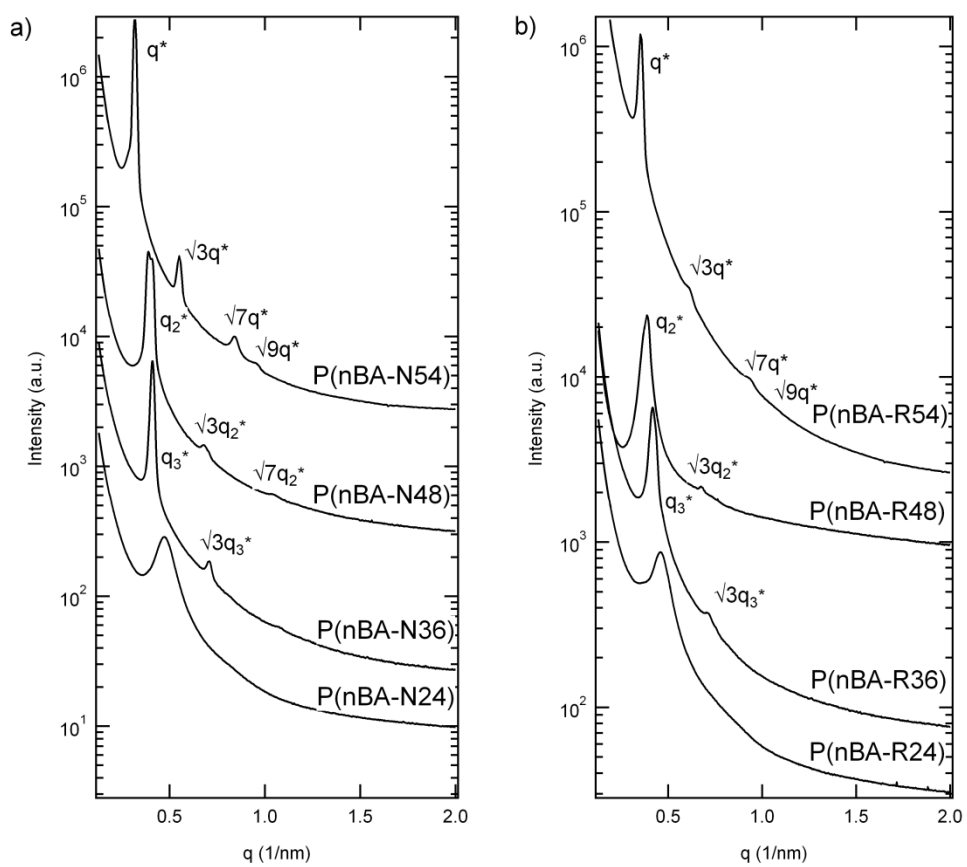


Figure 5.2. SAXS of P(nBA-peptoid) Block Copolymers. SAXS indicates self-assembly of P(nBA-peptoid) block copolymers.

indicating a change in packing due to the steric effects of the peptoid chain shape. These block copolymers also show a larger deviation from the predicted scaling relationship, as might be expected if the chains are more rod-like and do not follow the expected $N^{2/3}$ scaling. This result may also indicate that the helical block copolymers are more strongly segregated than the racemic block copolymers. Previously, Ho et. al measured the order-disorder transition temperatures (ODTs) of chiral polystyrene-poly(L-lactide) block copolymers and found them to be higher (more strongly segregated) than those of racemic polystyrene-poly(lactide) block copolymers of comparable molecular weight.¹⁷ The higher incompatibility between the poly(L-lactide) and polystyrene was attributed to a difference in the packing energy of the chiral polymer chains, which in turn affects the cohesive energy of the block. In particular, it was suggested that the chiral effect leads to the formation of a partially ordered microdomain, causing a decrease in the Gibbs free energy state. Stringer et. al previously crystallized a tetramer peptoid helix and found that the bulky side chains of the helix are situated between the side chains of the neighboring helices.²⁸ It is possible that a similar situation exists within the cylindrical microdomains and that the helices are interdigitated or somewhat ordered.

The change in domain spacing between the chiral and achiral block copolymer systems can further be probed by introducing precise chiral interactions into the peptoid block because the polypeptoids are sequence-specific and their residue location can be dictated exactly. A 36-mer polypeptoid was made that contained both a helical and a racemic domain (each 18 monomers in length), with the helical domain immediately adjacent to the block copolymer junction (PnBA-NR36). This block copolymer had a domain spacing intermediate to that of both the fully chiral or fully racemic block copolymers (Figure 5.4a), indicating that the change in domain spacing stems from the steric hindrance of the homochiral part of the peptoid chain only and that this does not influence the rest of the peptoid chain. This result is supported by circular dichroism (Appendix), which shows a decreased ellipticity per number of residues as compared to the homochiral peptoids. Neither chiral amplification nor disordering of the helical domain takes place.

When the locations of the helical and racemic domains are flipped such that the racemic region is adjacent to the block copolymer junction (PnBA-RN36), the self-assembled domain spacing is equal to that of PnBA-R36, the fully chiral block copolymer (~18.3 nm). This is likely an effect of originating the helix at the carboxamide terminus of the chain instead of the N-terminus, which in this case is covalently bound to the butyl acrylate block. Previously, it was shown that having chiral residues at the carboxamide terminus stabilized peptoid helix formation compared to starting the helical region at the opposite end of the chain.²¹ This sequence effect is also seen here, as indicated by the increased CD signal at 220 nm for RN36 compared to its retropeptoid, NR36 (Figure 5.4b). The helix stabilization may stiffen the rest of the polypeptoid chain, resulting in a larger domain spacing.

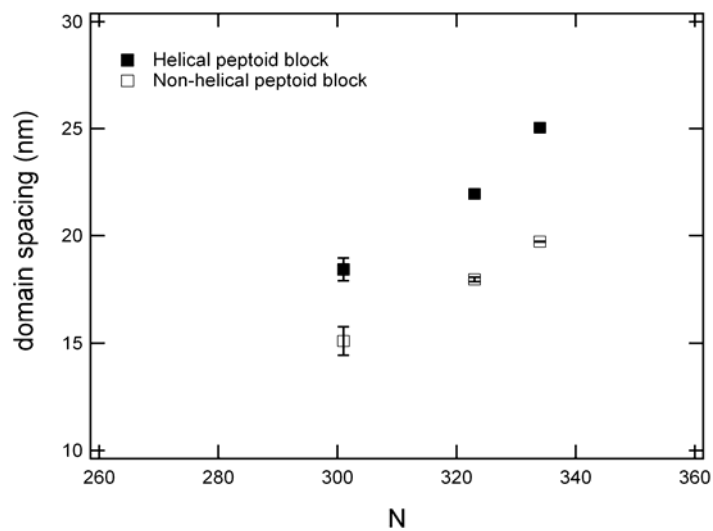


Figure 5.3. Domain Spacing of P(nBA-peptoid) Block Copolymers. Chiral peptoid blocks lead to larger domain spacings for the block copolymers.

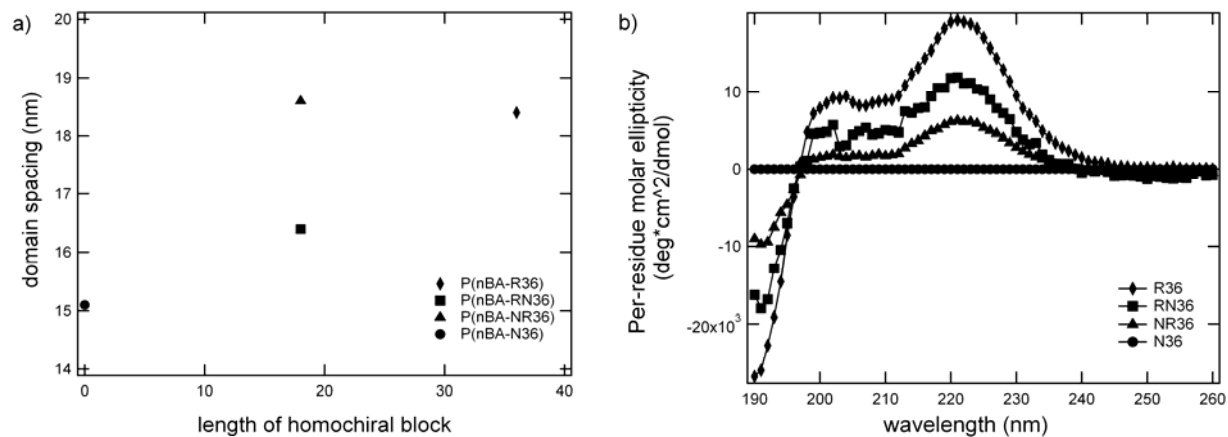


Figure 5.4. Domain Spacing and CD of Sequence Specific P(nBA-peptoid) Block Copolymers. a) Domain spacing can be tuned with the length of the homochiral block, although sequence is also important; b) placing chiral residues at the C-terminus stabilizes peptoid helix formation, as indicated by increased signal in circular dichroism.

As an achiral comparison, a polypeptoid was designed to have the same molecular weight and molecular composition as the helical polypeptoid. This design was accomplished by using 50% phenylethylglycine residues instead of *N-R- α* -methylbenzylglycines. A block copolymer containing this peptoid block and the same butyl acrylate block (PnBA-P36) still forms hexagonally-packed cylinders with a domain spacing similar to that of PnBA-N36. This result reinforces the unstructured nature of the racemic polypeptoid.

5.4 Conclusions

In this study, polypeptoid chain shape was controlled with chirality. Enantiomeric polypeptoids had a helical chain shape, and racemic polypeptoids possessed a more disordered chain shape. Block copolymers with a poly(*n*-butyl acrylate) block provided insight into the chain shape effects on self-assembly. In particular, a change in statistical segment length leads to an increase in the size of the morphological domain spacing. Precisely placed chiral residues show that helix stabilization at the C-terminus leads to larger domain spacings than peptoid sequences with chiral residues placed at the N-terminus. These studies show that polypeptoids are a useful platform for investigating chiral interactions in block copolymers and may show interesting behavior in applications where chirality is important, such as separations.

5.5 Acknowledgements

We gratefully acknowledge funding from the Office of Naval Research via a Presidential Early Career Award in Science and Engineering. A.M.R. also gratefully acknowledges the National Science Foundation for a graduate fellowship. Polypeptoid synthesis and associated chemical characterization were performed at the Molecular Foundry, a Lawrence Berkeley National Laboratory user facility supported by the Office of Science, Office of Basic Energy Sciences, U.S. Department of Energy, under Contract DE-AC02-05CH11231. SAXS studies at the Advanced Light Source (beamline 7.3.3) were supported by the U.S. Department of Energy under contract number DE-AC02-05CH11231, and SAXS studies at the Stanford Synchrotron Radiation Laboratory (beamline 1-4) were facilitated by Stanford University on behalf of the U.S. Department of Energy.

5.6 Appendix

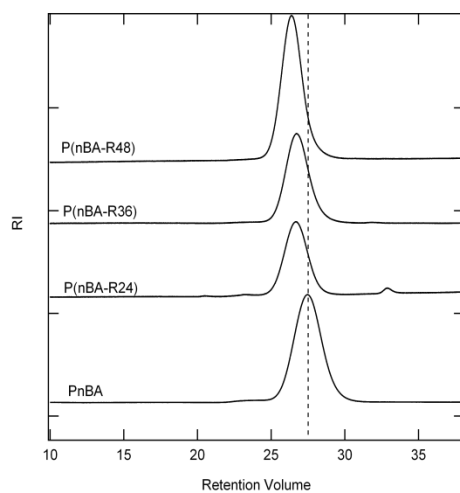


Figure 5.5. Representative GPC Traces for Block Copolymers. The dashed vertical line is a guide to the eye so that the peak shifts can be seen more clearly.

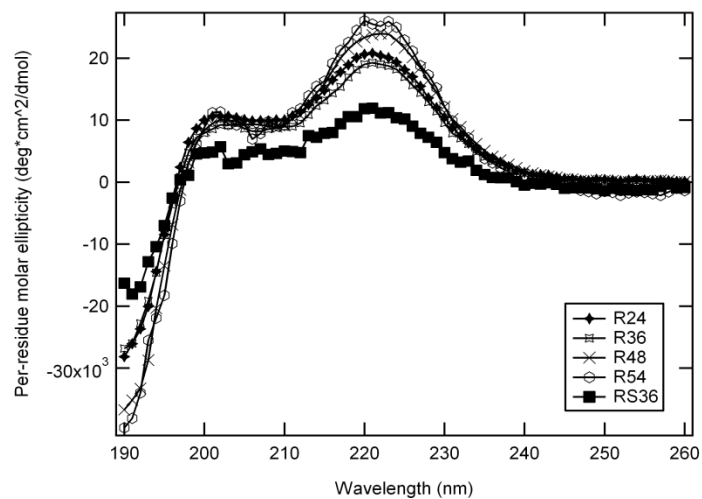


Figure 5.6. Circular Dichroism for Peptoid Homopolymers. Helical peptoid homopolymers show similar CD signals to the peptoids in block copolymers. RS36 contains both a helical and a racemic domain (each 18 monomers in length), and the CD signal is approximately half that of R36.

Domain Spacing Scaling Relationship

Matsen and Bates previously described the change in domain spacing for strongly segregated block copolymers according to the conformational asymmetry between the two blocks, the molecular composition, and the geometry of the self-assembled structure (Equation 5.1).

$$R = a \left(\frac{\beta}{2(\alpha^A + \alpha^B)} \right)^{\frac{1}{3}} \chi^{\frac{1}{6}} N^{\frac{2}{3}} \quad 5.1$$

where

$$D^* = \left(\frac{3\pi^4}{4} \right)^{\frac{1}{6}} R \quad \text{for cylinders} \quad 5.2$$

In this relationship, D^* is the domain spacing (as calculated from the primary SAXS peak), a is the average statistical segment length of the block copolymer, χ is the Flory-Huggins parameter, and N is the total number of monomers. For poly(n-butyl acrylate), $a_{\text{PhBA}} = 12.32$ Å. The statistical segment length of the peptoid can be related to the persistence length, which was measured previously in acetonitrile solution. Assuming the flexibility of the chain in the bulk is similar to that measured in solution, $a_{\text{racemic}} = 4.3$ Å. The coefficients α^A , α^B , and β all depend on the geometry of the structure, the volume fraction of the peptoid block, and the statistical segment lengths. To yield the representation of Equation 5.1 in Figure 5.7, the Flory-Huggins parameter χ was treated as a fitting parameter, and it was found that $\chi \sim 0.02$ showed reasonable agreement with the measured domain spacings of the block copolymer. For the range of chain lengths studied here (N), this value of χ yields χN values of approximately 5 – 6, which is below the predicted χN of 10.5 at the critical point. This indicates that these block copolymers are likely weakly segregated, and their domain spacing scaling may be better described as following $N^{1/2}$. For the chiral block copolymers, Equation 5.1 was applied to the data with a statistical segment length $a_{\text{chiral}} = 6.0$ Å, as previously measured, and χ was fit to be ~ 0.05 . However, the chiral block copolymers show an even larger deviation from the predicted scaling relationship.

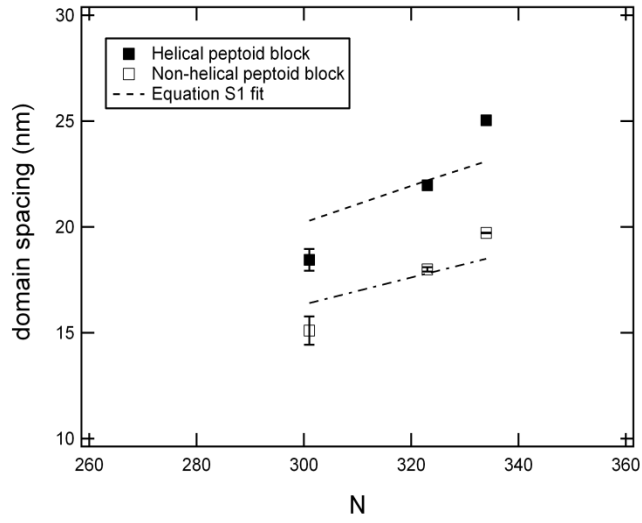


Figure 5.7. Domain spacings of the block copolymers with Equation 5.1 fits. The P(nBA-R) block copolymers deviate more from the predicted domain spacings.

4.7 References

- (1) Shoulders, M. D.; Raines, R. T. *Annual Review of Biochemistry* **2009**, *78*, 929.
- (2) Nakano, T.; Okamoto, Y. *Chemical Reviews* **2001**, *101*, 4013.
- (3) Fujiki, M. *Macromolecular Rapid Communications* **2001**, *22*, 539.
- (4) Green, M. M.; Reidy, M. P.; Johnson, R. D.; Darling, G.; O'Leary, D. J.; Willson, G. J. *Am. Chem. Soc.* **1989**, *111*, 6452.
- (5) Nolte, R. J. M. *Chemical Society Reviews* **1994**, *23*, 11.
- (6) Lam, J. W. Y.; Tang, B. Z. *Accounts of Chemical Research* **2005**, *38*, 745.
- (7) Cornelissen, J. J. L. M.; Rowan, A. E.; Nolte, R. J. M.; Sommerdijk, N. A. J. M. *Chemical Reviews* **2001**, *101*, 4039.
- (8) Yashima, E.; Maeda, K. *Macromolecules* **2007**, *41*, 3.
- (9) Nagai, K.; Sakajiri, K.; Maeda, K.; Okoshi, K.; Sato, T.; Yashima, E. *Macromolecules* **2006**, *39*, 5371.
- (10) Maeda, K.; Takeyama, Y.; Sakajiri, K.; Yashima, E. *J. Am. Chem. Soc.* **2004**, *126*, 16284.
- (11) Dellaportas, P.; Jones, R. G.; Holder, S. J. *Macromolecular Rapid Communications* **2002**, *23*, 99.
- (12) Majidi, M. R.; Kane-Maguire, L. A. P.; Wallace, G. G. *Polymer* **1995**, *36*, 3597.
- (13) Prince, R. B.; Barnes, S. A.; Moore, J. S. *J. Am. Chem. Soc.* **2000**, *122*, 2758.
- (14) Hanson, J. A.; Li, Z.; Deming, T. J. *Macromolecules* **2010**, *43*, 6268.
- (15) Bloksma, M. M.; Hoepfener, S.; D'Haese, C.; Kempe, K.; Mansfeld, U.; Paulus, R. M.; Gohy, J.-F.; Schubert, U. S.; Hoogenboom, R. *Soft Matter* **2012**, *8*, 165.
- (16) Chiang, Y.-W.; Ho, R.-M.; Burger, C.; Hasegawa, H. *Soft Matter* **2011**, *7*, 9797.
- (17) Ho, R. M.; Chiang, Y. W.; Chen, C. K.; Wang, H. W.; Hasegawa, H.; Akasaka, S.; Thomas, E. L.; Burger, C.; Hsiao, B. S. *J. Am. Chem. Soc.* **2009**, *131*, 18533.
- (18) Ho, R. M.; Li, M. C.; Lin, S. C.; Wang, H. F.; Lee, Y. D.; Hasegawa, H.; Thomas, E. L. *J. Am. Chem. Soc.* **2012**, *134*, 10974.
- (19) Figliozzi, G. M.; Goldsmith, R.; Ng, S. C.; Banville, S. C.; Zuckermann, R. N. *Methods Enzymol.* **1996**, *267*, 437.
- (20) Rosales, A. M.; McCulloch, B. L.; Zuckermann, R. N.; Segalman, R. A. *Macromolecules* **2012**, *45*, 6027.
- (21) Wu, C. W.; Sanborn, T. J.; Huang, K.; Zuckermann, R. N.; Barron, A. E. *J. Am. Chem. Soc.* **2001**, *123*, 6778.
- (22) Wu, C. W.; Sanborn, T. J.; Zuckermann, R. N.; Barron, A. E. *J. Am. Chem. Soc.* **2001**, *123*, 2958.
- (23) Holub, J. M.; Jang, H. J.; Kirshenbaum, K. *Org. Biomol. Chem.* **2006**, *4*, 1497.
- (24) Rosales, A. M.; Murnen, H. K.; Kline, S. R.; Zuckermann, R. N.; Segalman, R. A. *Soft Matter* **2012**, *8*, 3673.
- (25) Kirshenbaum, K.; Barron, A. E.; Goldsmith, R. A.; Armand, P.; Bradley, E. K.; Truong, K. T. V.; Dill, K. A.; Cohen, F. E.; Zuckermann, R. N. *Proceedings of the National Academy of Sciences* **1998**, *95*, 4303.
- (26) Bates, F. S.; Fredrickson, G. H. *Phys. Today* **1999**, *52*, 32.
- (27) Matsen, M. W.; Bates, F. S. *J. Polym. Sci. Pt. B-Polym. Phys.* **1997**, *35*, 945.
- (28) Stringer, J. R.; Crapster, J. A.; Guzei, I. A.; Blackwell, H. E. *J. Am. Chem. Soc.* **2011**, *133*, 15559.

Chapter 6. Conclusions and Future Outlook

In summary, polypeptoids are non-natural polymers that offer the ability to examine the effect of monomer sequence on polymer properties and self-assembly. In Chapter 2, we controlled the melting and crystallization behavior of short peptoid homopolymers with sequence. While many peptoid molecules had been previously explored in solution, little was known about the properties of peptoid polymers, especially in the solid state. Because the thermal properties of polypeptides were known to be significantly affected by hydrogen bonding, it was anticipated that polypeptoids (which lack this hydrogen bonding) would exhibit drastically different thermal behavior. Analogous peptide and peptoid molecules showed this was exactly the case, and the polypeptoids demonstrated lower melting transitions or glass transitions than their peptide analogs, indicating polymer chains with much more mobility. This result was further reinforced with conformational studies of polypeptoid chains in dilute solution (Chapter 3). Using small angle neutron scattering (SANS), several polypeptoids were shown to have a low persistence length, which could be slightly altered by the presence of helical secondary structure. Thus, these studies have furthered our understanding of polypeptoids as flexible polymer chains in which the properties can be tuned with the choice of side chains.

Our findings with peptoid homopolymers have also informed our work with peptoid-containing block copolymers (Chapters 4 and 5). Because of the conformational flexibility of the peptoid chains, we have been able to design block copolymers that self-assemble into morphologies with curved interfaces. This is difficult to achieve with peptidic systems due to the very strong dipole interactions present in peptide secondary structures. With the polypeptoids, however, we are able to achieve equilibrium block copolymer phases with order-disorder transitions that can be tuned according to the peptoid sequence. In addition, the changes in persistence length that we measured in Chapter 3 are manifested as changes in the block copolymer domain spacing.

While this work provides significant progress toward understanding the relationship between structure and sequence of non-natural polymers, there still remain several open questions that can guide future work. For example, the crystalline peptoid homopolymers were short enough to form extended chain crystals, and at the time, the only route to achieving truly polymeric peptoids was the use of chemical ligation techniques. However, recent developments in peptoid polymerization using N-carboxyanhydrides (NCA) have allowed access to polypeptoids of high molecular weight. Although NCA polymerizations are not sequence specific, they provide the opportunity to compare the material properties of the solid-phase synthesized peptoid oligomers and the NCA-polymerized peptoid polymers. Such a comparison will provide insight on the influence of side chain composition on crystalline properties across a large molecular weight range. Furthermore, the two synthesis methods offer the opportunity to compare sequenced copolymers against random copolymers of comparable molecular weights.

Our work on the conformational studies of polypeptoids (Chapter 3) has aided in the design of subsequent peptoid systems, as well as informed modeling studies. Since this work was conducted, several new routes to stabilize the peptoid helix have been implemented by other groups, such as increasing the steric bulk of the side chain or incorporating functional groups capable of forming hydrogen bonds or covalent bonds along a helix face. While techniques such as NMR and CD have shown an increase in the conformational homogeneity of these modified helices, a quantitative measure of their chain stiffness remains unknown. A more complete set of measurements would greatly aid the prediction of well-folded self-assembled structures both in solution and the solid state.

Although this work has established a platform for investigating the role of monomer sequence on block copolymer self-assembly, a fully sequence-specific self-assembling system has yet to be achieved in the solid state. Because the chemical difference between two peptoid blocks is controlled by the side chains, diblock copolypeptoids typically have very low strengths of segregation. This is compounded by the low molecular weights achieved with solid phase synthesis methods. Future work will surely focus on enhancing the strength of segregation, such as by adding selective solvents or salts to one of the peptoid blocks. Chemical ligation could also prove to be a convenient way to increase the strength of segregation by increasing the molecular weight. A fully sequence-specific peptoid system will be essential for probing fundamental questions such as the limits of block architecture using gradient, tapered, and other monomer sequences.

In a larger context, polypeptoids have shown to be an ideal sequence-specific model system, but their application to materials use will require several improvements. Higher molecular weight materials will confer additional stability and enhanced mechanical properties, though current synthesis methods require monomer synthesis and lead to the loss of sequence specificity. In addition, many bulk properties, such as rheological or mechanical properties, are currently unknown because a thorough investigation would require large quantities of polypeptoid. Thus, synthesis methods need to be further optimized for yield as well as molecular weight.

The exploration of monomer sequence effects on polymer properties will continue to be important, especially as materials are applied to highly specific functions. Our work on understanding this relationship with polypeptoids provides a valuable basis for the design of sequence-defined materials with hierarchical levels of structure.